

EUROPEAN ORGANISATION FOR NUCLEAR RESEARCH (CERN)



Submitted to: Physical Review D



CERN-EP-2016-167

April 5, 2022

Measurement of $W^\pm W^\pm$ vector-boson scattering and limits on anomalous quartic gauge couplings with the ATLAS detector

The ATLAS Collaboration

This paper presents the extended results of measurements of $W^\pm W^\pm jj$ production and limits on anomalous quartic gauge couplings using 20.3 fb^{-1} of proton–proton collision data at $\sqrt{s} = 8 \text{ TeV}$ recorded by the ATLAS detector at the Large Hadron Collider. Events with two leptons (e or μ) with the same electric charge and at least two jets are analyzed. Production cross-sections are determined in two fiducial regions, with different sensitivities to the electroweak and strong production mechanisms. An additional fiducial region, particularly sensitive to anomalous quartic gauge coupling parameters α_4 and α_5 , is introduced, which allows more stringent limits on these parameters compared to the previous ATLAS measurement.

© 2022 CERN for the benefit of the ATLAS Collaboration.

Reproduction of this article or parts of it is allowed as specified in the CC-BY-4.0 license.

arXiv:1611.02428v1 [hep-ex] 8 Nov 2016

1 Introduction

Vector-boson scattering (VBS) processes provide a unique method to examine the mechanism of Electroweak Symmetry Breaking and to search for physics beyond the Standard Model (SM) [1–3]. In the SM, the Higgs boson prevents the longitudinal scattering amplitude of the $VV \rightarrow VV$ ($V = W$ or Z) process from continuously increasing as a function of the center-of-mass energy of the diboson system, which would violate unitarity at energies above approximately 1 TeV [4–6]. In many new physics scenarios [7, 8], the Higgs boson has non-SM HVV couplings below current experimental sensitivity and additional resonances are introduced to restore unitarity in the high-energy regime. The energy dependence of the VBS production cross-section above the Higgs boson mass scale can be used to test whether the Higgs boson discovered at the Large Hadron Collider (LHC) [9, 10] unitarizes the scattering amplitude fully or only partially [2].

The VBS topology consists of a proton–proton collision with two initial quarks that each radiate an electroweak boson. The two bosons subsequently scatter and then decay. The two outgoing quarks are often close to the beam direction. Multiple processes can produce the same final state of two bosons (V) and two jets (j) from the fragmentation of the two outgoing quarks ($VVjj$). The production of $VVjj$ at tree level is composed of electroweak production involving only electroweak-interaction vertices (denoted by “ $VVjj$ -EW”), and strong production involving at least one strong-interaction vertex (denoted by “ $VVjj$ -QCD”). The electroweak production is further categorized into two components. The first component is the EW VBS production with actual scattering of the two electroweak bosons. The scattering occurs via triple or quartic gauge vertices, the s - and t -channel exchange of a Higgs boson, or a W/Z boson (throughout this paper, the notation “ Z boson” means “ Z/γ^* boson”, unless specified otherwise). The second component is the EW non-VBS production with electroweak vertices only, where the two bosons do not scatter. The EW non-VBS component cannot be separated from the EW VBS component in a gauge invariant way [1]. It is therefore included in the signal generation and cannot be distinguished from the EW VBS. Representative Feynman diagrams at tree level are shown in Figure 1 for EW VBS production, in Figure 2 for EW non-VBS production, and in Figure 3 for $VVjj$ -QCD production. Triboson production with one of the bosons decaying hadronically also yields the same $VVjj$ final state. The resonant decay of a boson into two quarks can be suppressed by applying a requirement on the invariant mass of the two quarks. As a consequence, triboson processes are suppressed in the EW VBS signal region.

The scattering of two massive vector bosons can lead to $W^\pm W^\pm jj$, $W^+ W^- jj$, $W^\pm Z jj$ or $ZZ jj$ diboson states. The $W^\pm W^\pm jj$ electroweak production does not involve diagrams with the s -channel exchange of a Higgs boson or a vector boson, and the contributions from strong production are greatly suppressed due to the lack of Feynman diagrams with two gluons or one quark and one gluon in the initial state [11]. The $W^\pm W^\pm jj$ channel is found to have the largest cross-section ratio of electroweak to strong production [12]. Leptonic decays of the W bosons ($W \rightarrow \ell\nu$)¹ are used, which allow the identification of the electric charges of the two W bosons. The presence of two leptons with the same electric charge in the final state significantly reduces SM backgrounds. For these reasons, $W^\pm W^\pm jj$ production is one of the best channels for VBS studies at the LHC [13].

Due to the non-Abelian nature of the SM electroweak theory, gauge bosons interact with each other. Besides the triple WWZ and $WW\gamma$ gauge boson vertices, the SM also predicts the existence of quartic

¹ Throughout this paper, $\ell = e, \mu$ where the notation “electrons” is used to mean “electrons or positrons” and the notation “muons” is used to mean “muons or antimuons”, unless specified otherwise. Additionally, ν indicates either a neutrino or an anti-neutrino.

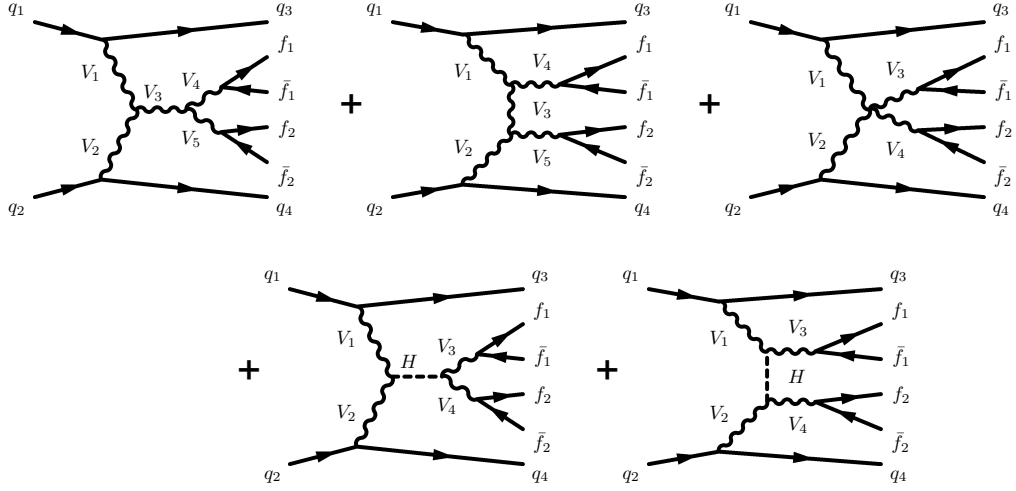


Figure 1: Representative Feynman diagrams for $VVjj$ -EW production with a scattering topology including either a triple gauge boson vertex with production of a W/Z boson in the s -channel (top left diagram), the t -channel exchange (top middle diagram), quartic gauge boson vertex (top right diagram), or the exchange of a Higgs boson in the s -channel (bottom left diagram) and t -channel (bottom right diagram). The lines are labeled by quarks (q), vector bosons ($V = W, Z$), and fermions (f).

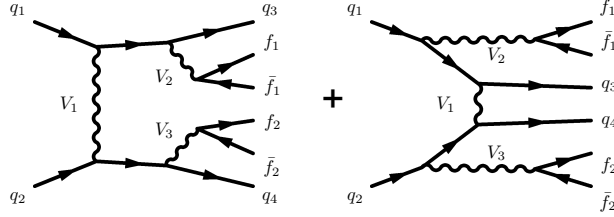


Figure 2: Representative Feynman diagrams for $VVjj$ -EW production without vector-boson scattering topology. The lines are labeled by quarks (q), vector bosons ($V = W, Z$), and fermions (f).

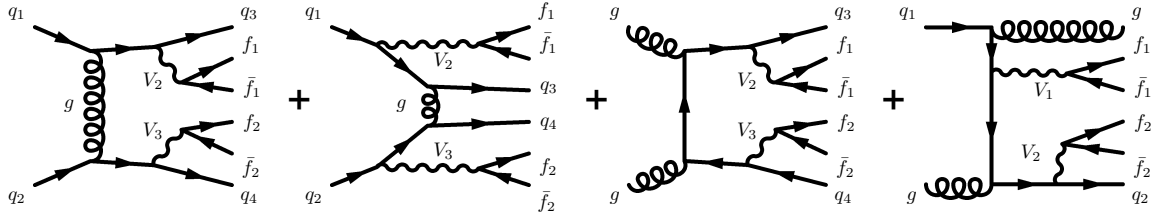


Figure 3: Representative Feynman diagrams for $VVjj$ -QCD production defined by VBS topologies with strong interaction vertices. The lines are labeled by quarks (q), vector bosons ($V = W, Z$), fermions (f), and gluons (g).

$WWWW$, $WW\gamma\gamma$, $WWZZ$, and $WWZ\gamma$ vertices. Possible physics beyond the SM can affect these vertices and introduce anomalous triple gauge couplings (aTGCs) or anomalous quartic gauge couplings (aQGCs). An effective field theory (EFT) framework [14–17] provides a generic platform for introducing the effect of new physics by adding additional terms in the SM chiral Lagrangian. The lowest-order terms contributing to aQGCs are the dimension-four operators \mathcal{L}_4 and \mathcal{L}_5 :

$$\alpha_4 \mathcal{L}_4 = \alpha_4 [\text{tr}(V_\mu V_\nu)]^2 \quad \text{and} \quad \alpha_5 \mathcal{L}_5 = \alpha_5 [\text{tr}(V_\mu V^\mu)]^2, \quad (1)$$

where α_4 and α_5 are dimensionless anomalous coupling parameters and $V_\mu = \Sigma(D_\mu \Sigma)^\dagger$ with D_μ being the covariant derivative operator. The field Σ is a 2×2 matrix, which transforms as $\Sigma \rightarrow U \Sigma V^\dagger$ under local $SU(2)_L$ transformations U and $U(1)_Y$ transformations V .

The EFT approach is applicable to many models of physics beyond the SM including, but not limited to, two- or multi-Higgs-doublet models, extended scalar sectors, Technicolor models, models of complete or partial compositeness, Little Higgs models, Twin Higgs models, etc. For example, certain heavy resonances would manifest as nonzero values of the α_5 coupling parameter among others, but not influence α_4 [18]. While other models of physics beyond the SM such as a Higgs triplet, W'/Z' , or Kaluza–Klein graviton would manifest as nonzero parameter points in the (α_4, α_5) plane [19].

Searches for processes containing QGCs have been performed by previous experiments, for example, $e^+e^- \rightarrow WW\gamma, \nu\nu\gamma\gamma, qq\gamma\gamma$ [20–23] by the LEP experiments, $p\bar{p} \rightarrow pW^+W^-\bar{p} \rightarrow pe^+\nu e^-\bar{\nu}\bar{p}$ by the D0 experiment [24], $pp \rightarrow WV\gamma \rightarrow \ell\nu qq\gamma$ [25] and $pp \rightarrow pW^+W^-p \rightarrow pe^\pm\nu\mu^\mp\nu p$ [26] by the CMS experiment, $\gamma\gamma \rightarrow W^+W^-$ [27] and $pp \rightarrow W\gamma\gamma \rightarrow \ell\nu\gamma\gamma$ [28] by the ATLAS experiment. None of these processes have been observed, which is expected due to their low SM cross sections and large backgrounds. These results are used to set limits on corresponding aQGCs with at least one photon involved.

Experimental investigation of QGCs with four massive vector bosons has only been attempted at the LHC. Using 20.3 fb^{-1} of data collected at $\sqrt{s} = 8 \text{ TeV}$, evidence of $W^\pm W^\pm$ decaying to $\ell^\pm\nu\ell^\pm\nu$ in association with two jets was recently presented [29] by the ATLAS Collaboration. Similar results were obtained by the CMS Collaboration [30] in the same final state. ATLAS has published a search for WZ production in association with two jets [31], WW/WZ production in association with a high-mass dijet system [32], and WWW production [33]. This paper completes and extends the results presented in the form of a letter in Ref. [29]. An updated Monte Carlo simulation for the signal is used, and a new signal region more sensitive to aQGCs is developed and more stringent limits on α_4 and α_5 are derived.

2 The ATLAS detector

The ATLAS detector [34] is a multipurpose particle detector designed to measure a wide range of physics processes from pp collisions at the TeV scale. It consists of an inner tracking detector (ID), calorimeters, a muon spectrometer (MS), and solenoidal and toroidal magnets in a cylindrical geometry with forward-backward symmetry.²

The ID consists of three subdetectors. The pixel detector and semiconductor tracker (SCT) are composed of silicon pixel and microstrip detectors and extend to $|\eta| = 2.5$. In this region, the pixel detector has 3 cylindrical layers and the SCT has 4 layers. The transition radiation tracker (TRT) is built of gas-filled

² The ATLAS reference system is a Cartesian right-handed coordinate system with its origin at the nominal interaction point (IP) in the center of the detector and the z -axis along the beam direction. The x -axis points from the IP to the center of the LHC ring and the y -axis points upward. Cylindrical coordinates (r, ϕ) are used in the plane that is transverse to the beam direction, where ϕ describes the azimuthal angle around the beam pipe as measured from the positive x -axis. Rapidity (y) is defined as $y = 1/2 \times \ln[(E + p_z)/(E - p_z)]$, where E (p_z) is the energy (the z -component of the momentum) of a particle. Pseudorapidity (η) is defined as $\eta = -\ln(\tan \theta/2)$ where θ is the polar angle. Transverse momentum (p_T) is defined relative to the beam axis and is calculated as $p_T = p \sin \theta$ where p is the momentum. The distance between two objects in the η - ϕ space is defined as $\Delta R = \sqrt{(\eta_1 - \eta_2)^2 + (\phi_1 - \phi_2)^2}$ where $\eta_{1,2}$ ($\phi_{1,2}$) represents the pseudorapidities (azimuthal angle) of the two objects.

straw-tube detectors and extends to $|\eta| = 2.0$. The ID is surrounded by a thin superconducting solenoid magnet that creates a 2 T axial magnetic field for charged-particle momentum measurements.

The calorimeter system consists of electromagnetic (EM) and hadronic calorimeters. A high-granularity sampling calorimeter with lead absorber layers and liquid argon (LAr) measures the energy and position of electromagnetic showers in the pseudorapidity region of $|\eta| < 3.2$. Hadronic showers are measured by steel and scintillator tile calorimeters for $|\eta| < 1.7$ and copper/LAr calorimeters for $1.5 < |\eta| < 3.2$. The forward calorimeter extends the coverage, spanning $3.1 < |\eta| < 4.9$ with additional copper/LAr and tungsten/LAr calorimeters.

The MS covers the pseudorapidity range of $|\eta| < 2.7$ and is instrumented with separate trigger and precision tracking chambers. A precision measurement of the track coordinates in the bending direction of the toroidal magnetic field is provided by drift tubes up to $|\eta| = 2.0$. At larger pseudorapidities, cathode strip chambers with higher granularity are used in the innermost station covering $2.0 < |\eta| < 2.7$. The muon trigger system consists of resistive plate chambers in the barrel ($|\eta| < 1.05$) and thin gap chambers in the endcap regions ($1.05 < |\eta| < 2.4$).

A three-level trigger system is used to record the events used in this analysis. The level-1 trigger is implemented in hardware and reduces the event rate to about 75 kHz. This is followed by two software-based trigger levels that together reduced the event rate to about 600 Hz during the 2012 data-taking period.

3 Event selection

Candidate events are collected by single-lepton triggers with thresholds of $p_T = 36$ GeV (muons) or $p_T = 60$ GeV (electrons) or single-isolated-lepton triggers with a lower threshold of $p_T = 24$ GeV. The events must also occur during stable beam conditions and with the relevant detector systems functional. The resulting total integrated luminosity is 20.3 fb^{-1} with an uncertainty of 2.8% [35].

Tracks used in this analysis are reconstructed using an “inside-out” algorithm starting with seeds made from hits in the pixel detector and the first layer of the SCT and attempting to extend these into the remaining silicon layers and finally into the TRT [36]. Proton–proton interaction vertices are reconstructed by extrapolating the z -position of tracks at the beamline, grouping two or more tracks into vertex candidates, and then reconstructing the vertex position and its corresponding error matrix. Tracks incompatible with the vertex by more than seven standard deviations are used to look for additional vertices. The vertex with the largest sum of squared transverse momenta of associated tracks ($\sum p_T^2$) is taken to be the primary vertex. The primary vertex is required to have at least three associated tracks with $p_T > 0.4$ GeV.

Three types of lepton identification criteria are defined for signal selection and background rejection, which are non-exclusive: a tight lepton criterion used to select the final two same-electric-charge leptons, a veto lepton used to reject events with an additional lepton present in $W^\pm Z$ or ZZ events, and a loose lepton category used to estimate the background contribution from events with non-prompt leptons from in-flight hadron decays or with jets misidentified as leptons.

Electrons are reconstructed from a combination of track information in the ID and cluster information in the electromagnetic calorimeter. Tight electrons must satisfy identification criteria similar to the tight definition used in Refs. [37–39], which includes requirements on the electron track, the shape of the shower in the EM calorimeter, and the ratio of energies deposited in the EM and hadronic calorimeters.

Additionally, the track hit information is used to identify and remove electrons arising from photon conversions. Electron candidates must have $p_T > 25$ GeV and $|\eta| < 2.47$. Electrons within the transition region ($1.37 < |\eta| < 1.52$) between the EM barrel and endcap calorimeters are excluded. The transverse (d_0) and longitudinal (z_0) impact parameters must satisfy $|d_0/\sigma_{d_0}| < 3$ and $|z_0 \times \sin \theta| < 0.5$ mm, where σ_{d_0} is the uncertainty in the measurement of d_0 . Finally, calorimeter and tracking isolation selections are applied as follows: the sum of the transverse energies of all calorimeter clusters (E_T^{iso}) and the sum of the transverse momenta of tracks (p_T^{iso}) within a cone of size $\Delta R = 0.3$, are required to be less than 14% and 6% of the electron's transverse energy, respectively. The energy from the electron itself is excluded in the calculations of E_T^{iso} and p_T^{iso} .

Veto and loose electrons are only required to pass a loose identification selection defined in Ref. [37]. The p_T threshold is lowered to 7 GeV, and the tracking isolation requirement is removed for veto electrons. For loose electrons, the impact parameter requirements are loosened to $|d_0/\sigma_{d_0}| < 10$ and $|z_0 \times \sin \theta| < 5$ mm, and the calorimeter and tracking isolation criteria are $0.14 < E_T^{\text{iso}}/p_T < 2$ and $0.06 < p_T^{\text{iso}}/p_T < 2$.

Muons are reconstructed from tracks in the ID and MS and fall into one of three categories: combined, standalone, and tagged [40]. Combined muons contain matching tracks in the ID and MS. Standalone muons consist only of a track in the MS, while tagged muons have an ID track that is matched to a track segment in the MS. In this analysis, tight muons are required to be reconstructed as combined muons with the same electric charge measured in the ID and MS. They must have $p_T > 25$ GeV and $|\eta| < 2.5$. The ID tracks associated with these muons must pass a number of quality requirements. The number of hits or dead sensors crossed in the pixel detector must be at least one, and in the SCT this number must be at least five. For muons with $0.1 < |\eta| < 1.9$, the track must have at least six hits in the TRT, and the fraction of these that are outliers must not exceed 90%. Tight muons have the same impact parameter requirements as tight electrons and have calorimeter and tracking isolation requirements defined by $E_T^{\text{iso}}/p_T < 0.07$ and $p_T^{\text{iso}}/p_T < 0.07$ where a cone of size $\Delta R = 0.3$ is used.

The selection of veto muons includes standalone and tagged muons. The p_T threshold is lowered to 6 GeV, the calorimeter isolation requirement is dropped, and the track isolation selection is loosened to be less than 15% of the muon p_T . Loose muons must be combined muons, but just as for loose electrons, the impact parameter requirements are loosened to $|d_0/\sigma_{d_0}| < 10$ and $|z_0 \times \sin \theta| < 5$ mm, and the calorimeter and tracking isolation criteria are $0.07 < p_T^{\text{iso}}/p_T < 2$ and $0.07 < p_T^{\text{iso}}/p_T < 2$.

To improve agreement between data and simulation, lepton selection efficiencies are measured in both data and simulation, and correction factors are applied to the simulation to account for differences with respect to data [39, 40]. Furthermore, the simulation is tuned to reproduce the calorimeter energy and the muon momentum scales and resolutions observed in data. The simulation also includes modeling of additional pp interactions in the same and neighboring bunch crossings.

Jets are reconstructed from topological clusters in the calorimeter using the anti- k_r algorithm [41] with a radius parameter of 0.4 [42]. Jets are required to have $p_T > 30$ GeV and $|\eta| < 4.5$. In order to reduce the probability of selecting a jet from a pileup interaction, jets with $|\eta| < 2.4$ and $p_T < 50$ GeV are required to have a jet vertex fraction greater than 50%. The jet vertex fraction is defined as the ratio of the sum of the p_T of all tracks associated with both the jet and the primary vertex to the sum of the p_T of all tracks in the jet [43]. Jets stemming from the fragmentation of a charm or bottom quark are identified with a neural network discriminator using input variables related to the impact parameter significance of tracks in the jet and secondary vertices reconstructed from these tracks [44]. The jet is classified as a b -jet if the output of this neural network discriminator exceeds a working point chosen to have a 70% efficiency for identifying jets from top quarks containing b -hadrons.

The measurement of the two-dimensional missing transverse momentum vector \vec{E}_T^{miss} and its magnitude E_T^{miss} [45] is based on the measurement of all topological clusters in the calorimeter, and muon tracks reconstructed by the ID and MS. The energies of clusters in the calorimeter are calibrated according to their association with a reconstructed object.

In order to deal with the case where a single particle is reconstructed as more than one object, an overlap removal procedure is followed. If the event contains a tight electron and a jet with $\Delta R(e, j) < 0.3$, the jet is removed since it is likely that it corresponds to the electron energy deposits picked up by the jet reconstruction algorithm. If the same is true for a jet and a tight muon, the event is rejected since the muon likely originates from the decay of a hadron within the jet. When estimating the background from non-prompt leptons, jets are also removed if they fall within $\Delta R = 0.3$ of a loose lepton. For electrons and muons separated by $\Delta R < 0.1$, the electron is removed since it is likely that it originates from a photon radiated from the muon.

Signal candidate events are selected by requiring two tight leptons with the same electric charge and an invariant mass ($m_{\ell\ell}$) greater than 20 GeV. Three final states are considered based on the lepton flavor, namely $e^\pm e^\pm$, $e^\pm \mu^\pm$, and $\mu^\pm \mu^\pm$. To reduce background contributions from the $W^\pm Z$ and ZZ processes, events with a third lepton of the veto type are rejected. An additional requirement is made in the $e^\pm e^\pm$ final state that the invariant mass of the two electrons differs from the combined world average of the Z pole mass [46] by at least 10 GeV. This selection criterion reduces the background from the $Z(\rightarrow e^+ e^-) + \text{jets}$ process where one electron's charge is misidentified. Since two neutrinos are produced from the decays of the two W bosons, E_T^{miss} is required to be greater than 40 GeV. Events are required to have at least two jets. In order to reduce the background from top-quark pair and single top-quark production, the event is rejected if any jet is classified as a b -jet. Remaining events with an invariant mass of the two leading- p_T jets (m_{jj}) greater than 500 GeV are selected. This selection level defines the inclusive signal region (denoted by ‘‘Inclusive SR’’), and both the electroweak and strong production of $W^\pm W^\pm jj$ are treated as signal. The VBS signal region (denoted by ‘‘VBS SR’’) is defined to consist of events in the inclusive signal region for which the separation in rapidity between the two leading- p_T jets ($|\Delta y_{jj}|$) is greater than 2.4. In this region only the electroweak production is considered as signal. The third signal region (denoted by ‘‘aQGC SR’’) additionally requires the estimated transverse mass of the WW system to be greater than 400 GeV in order to optimize the sensitivity to the new-physics parameters α_4 and α_5 . The variable, $m_{WW,T}$, is defined as

$$m_{WW,T} = \sqrt{\left(\mathbf{P}_{\ell_1} + \mathbf{P}_{\ell_2} + \mathbf{P}_{E_T^{\text{miss}}}\right)^2} \quad (2)$$

where $\mathbf{P}_{\ell_1, \ell_2}$ are the four-momenta of the two selected lepton candidates and $\mathbf{P}_{E_T^{\text{miss}}}$ is the massless four-vector constructed from the \vec{E}_T^{miss} measurement with the z -component of $\mathbf{P}_{E_T^{\text{miss}}}$ defined as zero. In the aQGC SR, both the electroweak and strong production predicted by the SM are considered as background, and only the contributions due to aQGCs are considered as signal.

Table 1 summarizes the kinematic selection criteria used for the three signal regions.

Signal Region		Selection Criteria
Inclusive	Lepton	Exactly two tight same-electric-charge leptons with $p_T > 25$ GeV
	Jet	At least two jets with $p_T > 30$ GeV and $ \eta < 4.5$
	$m_{\ell\ell}$	$m_{\ell\ell} > 20$ GeV
	E_T^{miss}	$E_T^{\text{miss}} > 40$ GeV
	Z veto	$ m_{\ell\ell} - m_Z > 10$ GeV (only for the $e^\pm e^\pm$ channel)
	Third-lepton veto	No third veto-lepton
	b -jet veto	No identified b -jets with $p_T > 30$ GeV and $ \eta < 2.5$
	m_{jj}	$m_{jj} > 500$ GeV
VBS	Δy_{jj}	$ \Delta y_{jj} > 2.4$
aQGC	$m_{WW,T}$	$m_{WW,T} > 400$ GeV

Table 1: Kinematic selection criteria used for three signal regions. These selection criteria are applied successively for each signal region such that the aQGC signal region has all requirements applied.

4 Monte Carlo simulation and theoretical predictions

Monte Carlo (MC) events are simulated at $\sqrt{s} = 8$ TeV and processed through the full ATLAS detector simulation [47] based on GEANT4 [48]. Additional proton–proton interactions modeled by PYTHIA 8 [49, 50] are included and reweighted to reproduce the observed distribution of the average number of proton–proton interactions per event. Contributions from interactions in nearby bunch crossings are also considered in the MC simulations. Events generated in the Inclusive and VBS signal regions are used to measure the production cross-sections, provide normalization factors for MC samples, and to compare with theoretical predictions. This section concentrates on the theoretical cross-sections and uncertainties for the $W^\pm W^\pm jj$ -EW and $W^\pm W^\pm jj$ -QCD processes in these two regions.

Definition of Inclusive and VBS fiducial phase-space regions at the particle level

Two fiducial phase-space regions are defined at particle level by selection criteria similar to the ‘‘Inclusive SR’’ and ‘‘VBS SR’’ described in Section 3. Particle level jets are reconstructed by running the anti- k_r algorithm with radius parameter $R = 0.4$ on all observable final-state stable particles after parton showering and hadronization. The inclusive fiducial phase-space region is defined with the following criteria: exactly two charged leptons (only considering electrons and muons) of the same electric charge, each with $p_T > 25$ GeV and $|\eta| < 2.5$, and at least two particle level jets with $p_T > 30$ GeV and $|\eta| < 4.5$. The jets are required to be separated from leptons by $\Delta R(\ell, j) > 0.3$. The events are further required to have a dilepton invariant mass $m_{\ell\ell} > 20$ GeV and $p_T^{v_1+v_2} > 40$ GeV, where $p_T^{v_1+v_2}$ is the magnitude of the vectorial sum of p_T of the two particle level neutrinos. The lepton four-momentum includes contributions from photons within $\Delta R(\ell, \gamma) = 0.1$ of the lepton direction. The two leptons are also required to be separated by $\Delta R > 0.3$. The two leading- p_T jets are required to have $m_{jj} > 500$ GeV. An additional requirement of $|\Delta y_{jj}| > 2.4$ is applied for the VBS fiducial phase-space region.

$W^\pm W^\pm jj$ -EW and $W^\pm W^\pm jj$ -QCD cross-sections and uncertainties

Both electroweak and strong production of $W^\pm W^\pm jj$ events are generated using the SHERPA version 1.4.5 event generator [51] at leading order (LO) in QCD with up to three partons. Matrix-element and parton-

shower matching for the two final-state jets are performed with the CKKW scheme [52]. Dynamic factorization (μ_F) and renormalization (μ_R) scales are set to be

$$\mu_{F,R} = \frac{1}{2} \sum_{i=1,2} \left[p_T(j_i) + \sqrt{m^2(W_i) + p_T^2(W_i)} \right], \quad (3)$$

where $p_T(j_i)$ is the momentum of the i^{th} leading- p_T jet, and $m(W_i)$ and $p_T(W_i)$ are the mass and transverse momentum of the i^{th} W boson. CT10 parton distribution functions (PDFs) [53] are used.

The $W^\pm W^\pm jj$ SHERPA samples are updated from those in the previous publication of the measurement of $W^\pm W^\pm jj$ [29] to include a more accurate representation of the QED final-state radiation. The impact of this effect reduces the final acceptance due to an additional 5% loss of leptons in the lepton-jet overlap removal in both fiducial phase-space regions.

The SHERPA cross-sections are scaled to account for the next-to-leading-order (NLO) cross-section predictions using POWHEG-BOX [54–56] with PYTHIA 8 for parton shower and hadronization in the fiducial phase-space regions. The dynamic scales defined in Eq. (3) are used. Contributions from non-resonant production are included, but are highly suppressed. Interference effects between the electroweak and strong production are studied using separated and combined electroweak and strong-mediated samples. The cross-section for the combined sample minus the sum of the cross-sections of purely electroweakly-mediated and purely strongly-mediated samples gives the size of the interference effect. The interference is found to enhance the total signal production cross-section by 10.7% in the Inclusive phase-space region and 6.5% in the VBS phase-space region.

The prediction for $W^\pm W^\pm jj$ -EW production is cross-checked using VBFNLO [57–59] and the results from the two generators are found to be consistent to within 5%. This 5% difference is taken as the generator uncertainty. Scale- and PDF-induced uncertainties are evaluated using VBFNLO. Scale-induced uncertainties are estimated by varying separately the factorization and renormalization scales from the central values as listed in Eq. (3) by factors ξ_F and ξ_R . The largest difference in the cross-section resulting from variations of (ξ_F, ξ_R) where $\xi_F, \xi_R = 0.5, 1, \text{ or } 2$ excluding extremum combinations $(\xi_F = 0.5, \xi_R = 2)$ and $(\xi_F = 2, \xi_R = 0.5)$ of scale variations is taken as the uncertainty. The PDF uncertainty is determined by adding in quadrature the CT10 eigenvector variations [53] and the difference of central values with respect to MSTW2008 [60].

Due to the selection criteria applied to jet transverse momenta and dijet mass, the parton shower has an effect on the fiducial cross-sections [61–64]. Two different parton-shower algorithms are applied to POWHEG-BOX NLO events and the difference in the signal yield is used to determine the uncertainty. The default algorithm relies on the PYTHIA 8 parton-shower model using the AU2 set of tuned parameters [65] for the underlying-event modeling. The second algorithm uses the HERWIG [66] parton-shower model with JIMMY [67] to model the underlying event.

The NLO cross-sections for the $W^\pm W^\pm jj$ -QCD production are also calculated using the POWHEG-BOX generator. Uncertainties due to the scale, PDF, and parton-shower model are evaluated in the same way as for the $W^\pm W^\pm jj$ -EW production.

Theoretical uncertainties in the predictions for $W^\pm W^\pm jj$ -EW and $W^\pm W^\pm jj$ -QCD production in the Inclusive and VBS fiducial phase-space regions are detailed in Table 2. The $W^\pm W^\pm jj$ -EW ($W^\pm W^\pm jj$ -QCD) production cross-section is predicted to be 1.00 ± 0.06 fb (0.35 ± 0.05 fb) in the Inclusive phase-space region and 0.88 ± 0.05 fb (0.098 ± 0.018 fb) in the VBS phase-space region. The interference between

Source of uncertainty	$W^\pm W^\pm jj$ -EW		$W^\pm W^\pm jj$ -QCD	
	Inclusive	VBS	Inclusive	VBS
MC sample size	1%	2%	4%	8%
Showering model	2%	4%	3%	7%
Scale	2%	2%	12%	13%
PDF	2%	3%	2%	2%
Generator	5%	3%	5%	5%
Total uncertainty	6%	6%	14%	18%

Table 2: Summary of theoretical uncertainties for the $W^\pm W^\pm jj$ -EW and $W^\pm W^\pm jj$ -QCD production in the Inclusive and VBS fiducial phase-space regions.

$W^\pm W^\pm jj$ -EW and $W^\pm W^\pm jj$ -QCD production enhances the cross-section by 0.16 ± 0.08 fb in the Inclusive phase-space region and 0.07 ± 0.04 fb in the VBS phase-space region. Both the electroweak and strong production of $W^\pm W^\pm jj$ and their interference are treated as signal in the Inclusive phase-space region. The total predicted signal cross-section in the Inclusive phase-space region is 1.52 ± 0.11 fb. For the VBS phase-space region, the electroweak production and the interference term are included in the total predicted cross-section, which is determined to be 0.95 ± 0.06 fb. For the rest of the paper, $W^\pm W^\pm jj$ -EW is used to indicate the combined contribution from the electroweak production and the interference effect, while $W^\pm W^\pm jj$ -EW+QCD indicates contributions from both electroweak and strong production as well as the interference effect.

5 Backgrounds

SM background processes producing the signature of two same-electric-charge leptons and E_T^{miss} with at least two jets in the final state are grouped in three categories: prompt background, non-prompt background, and conversions. The prompt background is due to WZ +jets, ZZ +jets, or $t\bar{t}V$ production when one or more leptons are either not reconstructed or not identified while the remaining two prompt leptons have the same electric charge. The non-prompt background is due to processes with one or two jets mis-reconstructed as tight leptons. The main contributions come from W +jets, $t\bar{t}$, single top quark, and multijet production. The conversion background events are mainly due to processes where two prompt electrons of opposite electric charge are produced but one radiates a photon that converts to e^+e^- . The main contribution comes from Z +jets production where the Z boson decays to e^+e^- . The background estimation for the prompt background category is based on MC-simulated samples, while estimations for the other two categories are based on data-driven methods. The modeling of the backgrounds is checked in several control regions.

5.1 Prompt background

The main source of prompt background is $WZjj$ production where both bosons decay leptonically and one lepton lies outside of the detector acceptance or fails the lepton identification requirements. Similarly to $W^\pm W^\pm jj$, there are strong and electroweak production mechanisms for $WZjj$, which contribute about 75% and 15% of the prompt background, respectively. The two production mechanisms are generated

using the SHERPA event generator at LO in QCD with up to three partons and normalized to NLO cross-sections calculated with vBFNLO in each fiducial phase-space region. The CT10 PDF set is used. The normalization of the electroweak production of $WZjj$ contains a further complication. This process receives a contribution from the production of a top quark in association with a Z boson and an additional parton (tZj), where the top quark further decays to a W boson and a b -quark. This class of diagrams is taken into account in SHERPA but is neglected in vBFNLO, even though it contributes almost a third of the events populating both phase-space regions. To account for this, a new normalization is derived using the b -quark in the initial state to select for tZj events. The samples are split into events that contain a b -quark in the initial state (using SHERPA at LO) and events without an initial b -quark (using vBFNLO at NLO). The cross-section used to normalize the SHERPA sample is given by $\sigma_{\text{fid}}^{\text{vBFNLO}}/A + \sigma_{\text{fid}}^{\text{SHERPA}} \times f_b$, where $\sigma_{\text{fid}}^{\text{vBFNLO}}$ is the NLO cross-section calculated using vBFNLO, $\sigma_{\text{fid}}^{\text{SHERPA}}$ is the sum of LO cross-sections calculated with and without a b -quark in the initial state using SHERPA, A is the parton-level acceptance of the SHERPA subsample without any b -quarks in the initial state, and f_b is the fraction of generated events containing a b -quark in the initial state. The overall cross-section for the electroweak $W^\pm Zjj$ production used for the normalization is 0.40 ± 0.09 fb (0.34 ± 0.09 fb) in the Inclusive (VBS) SR, while the corresponding cross-section for the strong production is 1.04 ± 0.17 fb (0.64 ± 0.08 fb).

Other processes with two prompt leptons with the same electric charge in the final state include the $t\bar{t}V$ process, $ZZjj$ production, and multiple parton–parton interactions (MPI) in one proton–proton interaction. The sum of these backgrounds contributes less than 10% of the total prompt background. The $t\bar{t}V$ events are generated using MADGRAPH [68] with PYTHIA 8 used for parton shower and hadronization. The CTEQ6L1 PDF [69] is used. The $ZZjj$ events are simulated using SHERPA with the CT10 PDF set. MPI processes such as $W^\pm j + W^\pm j$, $W^\pm j + Zj$, or $Zj + Zj$ are simulated with PYTHIA 8 with CTEQ6L1 and the overall contribution is found to be negligible.

5.2 Non-prompt background

Non-prompt backgrounds come from processes with jets misidentified as leptons or leptons from hadron decays (including b - and c -hadron decays). Since the MC simulation may not accurately model the details of these processes, a data-driven fake-factor method is employed to estimate this contribution.

The fake-factor method estimates a fake factor using the ratio of the number of jets satisfying the tight lepton identification criteria to the number of jets satisfying the loose lepton identification criteria in a jet-enriched sample. A new data sample, referred to as the “tight+loose” sample, is selected with the same set of criteria as the signal region but one lepton is required to be a loose lepton. This sample is dominated by contributions from W +jets, $t\bar{t}$, and single-top-quark processes. The fake factor is measured, as discussed below, as a function of the loose lepton p_T and applied to the tight+loose sample event-by-event as a global event weight to estimate the non-prompt background. The contribution from multijet background with two jets satisfying the tight lepton requirements is estimated by selecting events with two loose leptons and using the product of the two factors computed for each lepton as the event weight. The contribution from multijet background is found to be less than 3.5% of the total non-prompt background.

The lepton fake factors are measured using a dijet sample. Events are selected with a ‘tag’ jet and a loose or tight lepton back-to-back in the azimuthal plane with $\Delta\phi(\ell, j) > 2.8$. The lepton is also referred to as an ‘underlying jet’ since it originates from a jet or hadronic decay. Both the lepton and the jet are required to have $p_T > 25$ GeV. The transverse mass of the lepton and E_T^{miss} system is required to be less

than 40 GeV to suppress the W +jets contamination. The tag jet and underlying jet recoil in the transverse plane and are assumed to have the same p_T . The underlying jet p_T is calculated as the sum of the lepton p_T plus the transverse energy deposited in a cone of radius $\Delta R < 0.3$ around the lepton. To account for the reduction in p_T from energy deposited outside the lepton isolation cone or loss due to neutrinos, the tag jet p_T distribution in the dijet sample is reweighted to match the underlying jet in the tight+loose sample. The energy loss is linearly dependent on p_T where the tag jet has 18% higher p_T than the underlying jet associated with an electron and 72% more for underlying jets associated with a muon. The energy loss for non-prompt muons is accountable by the loss from neutrinos given these events are derived mainly from c - and b -hadron decays. In addition, a correction factor is applied to the tight+loose sample to take into account the lower trigger efficiency of isolated lepton triggers for loose leptons. The final fake factors are on the order of 2% for electrons and less than 1% for muons.

5.3 Conversion background

The conversion background is divided into two categories: events containing two prompt leptons with opposite electric charge, which can mimic the same final state if the electric charge of one lepton is misidentified (denoted by “Charge misID”), and $W\gamma$ production with the photon misreconstructed as an electron (denoted by “ $W\gamma$ ”).

The dominant mechanism responsible for charge misidentification of prompt electrons is the radiation of an energetic photon, which subsequently converts into an e^+e^- pair. The charge misidentification rate for muons is negligible and is therefore not considered. Events entering the signal regions due to conversions consist mainly of fully leptonic $t\bar{t}$ decays and Drell–Yan lepton pair production.

The rate of electron charge misidentification is measured in a data sample enriched in $Z \rightarrow e^+e^-$ events. This sample is required to have two tight electrons with the dielectron invariant mass between 70 GeV and 100 GeV. The asymmetric window around the pole mass of the Z boson is used to account for the reduced reconstructed energy when an electron’s charge is misidentified. Contributions to this mass region from other processes are found to be less than 1%. No requirement is made on the charges of the two electrons. The per-electron misidentification rate is derived from the number of same-electric-charge events and the total number of dielectron events.

A likelihood fit is used to measure the charge misidentification rate as a function of the electron p_T and η , taking into account that either electron in a same-electric-charge pair could be the misidentified one. The numbers of dielectron events and same-electric-charge events are counted in bins of the electron p_T and η . While the process of charge misidentification is inherently binomial, given the large number of events and the relatively small charge-flip rate a Poisson distribution is assumed. Given the total number of observed dielectron events, $N^{i,j}$, and the charge misidentification rates, ϵ^i and ϵ^j , where the efficiency is given for bins of p_T and η for the two electrons, i and j , the expected number of same-electric-charge events ($\tilde{N}_{SS}^{i,j}$) is given by

$$\tilde{N}_{SS}^{i,j} = \left[\epsilon^i (1 - \epsilon^j) + \epsilon^j (1 - \epsilon^i) \right] N^{i,j} \approx (\epsilon^i + \epsilon^j) N^{i,j} . \quad (4)$$

The approximation is valid for very small charge misidentification rates. The log-likelihood function for the number of observed dielectron events with same electric charge ($N_{SS}^{i,j}$) with respect to an expectation

of $\tilde{N}_{SS}^{i,j}$ is therefore given by

$$\ln L_{\text{misID}} = \ln \prod_{i,j} \frac{[(\epsilon^i + \epsilon^j) N_{SS}^{i,j}]^{N_{SS}^{i,j}}}{N_{SS}^{i,j}!} e^{-(\epsilon^i + \epsilon^j) N_{SS}^{i,j}} = \sum_{i,j} N_{SS}^{i,j} \ln [N_{SS}^{i,j} (\epsilon^i + \epsilon^j)] - N_{SS}^{i,j} (\epsilon^i + \epsilon^j) - \sum_{i,j} \ln [N_{SS}^{i,j}!], \quad (5)$$

Charge misidentification rates are determined for each p_T and η bin by maximizing the above log-likelihood function given the observed counts. Since the rates for bremsstrahlung and photon conversion depend on the amount of material traversed, the charge misidentification rate exhibits a strong dependence on the η of the electron with the rate generally increasing with $|\eta|$. The charge misidentification rate is observed to be a few tenths of a percent over most of the η range with a maximum of about 2% near $|\eta| = 2.5$.

The measured electron charge misidentification rate is cross-checked using a tag-and-probe method applied to the $Z \rightarrow e^+ e^-$ sample. Tighter requirements on the quality of the cluster in the calorimeter and the matched track are imposed on the tag electron to make sure its electric charge is correctly determined. The electric charge of the second electron is used to measure the electron charge misidentification rate. Good agreement between the estimates from these two methods is found.

To predict the amount of background from charge misidentification, data events are selected using all of the signal region criteria but requiring the two leptons to have opposite-sign electric charges. For each electron in this data sample, the corresponding charge misidentification rate is included in the global event weight. In the case of events with two electrons, this procedure is applied to each electron separately. In addition, an energy correction is applied to the electron with the charge misidentification rate assigned to take into account that electrons with misidentified charge tend to have lower reconstructed energy than their correctly identified counterparts and also yield a wider dielectron invariant mass peak for the Z boson. This energy correction is determined using the electron generator-level and reconstructed energies in MC-simulated $Z \rightarrow e^+ e^-$ events.

Production of $W\gamma$ events can yield same-electric-charge leptons if the photon converts in the detector and one conversion electron is not reconstructed. Both electroweak and strong $W\gamma jj$ production can arise and their contributions are also estimated using MC-simulated samples. The electroweak production is estimated using SHERPA, while the strong production is estimated using ALPGEN [70]. The CTEQ6L1 PDF set is used for both samples.

5.4 Control regions

Four control regions (CRs), referred to as the “ ≤ 1 jet CR”, “trilepton CR”, “ b -tag CR”, and “low- m_{jj} CR”, are used to validate background predictions. For all CRs, the contributions from $W^\pm W^\pm jj$ -EW and $W^\pm W^\pm jj$ -QCD production are normalized to the SM prediction. The definitions of all four control regions, the number of observed data events and the SM predictions as well as a few kinematic distributions in each region are presented below. Good agreement is observed between the data and the prediction for all regions.

≤ 1 jet control region

The ≤ 1 jet CR is used to test the modeling of lepton kinematics in the WZ/ZZ background where one of the leptons from the Z boson decay is not reconstructed. It is defined by inverting the signal region

selection on the jet multiplicity to accept only events with at most one jet. As a consequence, selection criteria using jet-based quantities such as m_{jj} and Δy_{jj} are also dropped. Figure 4 shows the dilepton invariant mass distribution and the leading-lepton p_T distribution for the $e^\pm\mu^\pm$ and $\mu^\pm\mu^\pm$ channels with the Z boson veto dropped. Table 3 shows the number of data events compared to the predictions from signal and various background sources.

≤ 1 jet Control Region					
	$e^\pm e^\pm$	$e^\pm\mu^\pm$	$\mu^\pm\mu^\pm$	Total	
$W^\pm W^\pm jj$ -EW+QCD	2.2 ± 0.3	7.0 ± 0.7	4.5 ± 0.5	13.7 ± 1.4	
Prompt	WZ, ZZ	46 ± 8	130 ± 23	75 ± 13	250 ± 40
	$t\bar{t}+W/Z$	0.3 ± 0.2	0.8 ± 0.4	0.6 ± 0.3	1.7 ± 0.7
Conversions	Charge misID	152 ± 17	24 ± 4	–	177 ± 21
	$W\gamma$	39 ± 11	59 ± 17	0.04 ± 0.04	98 ± 29
Non-prompt	38 ± 15	65 ± 26	8 ± 5	111 ± 30	
Total predicted	278 ± 28	290 ± 40	88 ± 14	650 ± 70	
Data	288	328	101	717	

Table 3: Predicted and observed numbers of events in the ≤ 1 jet control region separately for the $e^\pm e^\pm$, $e^\pm\mu^\pm$, and $\mu^\pm\mu^\pm$ channels as well as for the sum of all three. The uncertainty is the combination of statistical and systematic uncertainties; correlations among systematic uncertainties are taken into account in the calculation of the total.

Trilepton control region

The trilepton CR provides a test of the modeling of lepton and jet kinematics of the $WZjj$ production. It is defined by selecting events with three charged leptons where the third lepton passes the veto-lepton requirements. Events containing a fourth lepton passing the veto-lepton definition are still rejected. In contrast, m_{jj} and Δy_{jj} selection criteria are also dropped to obtain more events. The m_{jj} and $|\Delta y_{jj}|$ distributions are shown in Figure 5. Table 4 shows the number of data events compared to the predictions from signal and various background sources.

Trilepton Control Region					
	$e^\pm e^\pm \ell^\mp$	$e^\pm\mu^\pm \ell^\mp$	$\mu^\pm\mu^\pm \ell^\mp$	Total	
$W^\pm W^\pm jj$ -EW+QCD	0.05 ± 0.02	0.13 ± 0.03	–	0.168 ± 0.029	
Prompt	WZ	32 ± 5	96 ± 16	57 ± 10	186 ± 31
	ZZ	2.2 ± 0.6	5.3 ± 1.3	1.8 ± 0.5	9.2 ± 2.1
	$t\bar{t}+W/Z$	0.7 ± 0.3	2.4 ± 1.0	1.0 ± 0.5	4.1 ± 1.7
Non-prompt	0.5 ± 0.3	4 ± 4	–	4 ± 4	
Total predicted	36 ± 6	108 ± 18	60 ± 10	204 ± 33	
Data	40	104	48	192	

Table 4: Predicted and observed numbers of events in the trilepton control region separately for the $e^\pm e^\pm$, $e^\pm\mu^\pm$, and $\mu^\pm\mu^\pm$ channels as well as for the sum of all three. The third lepton is required to pass the veto-lepton requirements. The uncertainty is the combination of statistical and systematic uncertainties; correlations among systematic uncertainties are taken into account in the calculation of the total. The conversion background is found to be negligible.

b -tag control region

The b -tag CR provides a test of the modeling of $t\bar{t} + W/Z$ and non-prompt background. It is defined by inverting the b -jet veto criteria to require the presence of at least one b -tagged jet in the event. The

m_{jj} and $|\Delta y_{jj}|$ selection criteria are also dropped. Transverse momentum distributions for the leading- and sub-leading-leptons are shown in Figure 6. Table 5 shows the number of data events compared to the predictions from signal and various background sources. The b -tagging efficiency is included in the systematic uncertainty described in Section 6.

b -tag Control Region					
	$e^\pm e^\pm$	$e^\pm \mu^\pm$	$\mu^\pm \mu^\pm$	Total	
$W^\pm W^\pm jj$ -EW+QCD	0.8 ± 0.1	2.6 ± 0.3	1.5 ± 0.2	4.9 ± 0.5	
Prompt	WZ, ZZ	2.3 ± 0.5	4.9 ± 0.9	2.2 ± 0.4	9.4 ± 1.6
	$t\bar{t}+W/Z$	7.1 ± 3.1	18 ± 8	11 ± 4	36 ± 15
Conversions	Charge misID	22 ± 5	27 ± 6	–	49 ± 11
	$W\gamma$	1.7 ± 0.7	2.3 ± 0.9	0.2 ± 0.2	4.2 ± 1.4
Non-prompt		6.7 ± 2.5	20 ± 8	10 ± 5	37 ± 10
Total predicted		41 ± 6	75 ± 13	25 ± 7	141 ± 22
Data		46	82	36	164

Table 5: Predicted and observed numbers of events in the b -tag control region separately for the $e^\pm e^\pm$, $e^\pm \mu^\pm$, and $\mu^\pm \mu^\pm$ channels as well as for the sum of all three. The uncertainty is the combination of statistical and systematic uncertainties; correlations among systematic uncertainties are taken into account in the calculation of the total.

Low- m_{jj} control region

The low- m_{jj} control region is used to check the background modeling in a region with background composition similar to the signal regions. It is defined by inverting the m_{jj} selection and dropping the $|\Delta y_{jj}|$ selection. The $|\Delta y_{jj}|$ and leading-jet p_T distributions in the low- m_{jj} control region are shown in Figure 7. Table 6 shows the number of data events compared to the predictions from signal and various background sources.

Low m_{jj} Control Region					
	$e^\pm e^\pm$	$e^\pm \mu^\pm$	$\mu^\pm \mu^\pm$	Total	
$W^\pm W^\pm jj$ -EW+QCD	5.9 ± 0.6	17.4 ± 1.8	10.6 ± 1.1	33.9 ± 3.4	
Prompt	WZ, ZZ	25 ± 4	54 ± 9	18.4 ± 3.1	98 ± 16
	$t\bar{t}+W/Z$	1.7 ± 0.7	3.8 ± 1.6	2.4 ± 1.0	7.9 ± 3.4
Conversions	Charge misID	19.4 ± 2.3	8.4 ± 1.4	–	27.8 ± 3.4
	$W\gamma$	14 ± 4	20 ± 6	–	34 ± 10
Non-prompt		9 ± 4	21 ± 8	8 ± 4	39 ± 10
Total predicted		75 ± 9	125 ± 16	39 ± 6	240 ± 27
Data		78	120	30	228

Table 6: Predicted and observed numbers of events in the low- m_{jj} control region separately for the $e^\pm e^\pm$, $e^\pm \mu^\pm$, and $\mu^\pm \mu^\pm$ channels as well as for the sum of all three. The uncertainty is the combination of statistical and systematic uncertainties; correlations among systematic uncertainties are taken into account in the calculation of the total.

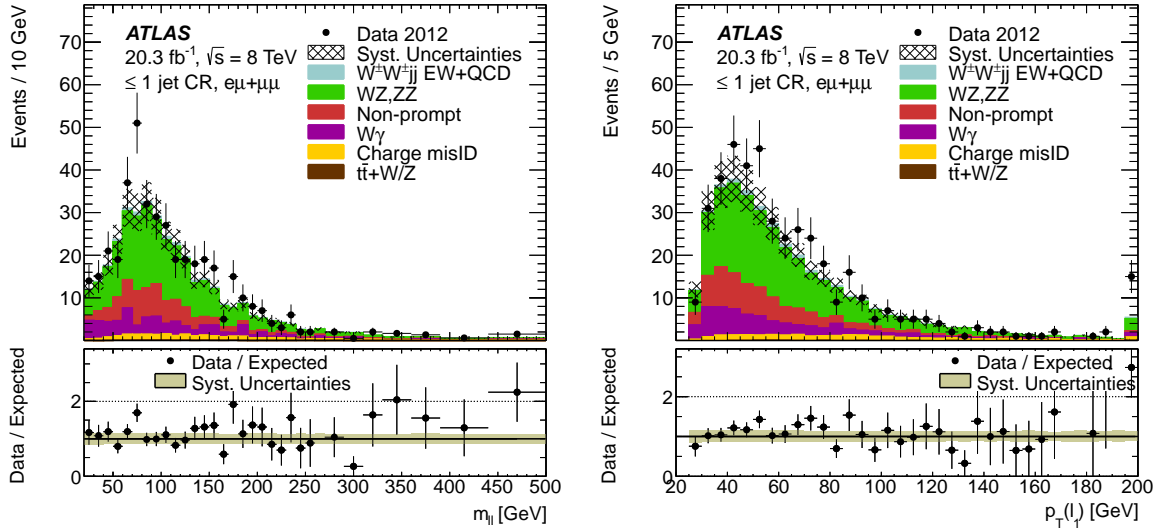


Figure 4: The invariant mass distribution of the dilepton pair (left) and the leading-lepton p_T distribution (right) for the $e^\pm\mu^\pm$ and $\mu^\pm\mu^\pm$ channels in the ≤ 1 jet CR without the Z boson veto requirement. The error bars on the data points include statistical uncertainty only. The hatched band represents the systematic uncertainty of the total prediction. The lower plot shows the ratio of the data to the expected background where the brown band indicates systematic uncertainty including the MC statistical uncertainty. The last bin includes overflow events.

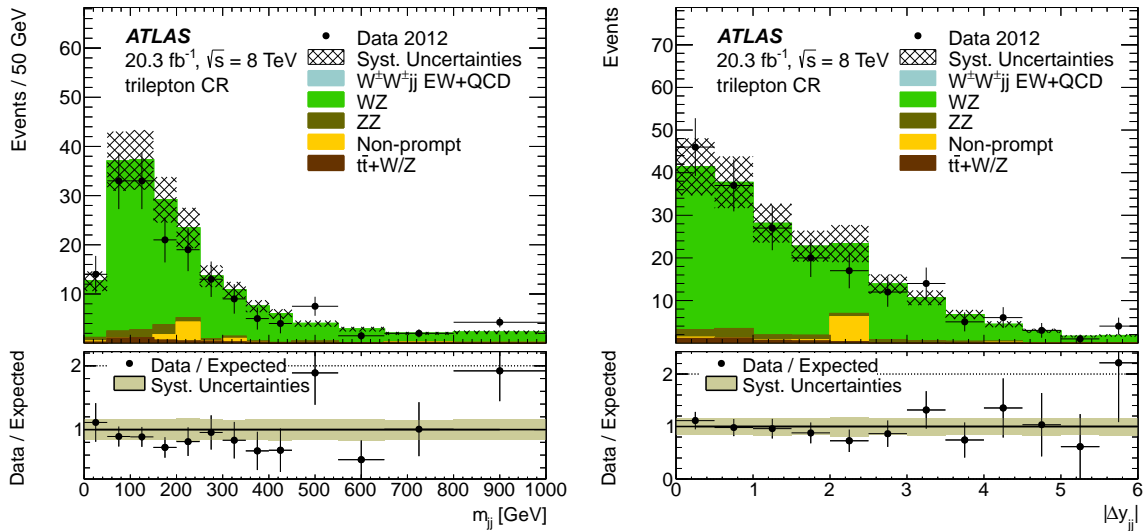


Figure 5: The m_{jj} distribution (left) and the distribution of the difference in rapidity (right) of the two jets with the highest p_T is shown summed over all lepton channels for the tripleton CR. Non-prompt background in this region is estimated using MC simulation. The error bars on the data points include statistical uncertainty only. The hatched band represents the systematic uncertainty of the total prediction. The lower plot shows the ratio of the data to the expected background where the brown band indicates systematic uncertainty including the MC statistical uncertainty. The last bin includes overflow events.

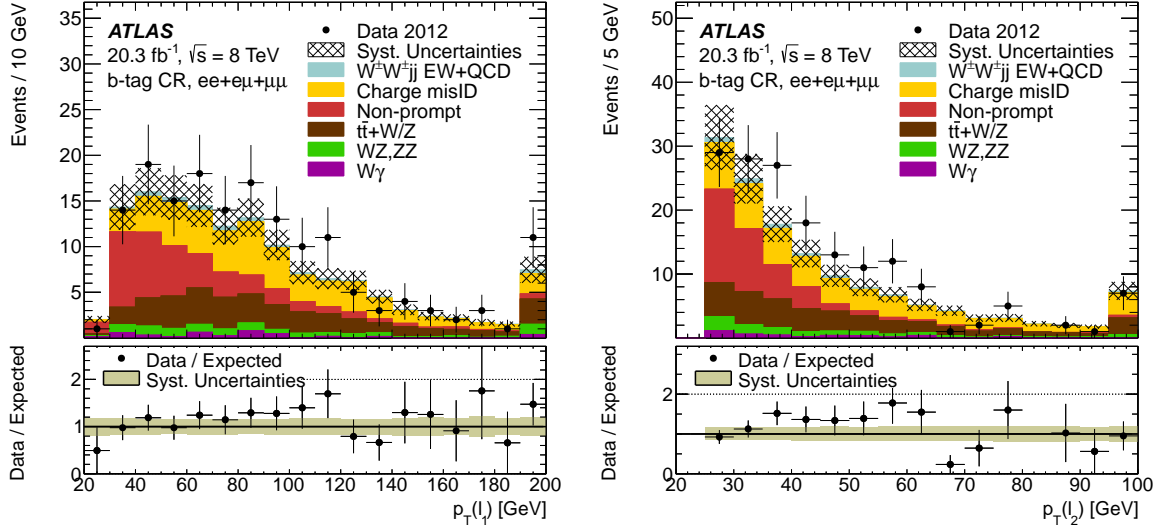


Figure 6: The leading (left) and sub-leading (right) lepton p_T distribution in the b -tag CR. The conversions background has been split into $W\gamma$ events and events with two prompt, opposite-sign (OS) leptons. The error bars on the data points include statistical uncertainty only. The hatched band represents the systematic uncertainty of the total prediction. The lower plot shows the ratio of the data to the expected background where the brown band indicates systematic uncertainty including the MC statistical uncertainty. The last bin includes overflow events.

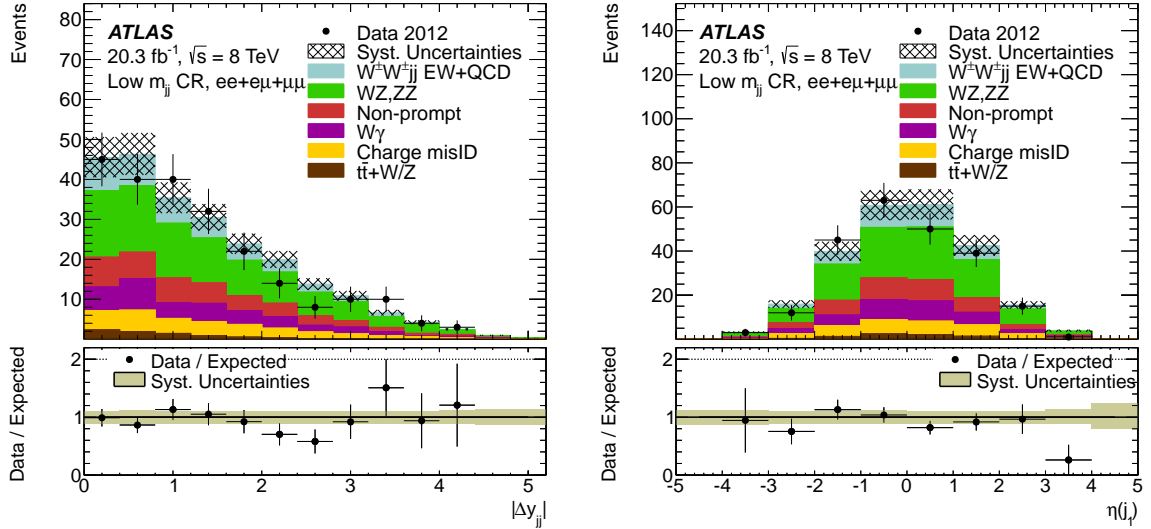


Figure 7: The distribution of the rapidity difference between the two jets with the highest p_T (left) and the distribution of the η of the leading-jet (right) for the sum of events in the $e^\pm e^\pm$, $e^\pm \mu^\pm$, and $\mu^\pm \mu^\pm$ channels for the low- m_{jj} CR. The conversions background has been split into $W\gamma$ events and events with two prompt OS leptons. The error bars on the data points include statistical uncertainty only. The hatched band represents the systematic uncertainty of the total prediction. The lower plot shows the ratio of the data to the expected background where the brown band indicates systematic uncertainty including the MC statistical uncertainty. The last bin includes overflow events.

6 Systematic uncertainties

Systematic uncertainties in the measured cross sections arise from uncertainties in the physics object reconstruction and identification, the procedures used to correct for detector effects, the background estimation, the usage of theoretical cross-sections for signal and background processes, and luminosity.

The experimental systematic uncertainties affecting the signal and prompt-background estimates include: the uncertainties due to the lepton energy scale, energy resolution, and identification efficiency [40, 71]; the uncertainties due to the jet energy scale and resolution [72]; the uncertainties in the E_T^{miss} calculation from energy deposits not associated with reconstructed objects [45]; and the uncertainties due to b -tagging efficiency and mistag rate [73]. An uncertainty is applied to MC samples to cover differences in efficiency observed between the trigger in data and the MC trigger simulation. The uncertainty in the integrated luminosity is 2.8%, affecting the overall normalization of both the signal and background processes estimated from MC simulation. It is derived following the methodology detailed in Ref. [35].

The uncertainty in the non-prompt-background estimate is between 39% and 52% depending on region and channel. It is dominated by prompt-lepton contamination in the dijet sample used to estimate the fake factors, uncertainty in the extrapolation of fake factors into the signal region, and the statistical uncertainty in the number of “tight+loose” events used to estimate the background.

The dominant systematic uncertainties from the conversion background arise from a possible method bias and the statistical uncertainty in the charge misidentification rate measurement. The total uncertainty in the estimation of the conversion background is found to be between 15% and 32% depending on signal region and lepton flavor.

The dominant theoretical uncertainty in the prompt background estimation comes from the predicted cross-section uncertainties for the $W^\pm Zjj$ -EW and $W^\pm Zjj$ -QCD production. Systematic uncertainties in the $W^\pm Zjj$ -EW background estimation are determined separately for the contribution with and without b -quarks. Uncertainties due to the choice of factorization and renormalization scales and PDF uncertainties are calculated with `VBFNLO`. Parton-shower effects are determined by applying two parton showering algorithms. LO `VBFNLO` events are used, since no NLO events are available. The difference between the `PYTHIA 8` parton-shower model with the AU2 tune for the underlying-event modeling and the `HERWIG` parton shower with `JIMMY` for the underlying-event modeling is used to estimate the parton-shower uncertainty. The same procedures are used to calculate the total NLO cross-sections, scale, PDF, and parton-shower uncertainties for the $W^\pm Zjj$ -QCD production. The $W^\pm Zjj$ -QCD final state also occurs through diagrams with zero or one parton but containing two jets after parton showering. This contribution is included in the `SHERPA` sample and has an additional parton-shower uncertainty. This effect is determined using a dedicated `MADGRAPH` sample with two different parton-shower models. A 52% uncertainty is obtained from this comparison, which results in an uncertainty of 6% in the total $W^\pm Zjj$ -QCD contribution. Other theoretical uncertainties include 30%, 19%, and 17% uncertainties in the predicted cross-sections of the $t\bar{t} + V$, electroweak and strong production of $ZZjj$, and $W\gamma$ processes, respectively.

A summary of the decomposition of the systematic uncertainties in the estimated number of background and signal events for the two SRs is given in Table 7. Most uncertainties do not have an inherent dependence on the flavor of the two leptons, but the size of the contribution to the total background uncertainty does depend on the channel due to differences in the composition of the background between channels. The fractional uncertainties listed are quoted as the effect on the background yield or signal yield in the $e^\pm e^\pm$, $e^\pm \mu^\pm$, and $\mu^\pm \mu^\pm$ channels separately. The largest uncertainty is the jet-related uncertainty for both the signal and background estimations.

Relative Systematic Uncertainties $e^\pm e^\pm/e^\pm \mu^\pm/\mu^\pm \mu^\pm$ [%]					
Background Yield			Signal Yield		
	Inclusive SR	VBS SR		Inclusive SR	VBS SR
Jet-related uncertainties	11/13/13	13/20/20	Jet-related uncertainties	6	5
$W^\pm Z jj$ -EW cross-section	6/8/11	5/5/8	$W^\pm W^\pm jj$ -EW cross-section	5	6
MC sample size	8/6/8	9/6/8	$W^\pm W^\pm jj$ -QCD cross-section	3.1	–
Non-prompt	4/7/7	4/7/7	Luminosity	2.8	2.8
Conversions	6/4/–	6/4/–	MC statistics	4/2.1/2.8	5/2.7/4
$W\gamma$ cross-section	2.8/2.6/–	3.1/2.6/–	E_T^{miss} reconstruction	1.1	1.1
E_T^{miss} reconstruction	2.2/2.4/1.8	2.9/3.2/1.4	Lepton reconstruction and identification	1.9/1.0/0.7	1.9/1.0/0.7
Luminosity	1.7/2.1/2.4	1.7/2.1/2.4	b -tagging efficiency	0.6	0.6
$W^\pm Z jj$ -QCD cross-section	–	0.9/1.5/2.6	Trigger efficiency	0.1/0.3/0.5	0.1/0.3/0.5
Lepton reconstruction and identification	1.6/1.2/1.2	1.7/1.1/1.1			
b -tagging efficiency	1.0/1.1/1.0	0.8/0.9/0.7			
Trigger efficiency	0.1/0.2/0.4	0.1/0.2/0.4			
Total	17/19/21	18/20/21		10/9/9	10/9/9

Table 7: The decomposition of the relative systematic uncertainties in the estimated number of background and signal events for the Inclusive and VBS SRs. The left columns represent the uncertainties of the total background predictions in each channel from the listed source, while the right columns represent the uncertainties of the total signal predictions from each source. Three numbers in the same cell indicate the uncertainties for the $e^\pm e^\pm$, $e^\pm \mu^\pm$ and $\mu^\pm \mu^\pm$ channels, respectively. If only one number is present in a given cell, it means all three channels have the same systematic uncertainty.

7 Events yields in the signal regions

The observed and predicted event yields in the Inclusive and VBS SRs are shown in Tables 8 and 9, broken down by $e^\pm e^\pm$, $e^\pm \mu^\pm$, and $\mu^\pm \mu^\pm$ channels as well as the sum of all three. The observed data events are consistent with the SM predictions including $W^\pm W^\pm jj$ production. Several kinematic distributions are shown in Figures 8–10. The uncertainties displayed are the systematic and statistical uncertainties added in quadrature. All three channels are combined in these plots, and correlations of a given systematic uncertainty with others are maintained across signal and background processes and channels. The contributions from electroweak and strong $W^\pm W^\pm$ production are normalized to the SM predictions. Figure 8 presents the dijet invariant mass distribution for the Inclusive SR before the final $m_{jj} > 500$ GeV selection is applied. Figure 9 presents the $|\Delta y_{jj}|$ distribution for the VBS SR before the $|\Delta y_{jj}| > 2.4$ selection is applied.

The lepton centrality is a measure of how central the leptons are with respect to the jets and is defined by $\zeta = \min[\eta(\ell_2) - \eta(j_2), \eta(j_1) - \eta(\ell_1)]$, where $\ell_{1,2}$ refers to the two leptons and $j_{1,2}$ refers here to the two jets with $\eta(j_1) > \eta(j_2)$, and $\eta(\ell_1) > \eta(\ell_2)$. Events tend to have a lepton centrality greater than zero in the VBS topology. The lepton centrality distribution together with the distribution of the scalar sum of the two leading leptons' transverse momenta in the VBS SR are shown in Figure 10. Good agreement between data and SM predictions with $W^\pm W^\pm jj$ production included is found for all distributions.

The data are also divided into W^+W^+ and W^-W^- channels. The W^+W^+ channel is favored by data and SM prediction as the LHC is a pp collider. These two channels are not split by leptonic final states due to the limited number of events. The event yields are shown in Table 10, and the observed charge distribution in data is found to be consistent with SM predictions.

Inclusive Signal Region				
	$e^\pm e^\pm$	$e^\pm \mu^\pm$	$\mu^\pm \mu^\pm$	Total
$W^\pm W^\pm jj$ -EW	2.82 ± 0.28	7.8 ± 0.7	4.6 ± 0.4	15.2 ± 1.3
$W^\pm W^\pm jj$ -QCD	0.86 ± 0.15	2.3 ± 0.4	1.45 ± 0.24	4.6 ± 0.7
Prompt	3.0 ± 0.7	6.1 ± 1.3	2.6 ± 0.6	11.6 ± 2.5
Conversions	Charge misID	2.1 ± 0.4	0.77 ± 0.27	2.8 ± 0.6
	$W\gamma$	1.1 ± 0.6	1.6 ± 0.8	2.7 ± 1.2
Non-prompt	0.61 ± 0.30	1.9 ± 0.8	0.41 ± 0.22	2.9 ± 0.8
Total predicted	10.4 ± 1.3	20.3 ± 2.5	9.1 ± 1.0	40 ± 4
Data	12	26	12	50

Table 8: Predicted and observed numbers of events in the inclusive SR are shown separately for the $e^\pm e^\pm$, $e^\pm \mu^\pm$, and $\mu^\pm \mu^\pm$ channels as well as for the sum of all three. The uncertainty is the combination of statistical and systematic uncertainties; correlations among systematic uncertainties are taken into account in the calculations of the total. The contributions from $W^\pm W^\pm jj$ -EW and $W^\pm W^\pm jj$ -QCD production are normalized to the SM prediction.

VBS Signal Region				
	$e^\pm e^\pm$	$e^\pm \mu^\pm$	$\mu^\pm \mu^\pm$	Total
$W^\pm W^\pm jj$ -EW	2.34 ± 0.23	6.3 ± 0.6	3.77 ± 0.35	12.4 ± 1.1
$W^\pm W^\pm jj$ -QCD	0.26 ± 0.06	0.67 ± 0.14	0.43 ± 0.09	1.36 ± 0.27
Prompt	2.2 ± 0.5	4.2 ± 1.0	1.9 ± 0.5	8.2 ± 1.9
Conversions	Charge misID	1.39 ± 0.27	0.64 ± 0.24	2.0 ± 0.5
	$W\gamma$	0.7 ± 0.4	1.3 ± 0.7	2.0 ± 1.0
Non-prompt	0.50 ± 0.26	1.5 ± 0.6	0.34 ± 0.19	2.3 ± 0.7
Total predicted	7.4 ± 1.0	14.5 ± 1.9	6.4 ± 0.7	28.3 ± 3.4
Data	6	18	10	34

Table 9: Predicted and observed numbers of events in the VBS SR are shown separately for the $e^\pm e^\pm$, $e^\pm \mu^\pm$, and $\mu^\pm \mu^\pm$ channels as well as for the sum of all three. The uncertainty is the combination of statistical and systematic uncertainties; correlations among systematic uncertainties are taken into account in the calculations of the total. The contributions from $W^\pm W^\pm jj$ -EW and $W^\pm W^\pm jj$ -QCD production are normalized to the SM prediction.

	Inclusive Signal Region		VBS Signal Region	
	$W^+ W^+$	$W^- W^-$	$W^+ W^+$	$W^- W^-$
$W^\pm W^\pm jj$ -EW	13.0 ± 1.2	3.9 ± 0.4	9.4 ± 0.8	2.90 ± 0.27
$W^\pm W^\pm jj$ -QCD	3.6 ± 0.6	1.14 ± 0.19	1.08 ± 0.21	0.26 ± 0.06
Prompt	8.0 ± 1.7	3.7 ± 0.8	6.0 ± 1.4	2.2 ± 0.6
Conversions	Charge misID	1.27 ± 0.28	1.57 ± 0.35	1.13 ± 0.28
	$W\gamma$	1.7 ± 0.8	1.0 ± 0.6	0.6 ± 0.4
Non-prompt	1.7 ± 0.5	1.2 ± 0.4	1.4 ± 0.4	0.95 ± 0.33
Total predicted	29.3 ± 3.3	12.5 ± 1.6	20.2 ± 2.5	8.1 ± 1.4
Data	35	15	23	11

Table 10: Event yields for predicted signal and background events as well as observed data in the VBS SR for the $W^+ W^+$ and $W^- W^-$ channels. The uncertainty is the combination of statistical and systematic uncertainties; correlations among systematic uncertainties are taken into account in the calculations of the total.

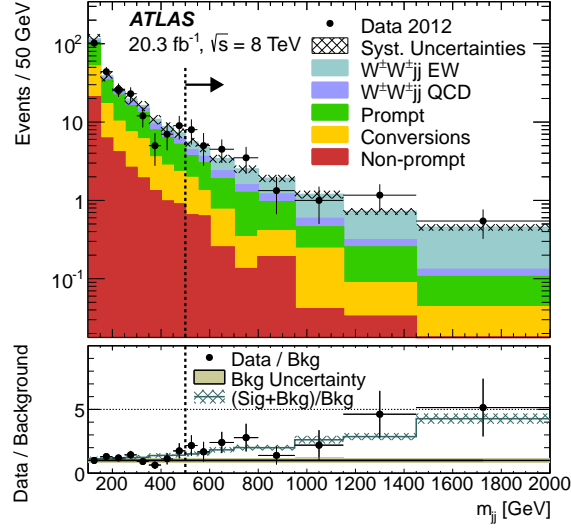


Figure 8: The m_{jj} distribution for the combined channels in the Inclusive SR prior to applying the requirement that $m_{jj} > 500$ GeV. The error bars on the data points represent statistical uncertainty only. The hatched band represents the systematic uncertainty of the total prediction. The lower plot shows the ratio of the data to the expected background where the brown band indicates systematic uncertainty including the MC statistical uncertainty. The ratio of the sum of the expected signal ($W^\pm W^\pm jj$ -EW and $W^\pm W^\pm jj$ -QCD) and background to the expected background is also shown.

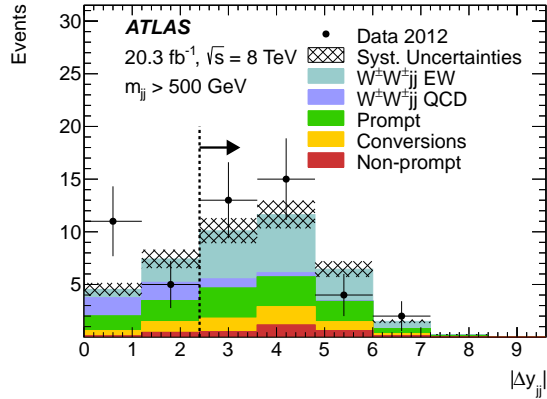


Figure 9: The rapidity difference distribution between the two jets with the highest p_T in the Inclusive SR for the combined channels. The region with $|\Delta y_{jj}| > 2.4$ denoted by the vertical dotted line indicates the VBS SR. The error bars on the data points include statistical uncertainty only. The hatched band represents the systematic uncertainty of the total prediction. The contributions from $W^\pm W^\pm jj$ -EW and $W^\pm W^\pm jj$ -QCD production are normalized to the SM prediction.

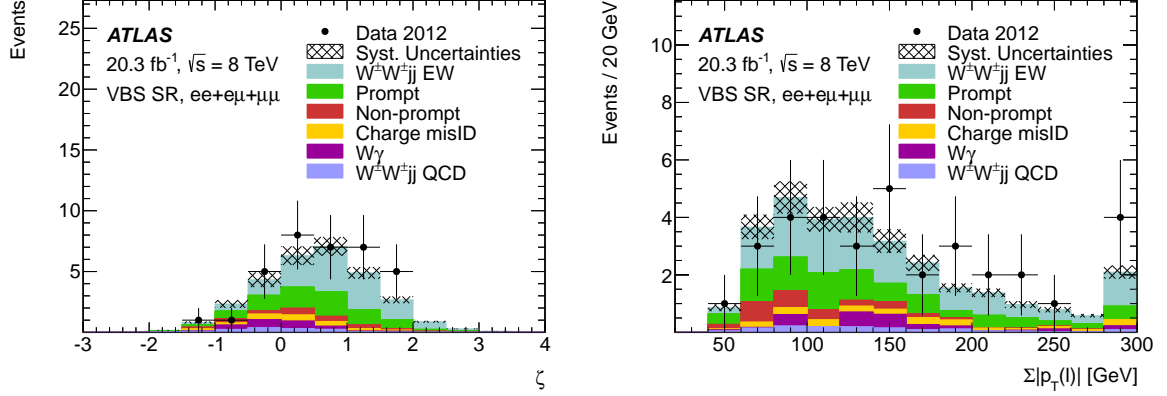


Figure 10: The lepton centrality (ζ) distribution (left) and the scalar sum of the two leading leptons' transverse momenta (right) for all channels combined in the VBS SR. The error bars on the data points include statistical uncertainty only. The hatched band represents the systematic uncertainty of the total prediction. The last bin includes overflow events.

8 Extraction of production cross sections

The excesses in data over the background-only predictions in the Inclusive and VBS SRs are consistent with the event topology for $W^\pm W^\pm jj$ production. The numbers of observed data and expected signal and background events are used to calculate the fiducial cross-sections in these two signal regions.

Cross-section extraction method

A likelihood function is used to extract the cross-sections in the two fiducial regions. The likelihood function uses Poisson distributions for each channel and global constraints for the nuisance parameters θ_j , which parameterize effects of systematic uncertainties. The number of expected events in a given decay channel c , N_c^{exp} , is a product of the integrated luminosity \mathcal{L} , the measured fiducial cross-section $\sigma_{W^\pm W^\pm jj}$, the relative acceptance for each channel, A_c , and the signal efficiency ϵ_c , in addition to the total number of background events in this channel, $\sum_b N_{c,b}$:

$$N_c^{\text{exp}} = \mathcal{L} \cdot \sigma_{W^\pm W^\pm jj} \cdot A_c \cdot \epsilon_c + \sum_b N_{c,b}. \quad (6)$$

The likelihood function is given by

$$L = \prod_c \text{Pois}(N_c^{\text{obs}} | N_c^{\text{exp}}) \prod_j g(0 | \theta_j, 1). \quad (7)$$

The function g is a Gaussian probability density function. The effect due to systematic uncertainties in ϵ_c and $N_{c,b}$ are parameterized by the nuisance parameters according to

$$\varepsilon_c(\theta_j) = \varepsilon_c^0 \prod_j (1 + \theta_j \delta_{c,j}^s), \quad (8)$$

$$N_{c,b}(\theta_j) = N_{c,b}^0 \prod_j (1 + \theta_j \delta_{c,j}^b) \quad (9)$$

with ε_c^0 and $N_{c,b}^0$ being the nominal estimates for the signal reconstruction efficiency and the background yields in channel c . The constants $\delta_{c,j}^s$ and $\delta_{c,j}^b$ represent the relative uncertainty in the signal reconstruction efficiency and the nominal background prediction, respectively, in channel c due to the source of systematic uncertainty, j .

The relative acceptances within the fiducial region are determined at particle level from the decay branching ratios of the two W bosons to $e^\pm e^\pm$, $e^\pm \mu^\pm$, and $\mu^\pm \mu^\pm$. Small deviations arise from the jet object definition at particle level, which accepts electrons as input objects to the jet clustering algorithm while muons are ignored. The acceptances in the corresponding channels are 0.232, 0.524, and 0.265 in the Inclusive SR and 0.235, 0.527, and 0.257 in the VBS SR, respectively.

The signal efficiency for channel c , ε_c , is estimated from simulated signal events. It is given by the number of events reconstructed in a given signal region divided by the number of events passing the corresponding definition of the fiducial phase-space region at the particle level. It accounts for the detector reconstruction, particle identification, and trigger efficiency as well as for the migration into and out of the fiducial volume due to detector resolution effects. The signal efficiency definition includes contributions from leptons originating from τ decays at the reconstruction level, while those events are vetoed at the particle level. The fraction of events where the electron or muon originates from a τ lepton in the signal yield at the reconstruction level is found to be 10%. The efficiencies in the $e^\pm e^\pm$, $e^\pm \mu^\pm$, and $\mu^\pm \mu^\pm$ channels are $(56.2 \pm 1.5)\%$, $(71.7 \pm 0.8)\%$, and $(77.0 \pm 0.9)\%$ in the Inclusive signal region and $(57.2 \pm 1.6)\%$, $(72.7 \pm 1.0)\%$, and $(82.7 \pm 1.2)\%$ in the VBS signal region, respectively.

The measured cross-sections are taken as those maximizing the log-likelihood function shown in Eq. (7). The quoted uncertainties are derived using the profile likelihood method [74] and correspond to likelihood intervals with a confidence level (CL) of 68.3%.

Measured fiducial cross-sections

The measured fiducial cross-section is $\sigma_{\text{Incl. } W^\pm W^\pm jj}^{\text{fid}} = 2.3 \pm 0.6(\text{stat}) \pm 0.3(\text{syst})$ fb for the $W^\pm W^\pm jj$ production, including both electroweak and strong production as well as the interference in the Inclusive SR. The measured fiducial cross-section is $\sigma_{\text{EW } W^\pm W^\pm jj}^{\text{fid}} = 1.5 \pm 0.5(\text{stat}) \pm 0.2(\text{syst})$ fb for electroweak $W^\pm W^\pm$ production, including interference with strong production in the VBS region. The measured cross-sections are in agreement with the respective SM predictions of 1.52 ± 0.11 fb and 0.95 ± 0.06 fb. The cross-sections are shown in Figure 11 for each channel and for the combined measurement. These results are shown numerically in Table 11. The observed combined significance over the background-only hypothesis is 4.5σ in the Inclusive SR and 3.6σ in the VBS SR, while the corresponding expected significances for a SM $W^\pm W^\pm jj$ signal are 3.1σ and 2.3σ , respectively.

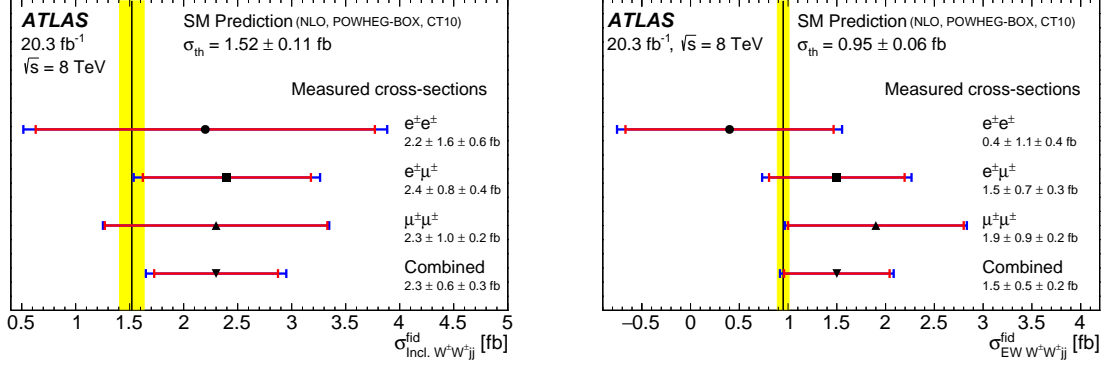


Figure 11: The measured cross-sections for the Inclusive SR (left) and the VBS SR (right) compared to the predictions for each channel and for the combined measurement. The inner error band represents the statistical uncertainty and the outer band represents the total uncertainty of each measurement.

9 Extraction of anomalous quartic gauge couplings

VBS events receive contributions from quartic gauge boson interactions and thus can be used to search for aQGCs. In general, the effective Lagrangian described in Section 1 does not ensure unitarity. The Higgs boson in the SM ensures unitarity of the SM VBS process, which is destroyed if anomalous couplings or additional resonances are added. A unitarization scheme has to be applied in order to avoid non-physical predictions. In the case of VBS with aQGC, the unitarization significantly impacts the differential and total cross-sections. The K-matrix unitarization scheme [17] is applied in this analysis where the elastic scattering eigen-amplitude $\mathcal{A}(s)$ is projected on the Argand circle $\mathcal{A}(s) \rightarrow \hat{\mathcal{A}}(s)$ such that $|\hat{\mathcal{A}}(s) - i/2| = 1/2$. This condition is derived from the optical theorem and ensures that the projected scattering amplitude meets the unitarity condition exactly. As a result, the cross-section saturates at the maximum value allowed by unitarity. The WHIZARD [75] event generator is used to calculate cross-sections and generate events with aQGCs at LO in QCD. The CTEQ6L1 PDF set is used. All samples use the parameterization in terms of α_4 and α_5 . The invariant mass of the system of two charged leptons and two neutrinos from the decay of the two W bosons, $m_{\ell\ell\nu\nu}$, is used as the renormalization and factorization scales, $\mu_R = \mu_F = m_{\ell\ell\nu\nu}$. The events are interfaced to PYTHIA 8 for modeling the parton shower, QED final-state radiation, decays of τ leptons, and the underlying event.

The expected sensitivity to α_4 and α_5 is improved significantly compared to the results obtained in the previous publication [29] by selecting a phase-space region that is more sensitive to anomalous contributions to the $WWWW$ vertex. This is achieved by an additional requirement: $m_{WW,T} > 400$ GeV. The effects from new-physics processes are expected to be seen predominantly at larger mass scales, which

	$e^\pm e^\pm$	$e^\pm \mu^\pm$	$\mu^\pm \mu^\pm$	Combined	SM prediction
$\sigma_{\text{Incl. } W^\pm W^\pm jj}^{\text{fid}}$ [fb]	$2.2 \pm 1.6 \pm 0.6$	$2.4 \pm 0.8 \pm 0.4$	$2.3 \pm 1.0 \pm 0.2$	$2.3 \pm 0.6 \pm 0.3$	1.52 ± 0.11
$\sigma_{\text{EW } W^\pm W^\pm jj}^{\text{fid}}$ [fb]	$0.4 \pm 1.1 \pm 0.4$	$1.5 \pm 0.7 \pm 0.3$	$1.9 \pm 0.9 \pm 0.2$	$1.5 \pm 0.5 \pm 0.2$	0.95 ± 0.06

Table 11: Measured fiducial cross-sections for the Inclusive and VBS SRs for each channel and for the combined measurement. The first uncertainty is statistical and the second is systematic.

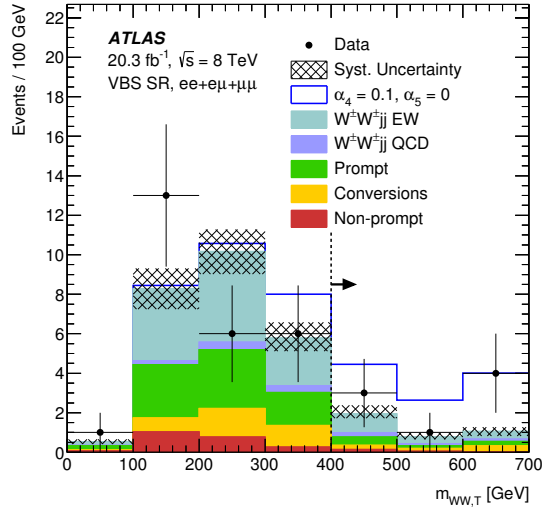


Figure 12: The $m_{WW,T}$ distribution for all channels combined in the VBS SR prior to applying the requirement of $m_{WW,T} > 400$ GeV. The $m_{WW,T}$ requirement is represented by a vertically dashed line. The expected signal contribution for the aQGC parameter point $\alpha_4 = 0.1$ and $\alpha_5 = 0$ is overlaid as a histogram and includes the aQGC signal and the background prediction. The error bars on the data points include statistical uncertainty only. The hatched band represents the systematic uncertainty of the total prediction. The last bin includes overflow events.

motivates the definition of the aQGC SR as defined in Section 3. The distribution of the transverse mass of the WW system before applying the final selection criteria is shown in Figure 12.

The signal in the aQGC region is defined as the α_4, α_5 -dependent excess of the $W^\pm W^\pm jj$ -EW production cross-section over the SM prediction of this process. No interference effects of the aQGC contribution with either the SM $W^\pm W^\pm jj$ -QCD or $W^\pm W^\pm jj$ -EW production are considered. The combined signal reconstruction efficiency in the three final states is found to be $(68.7 \pm 2.2)\%$ with no significant dependence on α_4 and α_5 .

Table 12 summarizes the expected and observed event yields in the aQGC SR. The theoretical uncertainties in the aQGC signal region are less than in the VBS region and the systematic uncertainties are consistent with those in the VBS signal region. Therefore, the VBS signal region systematic uncertainties as described in Section 6 are applied. A total of 3.8 ± 0.6 events are expected from SM background processes. The expected number of additional events for the aQGC parameter point $\alpha_4 = 0.1$ and $\alpha_5 = 0$ is also shown. In total 8 events are observed in data, which corresponds to an excess with a significance of 1.8σ .

A CL_s upper limit [76] on the visible cross-section in the aQGC SR is reported. The visible cross-section σ^{vis} is defined at the detector level as the excess of data events (N^{obs}) over the background prediction (N^{bkg}) divided by the integrated luminosity:

$$\sigma^{\text{vis}} = \frac{N^{\text{obs}} - N^{\text{bkg}}}{\mathcal{L}}. \quad (10)$$

The CL_s upper limit is derived with a likelihood function equivalent to the one defined in Eq. (7) for a single channel by replacing $\sigma_{W^\pm W^\pm jj} \cdot A_c \cdot \varepsilon_c$ with σ^{vis} in Eq. (6) where σ^{vis} is affected by uncertainties in

	aQGC Signal Region
Non-prompt	$0.2 \pm 0.1 \pm 0.1$
Conversions	$0.7 \pm 0.2 \pm 0.1$
Prompt	$0.8 \pm 0.1 \pm 0.3$
SM $W^\pm W^\pm jj$ -EW	$1.7 \pm 0.1 \pm 0.2$
SM $W^\pm W^\pm jj$ -QCD	$0.4 \pm 0.0 \pm 0.1$
Total background	$3.8 \pm 0.3 \pm 0.5$
$\alpha_4 = 0.1, \alpha_5 = 0$	$7.3 \pm 0.4 \pm 0.6$
Data	8

Table 12: Expected and observed event yields in the aQGC SR. The first quoted uncertainty is statistical and the second is systematic. The row corresponding to the BSM contribution indicates the additional events expected given $\alpha_4 = 0.1$ and $\alpha_5 = 0$.

the background prediction and the integrated luminosity, but not by reconstruction efficiencies or uncertainties in the theoretical cross-sections of the SM $W^\pm W^\pm jj$ production. The observed (expected) 95% CL upper limit on σ^{vis} in the aQGC SR is 0.50 fb (0.25 fb). These limits are converted to upper limits on the fiducial cross-section, assuming the same signal reconstruction efficiency as that of the $W^\pm W^\pm jj$ -EW production. Models predicting contributions to the aQGC fiducial phase-space region at the particle level of more than 0.72 fb (0.37 fb) are excluded at the 95% CL.

The upper limits on the fiducial cross-section in the aQGC phase-space region at the particle level are used to derive constraints in the (α_4, α_5) parameter space. The expected and observed two-dimensional exclusion contours are shown in Figure 13. The expected one-dimensional confidence intervals at the 95% CL are

$$\alpha_4 \in [-0.06, 0.07], \text{ and } \alpha_5 \in [-0.10, 0.11] \text{ (expected) .}$$

The observed one-dimensional confidence intervals at the 95% CL are

$$\alpha_4 \in [-0.14, 0.15], \text{ and } \alpha_5 \in [-0.22, 0.22] \text{ (observed) .}$$

This result constitutes a 35% improvement in the expected aQGC sensitivity with respect to the analysis published in Ref. [29]. The observed exclusion is only marginally more restrictive because of the small excess observed in the aQGC signal region. The sensitivity is similar to that in Ref. [32], where the observed results are more constraining.

10 Summary

This paper presents results from the ATLAS detector at the LHC using 20.3 fb^{-1} of proton–proton collision data at $\sqrt{s} = 8 \text{ TeV}$ from the measurement of the $W^\pm W^\pm jj$ production cross-sections. Events with two leptons (electrons or muons) with the same electric charge, E_T^{miss} , and at least two jets are investigated in the Inclusive signal region. An additional selection on the rapidity difference of the leading jets is used to measure the fiducial cross-section for the $W^\pm W^\pm jj$ -EW production in the VBS signal region.

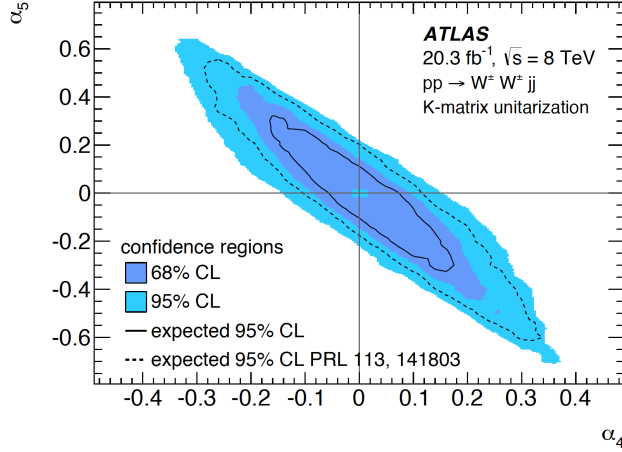


Figure 13: Two-dimensional confidence regions in the aQGC parameter plane (α_4, α_5). The area outside the solid light blue region is excluded by the data at the 95% CL. The area outside the solid dark blue region is excluded at the 68% CL. The expected exclusion contour at the 95% CL is marked by the solid black line. For comparison, the expected exclusion contour at the 95% CL from the previous analysis of this final state [29] is shown as a black dashed line.

The further requirement of a high transverse mass of the system of two leptons and E_T^{miss} is used to define a restricted phase-space region more sensitive to aQGC parameters.

In the Inclusive signal region, a total of 50 signal candidates are observed and 20 background events are expected. The excess of events over the background-only prediction is interpreted as evidence for the sum of the $W^\pm W^\pm jj$ -EW and $W^\pm W^\pm jj$ -QCD processes. The measured fiducial cross-section for $W^\pm W^\pm jj$ production is $2.3 \pm 0.6(\text{stat.}) \pm 0.3(\text{syst.})$ fb, with a significance of 4.5σ (3.1σ expected). In the VBS signal region, the background-only prediction includes the $W^\pm W^\pm jj$ -QCD production, and a total of 34 events are observed and 16 background events are predicted. The excess is interpreted as evidence for the $W^\pm W^\pm jj$ -EW processes. The measured fiducial cross-section for the $W^\pm W^\pm jj$ -EW production, including the interference with the $W^\pm W^\pm jj$ -QCD production, is $1.5 \pm 0.5(\text{stat.}) \pm 0.2(\text{syst.})$ fb with a significance of 3.6σ (2.3σ expected). The measured cross-sections are consistent with the SM predictions.

In the aQGC signal region, the background prediction includes both the $W^\pm W^\pm jj$ -EW and $W^\pm W^\pm jj$ -QCD processes. A total of 8 events are observed and 3.8 background events are expected. These numbers are used to constrain the aQGC parameters α_4 and α_5 . The observed one-dimensional 95% confidence level intervals are $-0.14 < \alpha_4 < 0.15$ and $-0.22 < \alpha_5 < 0.22$. The expected 95% confidence level intervals are $-0.06 < \alpha_4 < 0.07$ and $-0.10 < \alpha_5 < 0.11$. These intervals constitute a 35% improvement in the expected aQGC sensitivity with respect to the analysis published in Ref. [29].

Acknowledgments

We thank CERN for the very successful operation of the LHC, as well as the support staff from our institutions without whom ATLAS could not be operated efficiently.

We acknowledge the support of ANPCyT, Argentina; YerPhI, Armenia; ARC, Australia; BMWFW and FWF, Austria; ANAS, Azerbaijan; SSTC, Belarus; CNPq and FAPESP, Brazil; NSERC, NRC and CFI,

Canada; CERN; CONICYT, Chile; CAS, MOST and NSFC, China; COLCIENCIAS, Colombia; MSMT CR, MPO CR and VSC CR, Czech Republic; DNRF and DNSRC, Denmark; IN2P3-CNRS, CEA-DSM/IRFU, France; GNSF, Georgia; BMBF, HGF, and MPG, Germany; GSRT, Greece; RGC, Hong Kong SAR, China; ISF, I-CORE and Benozziyo Center, Israel; INFN, Italy; MEXT and JSPS, Japan; CNRST, Morocco; FOM and NWO, Netherlands; RCN, Norway; MNiSW and NCN, Poland; FCT, Portugal; MNE/IFA, Romania; MES of Russia and NRC KI, Russian Federation; JINR; MESTD, Serbia; MSSR, Slovakia; ARRS and MIZŠ, Slovenia; DST/NRF, South Africa; MINECO, Spain; SRC and Wallenberg Foundation, Sweden; SERI, SNSF and Cantons of Bern and Geneva, Switzerland; MOST, Taiwan; TAEK, Turkey; STFC, United Kingdom; DOE and NSF, United States of America. In addition, individual groups and members have received support from BCKDF, the Canada Council, CANARIE, CRC, Compute Canada, FQRNT, and the Ontario Innovation Trust, Canada; EPLANET, ERC, FP7, Horizon 2020 and Marie Skłodowska-Curie Actions, European Union; Investissements d’Avenir Labex and IDEX, ANR, Région Auvergne and Fondation Partager le Savoir, France; DFG and AvH Foundation, Germany; Herakleitos, Thales and Aristeia programmes co-financed by EU-ESF and the Greek NSRF; BSF, GIF and Minerva, Israel; BRF, Norway; Generalitat de Catalunya, Generalitat Valenciana, Spain; the Royal Society and Leverhulme Trust, United Kingdom.

The crucial computing support from all WLCG partners is acknowledged gratefully, in particular from CERN, the ATLAS Tier-1 facilities at TRIUMF (Canada), NDGF (Denmark, Norway, Sweden), CC-IN2P3 (France), KIT/GridKA (Germany), INFN-CNAF (Italy), NL-T1 (Netherlands), PIC (Spain), ASGC (Taiwan), RAL (UK) and BNL (USA), the Tier-2 facilities worldwide and large non-WLCG resource providers. Major contributors of computing resources are listed in Ref. [77].

References

- [1] V. D. Barger et al., *Strong W^+W^+ scattering signals at pp supercolliders*, [Phys. Rev. D **42** \(1990\) 3052](#).
- [2] J. Bagger et al., *Strongly interacting WW system: Gold-plated modes*, [Phys. Rev. D **49** \(1994\) 1246](#).
- [3] J. Bagger et al., *CERN LHC analysis of the strongly interacting WW system: Gold-plated modes*, [Phys. Rev. D **52** \(1995\) 3878](#).
- [4] M. J. G. Veltman, *Second Threshold in Weak Interactions*, *Acta Phys. Polon. B* **8** (1977) 475.
- [5] B. W. Lee, C. Quigg, and H. B. Thacker, *Strength of weak interactions at very high energies and the Higgs boson mass*, [Phys. Rev. Lett. **38** \(1977\) 883](#).
- [6] B. W. Lee, C. Quigg, and H. B. Thacker, *Weak interactions at very high energies: The role of the Higgs-boson mass*, [Phys. Rev. D **16** \(1977\) 1519](#).
- [7] D. Espriu and B. Yencho, *Longitudinal WW scattering in light of the “Higgs boson” discovery*, [Phys. Rev. D **87** \(2013\) 055017](#), arXiv:1212.4158.
- [8] J. Chang et al., *WW scattering in the era of post-Higgs-boson discovery*, [Phys. Rev. D **87** \(2013\) 093005](#), arXiv:1303.6335.

- [9] ATLAS Collaboration, *Observation of a new particle in the search for the Standard Model Higgs boson with the ATLAS detector at the LHC*, *Phys. Lett. B* **716** (2012) 1, arXiv:1207.7214.
- [10] CMS Collaboration, *Observation of a new boson at a mass of 125 GeV with the CMS experiment at the LHC*, *Phys. Lett. B* **716** (2012) 30, arXiv:1207.7235.
- [11] E. Accomando et al., *Boson-boson scattering and Higgs production at the LHC from a six fermion point of view: Four jets + $\ell\nu$ processes at $O(\alpha_{\text{em}}^6)$* , *JHEP* **03** (2006) 093, arXiv:hep-ph/0512219.
- [12] B. Zhu et al., *Same sign WW scattering process as a probe of Higgs boson in pp collision at $\sqrt{s} = 10$ TeV*, *Eur. Phys. J. C* **71** (2011) 1514, arXiv:1010.5848.
- [13] M. Szleper, *The Higgs boson and the physics of WW scattering before and after Higgs discovery*, (2014), arXiv:1412.8367.
- [14] T. Appelquist and C. W. Bernard, *Strongly Interacting Higgs Bosons*, *Phys. Rev. D* **22** (1980) 200.
- [15] A. C. Longhitano, *Heavy Higgs bosons in the Weinberg-Salam model*, *Phys. Rev. D* **22** (1980) 1166.
- [16] W. Kilian, *Electroweak symmetry breaking: The bottom-up approach*, *Springer Tracts Mod. Phys.* **198** (2003) 1.
- [17] A. Alboteanu, W. Kilian, and J. Reuter, *Resonances and Unitarity in Weak Boson Scattering at the LHC*, *JHEP* **11** (2008) 010, arXiv:0806.4145.
- [18] M. Baak et al., *Working Group Report: Precision Study of Electroweak Interactions*, (2013), arXiv:1310.6708.
- [19] J. Reuter, W. Kilian, and M. Sekulla, *Simplified Models for New Physics in Vector Boson Scattering - Input for Snowmass 2013*, (2013), arXiv:1307.8170.
- [20] OPAL Collaboration, G. Abbiendi, et al., *Constraints on anomalous quartic gauge boson couplings from $\nu\bar{\nu}\gamma\gamma$ and $q\bar{q}\gamma\gamma$ events at CERN LEP2*, *Phys. Rev. D* **70** (2004) 032005.
- [21] OPAL Collaboration, G. Abbiendi, et al., *A Study of $W^+W^-\gamma$ events at LEP*, *Phys. Lett. B* **580** (2004) 17, arXiv:hep-ex/0309013.
- [22] DELPHI Collaboration, J. Abdallah, et al., *Measurement of the $e^+e^- \rightarrow W^+W^-\gamma$ cross-section and limits on anomalous quartic gauge couplings with DELPHI*, *The European Physical Journal C - Particles and Fields* **31** (2003) 139–147.
- [23] L3 Collaboration, P. Achard, et al., *Study of the $W^+W^-\gamma$ process and limits on anomalous quartic gauge boson couplings at LEP*, *Phys. Lett. B* **527** (2002) 29–38, arXiv:hep-ex/0111029.
- [24] D0 Collaboration, V. M. Abazov, et al., *Search for anomalous quartic WW $\gamma\gamma$ couplings in dielectron and missing energy final states in $p\bar{p}$ collisions at $\sqrt{s} = 1.96$ TeV*, *Phys. Rev. D* **88** (2013) 012005, arXiv:1305.1258.
- [25] CMS Collaboration, *Measurement of the sum of WW and WZ production with W+di-jet events in pp collisions at $\sqrt{s} = 7$ TeV*, *Eur. Phys. J. C* **73** (2013) 2283, arXiv:1210.7544.

- [26] CMS Collaboration, *Evidence for exclusive $\gamma\gamma \rightarrow W^+W^-$ production and constraints on anomalous quartic gauge couplings at $\sqrt{s} = 7$ and 8 TeV*, (2016), arXiv:[1604.04464](#).
- [27] ATLAS Collaboration, *Measurement of exclusive $\gamma\gamma \rightarrow W^+W^-$ production and search for exclusive Higgs boson production in pp collisions at $\sqrt{s} = 8$ TeV using the ATLAS detector*, (2016), arXiv:[1607.03745](#).
- [28] ATLAS Collaboration, *Evidence of $W\gamma\gamma$ production in pp collisions at $\sqrt{s} = 8$ TeV and limits on anomalous Quartic Gauge Couplings with the ATLAS detector*, *Phys. Rev. Lett.* **115** (2015) 031802, arXiv:[1503.03243](#).
- [29] ATLAS Collaboration, *Evidence for Electroweak Production of $W^\pm W^\pm jj$ in pp Collisions at $\sqrt{s} = 8$ TeV with the ATLAS Detector*, *Phys. Rev. Lett.* **113** (2014) 141803, arXiv:[1405.6241](#).
- [30] CMS Collaboration, *Study of vector boson scattering and search for new physics in events with two same-sign leptons and two jets*, *Phys. Rev. Lett.* **114** (2015) 051801, arXiv:[1410.6315](#).
- [31] ATLAS Collaboration, *Measurements of $W^\pm Z$ production cross sections in pp collisions at $\sqrt{s} = 8$ TeV with the ATLAS detector and limits on anomalous gauge boson self-couplings*, *Phys. Rev. D* **93** (2016) 092004, arXiv:[1603.02151](#).
- [32] ATLAS Collaboration, *Search for anomalous electroweak production of WW/WZ in association with a high-mass dijet system in pp collisions at $\sqrt{s}=8$ TeV with the ATLAS detector*, Submitted to *Phys. Rev. D* (2016), arXiv:[1609.05122](#).
- [33] ATLAS Collaboration, *Search for triboson $W \pm W \pm W^\mp$ production in pp collisions at $\sqrt{s}=8$ TeV with the ATLAS detector*, Submitted to *Eur. Phys. C* (2016), arXiv:[1610.05088](#).
- [34] ATLAS Collaboration, *The ATLAS Experiment at the CERN Large Hadron Collider*, *JINST* **3** (2008) S08003.
- [35] ATLAS Collaboration, *Improved luminosity determination in pp collisions at $\sqrt{s} = 7$ TeV using the ATLAS detector at the LHC*, *Eur. Phys. J. C* **73** (2013) 2518, arXiv:[1302.4393](#).
- [36] ATLAS Collaboration, *Performance of primary vertex reconstruction in proton-proton collisions at $\sqrt{s} = 7$ TeV in the ATLAS experiment*, ATLAS-CONF-2010-069 (2010), URL: <http://cds.cern.ch/record/1281344>.
- [37] ATLAS Collaboration, *Electron reconstruction and identification efficiency measurements with the ATLAS detector using the 2011 LHC proton-proton collision data*, *Eur. Phys. J. C* **74** (2014) 2941, arXiv:[1404.2240](#).
- [38] ATLAS Collaboration, *Electron performance measurements with the ATLAS detector using the 2010 LHC proton-proton collision data*, *Eur. Phys. J. C* **72** (2012) 1909, arXiv:[1110.3174](#).
- [39] ATLAS Collaboration, *Electron efficiency measurements with the ATLAS detector using the 2012 LHC proton-proton collision data*, ATLAS-CONF-2014-032 (2014), URL: <http://cds.cern.ch/record/1706245>.
- [40] ATLAS Collaboration, *Measurement of the muon reconstruction performance of the ATLAS detector using 2011 and 2012 LHC proton-proton collision data*, *Eur. Phys. J. C* **74** (2014) 3130, arXiv:[1407.3935](#).
- [41] M. Cacciari, G. P. Salam, and G. Soyez, *The anti- k_t jet clustering algorithm*, *JHEP* **04** (2008) 063, arXiv:[0802.1189](#).

- [42] ATLAS Collaboration, *Jet energy measurement with the ATLAS detector in proton-proton collisions at $\sqrt{s} = 7$ TeV*, *Eur. Phys. J. C* **73** (2013) 2304, arXiv:1112.6426.
- [43] ATLAS Collaboration, *Tagging and suppression of pileup jets with the ATLAS detector*, ATLAS-CONF-2014-018 (2014), URL: <http://cds.cern.ch/record/1700870>.
- [44] ATLAS Collaboration, *Performance of b-jet identification in the ATLAS experiment*, *JINST* **11** (2016) P04008, arXiv:1512.01094.
- [45] ATLAS Collaboration, *Performance of missing transverse momentum reconstruction in proton-proton collisions at 7 TeV with ATLAS*, *Eur. Phys. J. C* **72** (2012) 1844, arXiv:1108.5602.
- [46] K. A. Olive et al., *Review of particle physics*, *Chin. Phys. C* **38** (2014) 090001.
- [47] ATLAS Collaboration, *The ATLAS simulation infrastructure*, *Eur. Phys. J. C* **70** (2010) 823, arXiv:1005.4568.
- [48] S. Agostinelli et al., *GEANT4: A Simulation toolkit*, *Nucl. Instrum. Meth. A* **506** (2003) 250–303.
- [49] T. Sjöstrand, S. Mrenna, and P. Z. Skands, *PYTHIA 6.4 physics and manual*, *JHEP* **05** (2006) 026, arXiv:hep-ph/0603175.
- [50] T. Sjöstrand, S. Mrenna, and P. Z. Skands, *A Brief Introduction to PYTHIA 8.1*, *Comput. Phys. Commun.* **178** (2008) 852, arXiv:0710.3820.
- [51] T. Gleisberg et al., *Event generation with SHERPA 1.1*, *JHEP* **02** (2009) 007, arXiv:0811.4622.
- [52] S. Catani et al., *QCD matrix elements + parton showers*, *JHEP* **11** (2001) 063, arXiv:hep-ph/0109231.
- [53] H.-L. Lai et al., *New parton distributions for collider physics*, *Phys. Rev. D* **82** (2010) 074024, arXiv:1007.2241.
- [54] P. Nason, *A New method for combining NLO QCD with shower Monte Carlo algorithms*, *JHEP* **11** (2004) 040, arXiv:hep-ph/0409146.
- [55] S. Frixione, P. Nason, and C. Oleari, *Matching NLO QCD computations with parton shower simulations: the POWHEG method*, *JHEP* **11** (2007) 070, arXiv:0709.2092.
- [56] S. Alioli et al., *A general framework for implementing NLO calculations in shower Monte Carlo programs: the POWHEG BOX*, *JHEP* **06** (2010) 043, arXiv:1002.2581.
- [57] K. Arnold et al., *VBFNLO: A Parton Level Monte Carlo for Processes with Electroweak Bosons – Manual for Version 2.5.0*, (2011), arXiv:1107.4038.
- [58] J. Baglio et al., *Release Note - VBFNLO 2.7.0*, (2014), arXiv:1404.3940.
- [59] K. Arnold et al., *VBFNLO: A Parton level Monte Carlo for processes with electroweak bosons*, *Comput. Phys. Commun.* **180** (2009) 1661–1670, arXiv:0811.4559.
- [60] A. D. Martin et al., *Parton distributions for the LHC*, *Eur. Phys. J. C* **63** (2009) 189, arXiv:0901.0002.
- [61] B. Jager, C. Oleari, and D. Zeppenfeld, *Next-to-leading order QCD corrections to W^+W^+jj and W^-W^-jj production via weak-boson fusion*, *Phys. Rev. D* **80** (2009) 034022, arXiv:0907.0580.
- [62] B. Jager and G. Zanderighi, *NLO corrections to electroweak and QCD production of W^+W^+ plus two jets in the POWHEGBOX*, *JHEP* **11** (2011) 055, arXiv:1108.0864.

- [63] T. Melia et al., *Next-to-leading order QCD predictions for W^+W^+jj production at the LHC*, *JHEP* **12** (2010) 053, arXiv:1007.5313.
- [64] T. Melia et al., *W^+W^+ plus dijet production in the POWHEGBOX*, *Eur. Phys. J. C* **71** (2011) 1670, arXiv:1102.4846.
- [65] ATLAS Collaboration, *Summary of ATLAS Pythia 8 tunes*, ATL-PHYS-PUB-2012-003 (2012), URL: <http://cds.cern.ch/record/1474107>.
- [66] G. Corcella et al., *HERWIG 6: An Event generator for hadron emission reactions with interfering gluons (including supersymmetric processes)*, *JHEP* **01** (2001) 010, arXiv:hep-ph/0011363.
- [67] J. M. Butterworth, J. R. Forshaw, and M. H. Seymour, *Multiparton interactions in photoproduction at HERA*, *Zeitschrift für Physik C: Particles and Fields* **72** (1996) 637–646.
- [68] J. Alwall et al., *The automated computation of tree-level and next-to-leading order differential cross sections, and their matching to parton shower simulations*, *JHEP* **07** (2014) 079.
- [69] J. Pumplin et al., *New generation of parton distributions with uncertainties from global QCD analysis*, *JHEP* **07** (2002) 012, arXiv:hep-ph/0201195.
- [70] M. L. Mangano et al., *ALPGEN, a generator for hard multiparton processes in hadronic collisions*, *JHEP* **07** (2003) 001, arXiv:hep-ph/0206293.
- [71] ATLAS Collaboration, *Electron and photon energy calibration with the ATLAS detector using LHC Run 1 data*, *Eur. Phys. J. C* **74** (2014) 3071, arXiv:1407.5063.
- [72] ATLAS Collaboration, *Jet energy measurement and its systematic uncertainty in proton-proton collisions at $\sqrt{s} = 7$ TeV with the ATLAS detector*, *Eur. Phys. J. C* **75** (2015) 17, arXiv:1406.0076.
- [73] ATLAS Collaboration, *Commissioning of the ATLAS high-performance b-tagging algorithms in the 7 TeV collision data*, ATL-CONF-2011-102 (2011), URL: <http://cds.cern.ch/record/1369219>.
- [74] G. Cowan et al., *Asymptotic formulae for likelihood-based tests of new physics*, *Eur. Phys. J. C* **71** (2011) 1554, [Erratum: *Eur. Phys. J. C* **73**, 2501 (2013)], arXiv:1007.1727.
- [75] W. Kilian, T. Ohl, and J. Reuter, *WHIZARD: Simulating multi-particle processes at LHC and ILC*, *Eur. Phys. J. C* **71** (2011) 1742, arXiv:0708.4233.
- [76] A. L. Read, *Presentation of search results: The $CL(s)$ technique*, *J. Phys.* **G28** (2002) 2693.
- [77] ATLAS Collaboration, *ATLAS Computing Acknowledgements 2016-2017*, ATL-GEN-PUB-2016-002, 2016, URL: <http://cds.cern.ch/record/2202407>.

The ATLAS Collaboration

M. Aaboud^{135d}, G. Aad⁸⁶, B. Abbott¹¹³, J. Abdallah⁶⁴, O. Abdinov¹², B. Abeloos¹¹⁷, R. Aben¹⁰⁷, O.S. AbouZeid¹³⁷, N.L. Abraham¹⁴⁹, H. Abramowicz¹⁵³, H. Abreu¹⁵², R. Abreu¹¹⁶, Y. Abulaiti^{146a,146b}, B.S. Acharya^{163a,163b,a}, L. Adamczyk^{40a}, D.L. Adams²⁷, J. Adelman¹⁰⁸, S. Adomeit¹⁰⁰, T. Adye¹³¹, A.A. Affolder⁷⁵, T. Agatonovic-Jovin¹⁴, J. Agricola⁵⁶, J.A. Aguilar-Saavedra^{126a,126f}, S.P. Ahlen²⁴, F. Ahmadov^{66,b}, G. Aielli^{133a,133b}, H. Akerstedt^{146a,146b}, T.P.A. Åkesson⁸², A.V. Akimov⁹⁶, G.L. Alberghi^{22a,22b}, J. Albert¹⁶⁸, S. Albrand⁵⁷, M.J. Alconada Verzini⁷², M. Aleksa³², I.N. Aleksandrov⁶⁶, C. Alexa^{28b}, G. Alexander¹⁵³, T. Alexopoulos¹⁰, M. Alhroob¹¹³, B. Ali¹²⁸, M. Aliev^{74a,74b}, G. Alimonti^{92a}, J. Alison³³, S.P. Alkire³⁷, B.M.M. Allbrooke¹⁴⁹, B.W. Allen¹¹⁶, P.P. Allport¹⁹, A. Aloisio^{104a,104b}, A. Alonso³⁸, F. Alonso⁷², C. Alpigiani¹³⁸, M. Alstaty⁸⁶, B. Alvarez Gonzalez³², D. Álvarez Piqueras¹⁶⁶, M.G. Alviggi^{104a,104b}, B.T. Amadio¹⁶, K. Amako⁶⁷, Y. Amaral Coutinho^{26a}, C. Amelung²⁵, D. Amidei⁹⁰, S.P. Amor Dos Santos^{126a,126c}, A. Amorim^{126a,126b}, S. Amoroso³², G. Amundsen²⁵, C. Anastopoulos¹³⁹, L.S. Ancu⁵¹, N. Andari¹⁹, T. Andeen¹¹, C.F. Anders^{59b}, G. Anders³², J.K. Anders⁷⁵, K.J. Anderson³³, A. Andreazza^{92a,92b}, V. Andrei^{59a}, S. Angelidakis⁹, I. Angelozzi¹⁰⁷, P. Anger⁴⁶, A. Angerami³⁷, F. Anghinolfi³², A.V. Anisenkov^{109,c}, N. Anjos¹³, A. Annovi^{124a,124b}, C. Antel^{59a}, M. Antonelli⁴⁹, A. Antonov^{98,*}, F. Anulli^{132a}, M. Aoki⁶⁷, L. Aperio Bella¹⁹, G. Arabidze⁹¹, Y. Arai⁶⁷, J.P. Araque^{126a}, A.T.H. Arce⁴⁷, F.A. Arduh⁷², J-F. Arguin⁹⁵, S. Argyropoulos⁶⁴, M. Arik^{20a}, A.J. Armbruster¹⁴³, L.J. Armitage⁷⁷, O. Arnaez³², H. Arnold⁵⁰, M. Arratia³⁰, O. Arslan²³, A. Artamonov⁹⁷, G. Artoni¹²⁰, S. Artz⁸⁴, S. Asai¹⁵⁵, N. Asbah⁴⁴, A. Ashkenazi¹⁵³, B. Åsman^{146a,146b}, L. Asquith¹⁴⁹, K. Assamagan²⁷, R. Astalos^{144a}, M. Atkinson¹⁶⁵, N.B. Atlay¹⁴¹, K. Augsten¹²⁸, G. Avolio³², B. Axen¹⁶, M.K. Ayoub¹¹⁷, G. Azuelos^{95,d}, M.A. Baak³², A.E. Baas^{59a}, M.J. Baca¹⁹, H. Bachacou¹³⁶, K. Bachas^{74a,74b}, M. Backes¹⁴⁸, M. Backhaus³², P. Bagiacchi^{132a,132b}, P. Bagnaia^{132a,132b}, Y. Bai^{35a}, J.T. Baines¹³¹, O.K. Baker¹⁷⁵, E.M. Baldwin^{109,c}, P. Balek¹⁷¹, T. Balestri¹⁴⁸, F. Balli¹³⁶, W.K. Balunas¹²², E. Banas⁴¹, Sw. Banerjee^{172,e}, A.A.E. Bannoura¹⁷⁴, L. Barak³², E.L. Barberio⁸⁹, D. Barberis^{52a,52b}, M. Barbero⁸⁶, T. Barillari¹⁰¹, M-S Barisits³², T. Barklow¹⁴³, N. Barlow³⁰, S.L. Barnes⁸⁵, B.M. Barnett¹³¹, R.M. Barnett¹⁶, Z. Barnovska-Blenessy⁵, A. Baroncelli^{134a}, G. Barone²⁵, A.J. Barr¹²⁰, L. Barranco Navarro¹⁶⁶, F. Barreiro⁸³, J. Barreiro Guimarães da Costa^{35a}, R. Bartoldus¹⁴³, A.E. Barton⁷³, P. Bartos^{144a}, A. Basalae¹²³, A. Bassalat¹¹⁷, R.L. Bates⁵⁵, S.J. Batista¹⁵⁸, J.R. Batley³⁰, M. Battaglia¹³⁷, M. Bause^{132a,132b}, F. Bauer¹³⁶, H.S. Bawa^{143,f}, J.B. Beacham¹¹¹, M.D. Beattie⁷³, T. Beau⁸¹, P.H. Beauchemin¹⁶¹, P. Bechtel²³, H.P. Beck^{18,g}, K. Becker¹²⁰, M. Becker⁸⁴, M. Beckingham¹⁶⁹, C. Becot¹¹⁰, A.J. Beddall^{20e}, A. Beddall^{20b}, V.A. Bednyakov⁶⁶, M. Bedognetti¹⁰⁷, C.P. Bee¹⁴⁸, L.J. Beemster¹⁰⁷, T.A. Beermann³², M. Beger²⁷, J.K. Behr⁴⁴, C. Belanger-Champagne⁸⁸, A.S. Bell⁷⁹, G. Bella¹⁵³, L. Bellagamba^{22a}, A. Bellerive³¹, M. Bellomo⁸⁷, K. Belotskiy⁹⁸, O. Beltramello³², N.L. Belyaev⁹⁸, O. Benary¹⁵³, D. Benchechroun^{135a}, M. Bender¹⁰⁰, K. Bendtz^{146a,146b}, N. Benekos¹⁰, Y. Benhammou¹⁵³, E. Benhar Noccioli¹⁷⁵, J. Benitez⁶⁴, D.P. Benjamin⁴⁷, J.R. Bensinger²⁵, S. Bentvelsen¹⁰⁷, L. Beresford¹²⁰, M. Beretta⁴⁹, D. Berge¹⁰⁷, E. Bergeaas Kuutmann¹⁶⁴, N. Berger⁵, J. Beringer¹⁶, S. Berlendis⁵⁷, N.R. Bernard⁸⁷, C. Bernius¹¹⁰, F.U. Bernlochner²³, T. Berry⁷⁸, P. Berta¹²⁹, C. Bertella⁸⁴, G. Bertoli^{146a,146b}, F. Bertolucci^{124a,124b}, I.A. Bertram⁷³, C. Bertsche⁴⁴, D. Bertsche¹¹³, G.J. Besjes³⁸, O. Bessidskaia Bylund^{146a,146b}, M. Bessner⁴⁴, N. Besson¹³⁶, C. Betancourt⁵⁰, A. Bethani⁵⁷, S. Bethke¹⁰¹, A.J. Bevan⁷⁷, R.M. Bianchi¹²⁵, L. Bianchini²⁵, M. Bianco³², O. Biebel¹⁰⁰, D. Biedermann¹⁷, R. Bielski⁸⁵, N.V. Biesuz^{124a,124b}, M. Biglietti^{134a}, J. Bilbao De Mendizabal⁵¹, T.R.V. Billoud⁹⁵, H. Bilokon⁴⁹, M. Bindi⁵⁶, S. Binet¹¹⁷, A. Bingul^{20b}, C. Bini^{132a,132b}, S. Biondi^{22a,22b}, T. Bisanz⁵⁶, D.M. Bjergaard⁴⁷, C.W. Black¹⁵⁰, J.E. Black¹⁴³, K.M. Black²⁴, D. Blackburn¹³⁸, R.E. Blair⁶, J.-B. Blanchard¹³⁶, T. Blazek^{144a}, I. Bloch⁴⁴, C. Blocker²⁵, W. Blum^{84,*}

U. Blumenschein⁵⁶, S. Blunier^{34a}, G.J. Bobbink¹⁰⁷, V.S. Bobrovnikov^{109,c}, S.S. Bocchetta⁸², A. Bocci⁴⁷, C. Bock¹⁰⁰, M. Boehler⁵⁰, D. Boerner¹⁷⁴, J.A. Bogaerts³², D. Bogovac¹⁴, A.G. Bogdanchikov¹⁰⁹, C. Bohm^{146a}, V. Boisvert⁷⁸, P. Bokan¹⁴, T. Bold^{40a}, A.S. Boldyrev^{163a,163c}, M. Bomben⁸¹, M. Bona⁷⁷, M. Boonekamp¹³⁶, A. Borisov¹³⁰, G. Borissov⁷³, J. Bortfeldt³², D. Bortoletto¹²⁰, V. Bortolotto^{61a,61b,61c}, K. Bos¹⁰⁷, D. Boscherini^{22a}, M. Bosman¹³, J.D. Bossio Sola²⁹, J. Boudreau¹²⁵, J. Bouffard², E.V. Bouhova-Thacker⁷³, D. Boumediene³⁶, C. Bourdarios¹¹⁷, S.K. Boutle⁵⁵, A. Boveia³², J. Boyd³², I.R. Boyko⁶⁶, J. Bracinik¹⁹, A. Brandt⁸, G. Brandt⁵⁶, O. Brandt^{59a}, U. Bratzler¹⁵⁶, B. Brau⁸⁷, J.E. Brau¹¹⁶, H.M. Braun^{174,*}, W.D. Breaden Madden⁵⁵, K. Brendlinger¹²², A.J. Brennan⁸⁹, L. Brenner¹⁰⁷, R. Brenner¹⁶⁴, S. Bressler¹⁷¹, T.M. Bristow⁴⁸, D. Britton⁵⁵, D. Britzger⁴⁴, F.M. Brochu³⁰, I. Brock²³, R. Brock⁹¹, G. Brooijmans³⁷, T. Brooks⁷⁸, W.K. Brooks^{34b}, J. Brosamer¹⁶, E. Brost¹⁰⁸, J.H. Broughton¹⁹, P.A. Bruckman de Renstrom⁴¹, D. Bruncko^{144b}, R. Bruneliere⁵⁰, A. Bruni^{22a}, G. Bruni^{22a}, L.S. Bruni¹⁰⁷, B.H. Brunt³⁰, M. Bruschi^{22a}, N. Brusino²³, P. Bryant³³, L. Bryngemark⁸², T. Buanes¹⁵, Q. Buat¹⁴², P. Buchholz¹⁴¹, A.G. Buckley⁵⁵, I.A. Budagov⁶⁶, F. Buehrer⁵⁰, M.K. Bugge¹¹⁹, O. Bulekov⁹⁸, D. Bullock⁸, H. Burckhart³², S. Burdin⁷⁵, C.D. Burgard⁵⁰, B. Burghgrave¹⁰⁸, K. Burka⁴¹, S. Burke¹³¹, I. Burmeister⁴⁵, J.T.P. Burr¹²⁰, E. Busato³⁶, D. Büscher⁵⁰, V. Büscher⁸⁴, P. Bussey⁵⁵, J.M. Butler²⁴, C.M. Buttar⁵⁵, J.M. Butterworth⁷⁹, P. Butti¹⁰⁷, W. Buttinger²⁷, A. Buzatu⁵⁵, A.R. Buzykaev^{109,c}, S. Cabrera Urbán¹⁶⁶, D. Caforio¹²⁸, V.M. Cairo^{39a,39b}, O. Cakir^{4a}, N. Calace⁵¹, P. Calafiura¹⁶, A. Calandri⁸⁶, G. Calderini⁸¹, P. Calfayan¹⁰⁰, G. Callea^{39a,39b}, L.P. Caloba^{26a}, S. Calvente Lopez⁸³, D. Calvet³⁶, S. Calvet³⁶, T.P. Calvet⁸⁶, R. Camacho Toro³³, S. Camarda³², P. Camarri^{133a,133b}, D. Cameron¹¹⁹, R. Caminal Armadans¹⁶⁵, C. Camincher⁵⁷, S. Campana³², M. Campanelli⁷⁹, A. Camplani^{92a,92b}, A. Campoverde¹⁴¹, V. Canale^{104a,104b}, A. Canepa^{159a}, M. Cano Bret^{35e}, J. Cantero¹¹⁴, R. Cantrill^{126a}, T. Cao⁴², M.D.M. Capeans Garrido³², I. Caprini^{28b}, M. Caprini^{28b}, M. Capua^{39a,39b}, R. Caputo⁸⁴, R.M. Carbone³⁷, R. Cardarelli^{133a}, F. Cardillo⁵⁰, I. Carli¹²⁹, T. Carli³², G. Carlino^{104a}, L. Carminati^{92a,92b}, S. Caron¹⁰⁶, E. Carquin^{34b}, G.D. Carrillo-Montoya³², J.R. Carter³⁰, J. Carvalho^{126a,126c}, D. Casadei¹⁹, M.P. Casado^{13,h}, M. Casolino¹³, D.W. Casper¹⁶², E. Castaneda-Miranda^{145a}, R. Castelijm¹⁰⁷, A. Castelli¹⁰⁷, V. Castillo Gimenez¹⁶⁶, N.F. Castro^{126a,i}, A. Catinaccio³², J.R. Catmore¹¹⁹, A. Cattai³², J. Caudron²³, V. Cavaliere¹⁶⁵, E. Cavallaro¹³, D. Cavalli^{92a}, M. Cavalli-Sforza¹³, V. Cavasinni^{124a,124b}, F. Ceradini^{134a,134b}, L. Cerda Alberich¹⁶⁶, B.C. Cerio⁴⁷, A.S. Cerqueira^{26b}, A. Cerri¹⁴⁹, L. Cerrito^{133a,133b}, F. Cerutti¹⁶, M. Cerv³², A. Cervelli¹⁸, S.A. Cetin^{20d}, A. Chafaq^{135a}, D. Chakraborty¹⁰⁸, S.K. Chan⁵⁸, Y.L. Chan^{61a}, P. Chang¹⁶⁵, J.D. Chapman³⁰, D.G. Charlton¹⁹, A. Chatterjee⁵¹, C.C. Chau¹⁵⁸, C.A. Chavez Barajas¹⁴⁹, S. Che¹¹¹, S. Cheatham⁷³, A. Chegwidan⁹¹, S. Chekanov⁶, S.V. Chekulaev^{159a}, G.A. Chelkov^{66,j}, M.A. Chelstowska⁹⁰, C. Chen⁶⁵, H. Chen²⁷, K. Chen¹⁴⁸, S. Chen^{35c}, S. Chen¹⁵⁵, X. Chen^{35f}, Y. Chen⁶⁸, H.C. Cheng⁹⁰, H.J. Cheng^{35a}, Y. Cheng³³, A. Cheplakov⁶⁶, E. Cheremushkina¹³⁰, R. Cherkaoui El Moursli^{135e}, V. Chernyatin^{27,*}, E. Cheu⁷, L. Chevalier¹³⁶, V. Chiarella⁴⁹, G. Chiarelli^{124a,124b}, G. Chiodini^{74a}, A.S. Chisholm¹⁹, A. Chitan^{28b}, M.V. Chizhov⁶⁶, K. Choi⁶², A.R. Chomont³⁶, S. Chouridou⁹, B.K.B. Chow¹⁰⁰, V. Christodoulou⁷⁹, D. Chromek-Burckhart³², J. Chudoba¹²⁷, A.J. Chuinard⁸⁸, J.J. Chwastowski⁴¹, L. Chytka¹¹⁵, G. Ciapetti^{132a,132b}, A.K. Ciftci^{4a}, D. Cinca⁴⁵, V. Cindro⁷⁶, I.A. Cioara²³, C. Ciocca^{22a,22b}, A. Ciocio¹⁶, F. Ciotto^{104a,104b}, Z.H. Citron¹⁷¹, M. Citterio^{92a}, M. Ciubancan^{28b}, A. Clark⁵¹, B.L. Clark⁵⁸, M.R. Clark³⁷, P.J. Clark⁴⁸, R.N. Clarke¹⁶, C. Clement^{146a,146b}, Y. Coadou⁸⁶, M. Cobal^{163a,163c}, A. Coccaro⁵¹, J. Cochran⁶⁵, L. Colasurdo¹⁰⁶, B. Cole³⁷, A.P. Colijn¹⁰⁷, J. Collot⁵⁷, T. Colombo³², G. Compostella¹⁰¹, P. Conde Muño^{126a,126b}, E. Coniavitis⁵⁰, S.H. Connell^{145b}, I.A. Connelly⁷⁸, V. Consorti⁵⁰, S. Constantinescu^{28b}, G. Conti³², F. Conventi^{104a,k}, M. Cooke¹⁶, B.D. Cooper⁷⁹, A.M. Cooper-Sarkar¹²⁰, K.J.R. Cormier¹⁵⁸, T. Cornelissen¹⁷⁴, M. Corradi^{132a,132b}, F. Corriveau^{88,l}, A. Corso-Radu¹⁶², A. Cortes-Gonzalez³², G. Cortiana¹⁰¹, G. Costa^{92a}, M.J. Costa¹⁶⁶, D. Costanzo¹³⁹, G. Cottin³⁰, G. Cowan⁷⁸, B.E. Cox⁸⁵, K. Cranmer¹¹⁰, S.J. Crawley⁵⁵, G. Cree³¹, S. Crépe-Renaudin⁵⁷,

F. Crescioli⁸¹, W.A. Cribbs^{146a,146b}, M. Crispin Ortuzar¹²⁰, M. Cristinziani²³, V. Croft¹⁰⁶,
 G. Crosetti^{39a,39b}, A. Cueto⁸³, T. Cuhadar Donszelmann¹³⁹, J. Cummings¹⁷⁵, M. Curatolo⁴⁹, J. Cúth⁸⁴,
 H. Czirr¹⁴¹, P. Czodrowski³, G. D'amen^{22a,22b}, S. D'Auria⁵⁵, M. D'Onofrio⁷⁵,
 M.J. Da Cunha Sargedas De Sousa^{126a,126b}, C. Da Via⁸⁵, W. Dabrowski^{40a}, T. Dado^{144a}, T. Dai⁹⁰,
 O. Dale¹⁵, F. Dallaire⁹⁵, C. Dallapiccola⁸⁷, M. Dam³⁸, J.R. Dandoy³³, N.P. Dang⁵⁰, A.C. Daniells¹⁹,
 N.S. Dann⁸⁵, M. Danninger¹⁶⁷, M. Dano Hoffmann¹³⁶, V. Dao⁵⁰, G. Darbo^{52a}, S. Darmora⁸,
 J. Dassoulas³, A. Dattagupta¹¹⁶, W. Davey²³, C. David¹⁶⁸, T. Davidek¹²⁹, M. Davies¹⁵³, P. Davison⁷⁹,
 E. Dawe⁸⁹, I. Dawson¹³⁹, R.K. Daya-Ishmukhametova⁸⁷, K. De⁸, R. de Asmundis^{104a},
 A. De Benedetti¹¹³, S. De Castro^{22a,22b}, S. De Cecco⁸¹, N. De Groot¹⁰⁶, P. de Jong¹⁰⁷, H. De la Torre⁸³,
 F. De Lorenzi⁶⁵, A. De Maria⁵⁶, D. De Pedis^{132a}, A. De Salvo^{132a}, U. De Sanctis¹⁴⁹, A. De Santo¹⁴⁹,
 J.B. De Vivie De Regie¹¹⁷, W.J. Dearnaley⁷³, R. Debbe²⁷, C. Debenedetti¹³⁷, D.V. Dedovich⁶⁶,
 N. Dehghanian³, I. Deigaard¹⁰⁷, M. Del Gaudio^{39a,39b}, J. Del Peso⁸³, T. Del Prete^{124a,124b},
 D. Delgove¹¹⁷, F. Deliot¹³⁶, C.M. Delitzsch⁵¹, A. Dell'Acqua³², L. Dell'Asta²⁴, M. Dell'Orso^{124a,124b},
 M. Della Pietra^{104a,k}, D. della Volpe⁵¹, M. Delmastro⁵, P.A. Delsart⁵⁷, D.A. DeMarco¹⁵⁸, S. Demers¹⁷⁵,
 M. Demichev⁶⁶, A. Demilly⁸¹, S.P. Denisov¹³⁰, D. Denysiuk¹³⁶, D. Derendarz⁴¹, J.E. Derkaoui^{135d},
 F. Derue⁸¹, P. Dervan⁷⁵, K. Desch²³, C. Deterre⁴⁴, K. Dette⁴⁵, P.O. Deviveiros³², A. Dewhurst¹³¹,
 S. Dhaliwal²⁵, A. Di Ciaccio^{133a,133b}, L. Di Ciaccio⁵, W.K. Di Clemente¹²², C. Di Donato^{132a,132b},
 A. Di Girolamo³², B. Di Girolamo³², B. Di Micco^{134a,134b}, R. Di Nardo³², A. Di Simone⁵⁰,
 R. Di Sipio¹⁵⁸, D. Di Valentino³¹, C. Diaconu⁸⁶, M. Diamond¹⁵⁸, F.A. Dias⁴⁸, M.A. Diaz^{34a},
 E.B. Diehl⁹⁰, J. Dietrich¹⁷, S. Diglio⁸⁶, A. Dimitrievska¹⁴, J. Dingfelder²³, P. Dita^{28b}, S. Dita^{28b},
 F. Dittus³², F. Djama⁸⁶, T. Djobava^{53b}, J.I. Djuvsland^{59a}, M.A.B. do Vale^{26c}, D. Dobos³², M. Dobre^{28b},
 C. Doglioni⁸², J. Dolejsi¹²⁹, Z. Dolezal¹²⁹, M. Donadelli^{26d}, S. Donati^{124a,124b}, P. Dondero^{121a,121b},
 J. Donini³⁶, J. Dopke¹³¹, A. Doria^{104a}, M.T. Dova⁷², A.T. Doyle⁵⁵, E. Drechsler⁵⁶, M. Dris¹⁰, Y. Du^{35d},
 J. Duarte-Campderros¹⁵³, E. Duchovni¹⁷¹, G. Duckeck¹⁰⁰, O.A. Ducu^{95,m}, D. Duda¹⁰⁷, A. Dudarev³²,
 A.Chr. Dudder⁸⁴, E.M. Duffield¹⁶, L. Duflot¹¹⁷, M. Dührssen³², M. Dumancic¹⁷¹, M. Dunford^{59a},
 H. Duran Yildiz^{4a}, M. Düren⁵⁴, A. Durglishvili^{53b}, D. Duschinger⁴⁶, B. Dutta⁴⁴, M. Dyndal⁴⁴,
 C. Eckardt⁴⁴, K.M. Ecker¹⁰¹, R.C. Edgar⁹⁰, N.C. Edwards⁴⁸, T. Eifert³², G. Eigen¹⁵, K. Einsweiler¹⁶,
 T. Ekelof¹⁶⁴, M. El Kacimi^{135c}, V. Ellajosyula⁸⁶, M. Ellert¹⁶⁴, S. Elles⁵, F. Ellinghaus¹⁷⁴, A.A. Elliot¹⁶⁸,
 N. Ellis³², J. Elmsheuser²⁷, M. Elsing³², D. Emelianov¹³¹, Y. Enari¹⁵⁵, O.C. Endner⁸⁴, J.S. Ennis¹⁶⁹,
 J. Erdmann⁴⁵, A. Ereditato¹⁸, G. Ernis¹⁷⁴, J. Ernst², M. Ernst²⁷, S. Errede¹⁶⁵, E. Ertel⁸⁴, M. Escalier¹¹⁷,
 H. Esch⁴⁵, C. Escobar¹²⁵, B. Esposito⁴⁹, A.I. Etienne¹³⁶, E. Etzion¹⁵³, H. Evans⁶², A. Ezhilov¹²³,
 F. Fabbri^{22a,22b}, L. Fabbri^{22a,22b}, G. Facini³³, R.M. Fakhruddinov¹³⁰, S. Falciano^{132a}, R.J. Falla⁷⁹,
 J. Faltova³², Y. Fang^{35a}, M. Fanti^{92a,92b}, A. Farbin⁸, A. Farilla^{134a}, C. Farina¹²⁵, E.M. Farina^{121a,121b},
 T. Farooque¹³, S. Farrell¹⁶, S.M. Farrington¹⁶⁹, P. Farthouat³², F. Fassi^{135e}, P. Fassnacht³²,
 D. Fassouliotis⁹, M. Fauci Giannelli⁷⁸, A. Favareto^{52a,52b}, W.J. Fawcett¹²⁰, L. Fayard¹¹⁷,
 O.L. Fedin^{123,n}, W. Fedorko¹⁶⁷, S. Feigl¹¹⁹, L. Felgioni⁸⁶, C. Feng^{35d}, E.J. Feng³², H. Feng⁹⁰,
 A.B. Fenyuk¹³⁰, L. Feremenga⁸, P. Fernandez Martinez¹⁶⁶, S. Fernandez Perez¹³, J. Ferrando⁵⁵,
 A. Ferrari¹⁶⁴, P. Ferrari¹⁰⁷, R. Ferrari^{121a}, D.E. Ferreira de Lima^{59b}, A. Ferrer¹⁶⁶, D. Ferrere⁵¹,
 C. Ferretti⁹⁰, A. Ferretto Parodi^{52a,52b}, F. Fiedler⁸⁴, A. Filipčič⁷⁶, M. Filipuzzi⁴⁴, F. Filthaut¹⁰⁶,
 M. Fincke-Keeler¹⁶⁸, K.D. Finelli¹⁵⁰, M.C.N. Fiolhais^{126a,126c}, L. Fiorini¹⁶⁶, A. Firan⁴², A. Fischer²,
 C. Fischer¹³, J. Fischer¹⁷⁴, W.C. Fisher⁹¹, N. Flaschel⁴⁴, I. Fleck¹⁴¹, P. Fleischmann⁹⁰, G.T. Fletcher¹³⁹,
 R.R.M. Fletcher¹²², T. Flick¹⁷⁴, A. Floderus⁸², L.R. Flores Castillo^{61a}, M.J. Flowerdew¹⁰¹,
 G.T. Forcolin⁸⁵, A. Formica¹³⁶, A. Forti⁸⁵, A.G. Foster¹⁹, D. Fournier¹¹⁷, H. Fox⁷³, S. Fracchia¹³,
 P. Francavilla⁸¹, M. Franchini^{22a,22b}, D. Francis³², L. Franconi¹¹⁹, M. Franklin⁵⁸, M. Frate¹⁶²,
 M. Fraternali^{121a,121b}, D. Freeborn⁷⁹, S.M. Fressard-Batraneanu³², F. Friedrich⁴⁶, D. Froidevaux³²,
 J.A. Frost¹²⁰, C. Fukunaga¹⁵⁶, E. Fullana Torregrosa⁸⁴, T. Fusayasu¹⁰², J. Fuster¹⁶⁶, C. Gabaldon⁵⁷,
 O. Gabizon¹⁷⁴, A. Gabrielli^{22a,22b}, A. Gabrielli¹⁶, G.P. Gach^{40a}, S. Gadatsch³², S. Gadomski⁵¹,

G. Gagliardi^{52a,52b}, L.G. Gagnon⁹⁵, P. Gagnon⁶², C. Galea¹⁰⁶, B. Galhardo^{126a,126c}, E.J. Gallas¹²⁰, B.J. Gallop¹³¹, P. Gallus¹²⁸, G. Galster³⁸, K.K. Gan¹¹¹, J. Gao^{35b}, Y. Gao⁴⁸, Y.S. Gao^{143.f}, F.M. Garay Walls⁴⁸, C. García¹⁶⁶, J.E. García Navarro¹⁶⁶, M. Garcia-Sciveres¹⁶, R.W. Gardner³³, N. Garelli¹⁴³, V. Garonne¹¹⁹, A. Gascon Bravo⁴⁴, K. Gasnikova⁴⁴, C. Gatti⁴⁹, A. Gaudiello^{52a,52b}, G. Gaudio^{121a}, L. Gauthier⁹⁵, I.L. Gavrilenko⁹⁶, C. Gay¹⁶⁷, G. Gaycken²³, E.N. Gazis¹⁰, Z. Gecse¹⁶⁷, C.N.P. Gee¹³¹, Ch. Geich-Gimbel²³, M. Geisen⁸⁴, M.P. Geisler^{59a}, C. Gemme^{52a}, M.H. Genest⁵⁷, C. Geng^{35b,o}, S. Gentile^{132a,132b}, C. Gentsos¹⁵⁴, S. George⁷⁸, D. Gerbaudo¹³, A. Gershon¹⁵³, S. Ghasemi¹⁴¹, H. Ghazlane^{135b}, M. Ghneimat²³, B. Giacobbe^{22a}, S. Giagu^{132a,132b}, P. Giannetti^{124a,124b}, B. Gibbard²⁷, S.M. Gibson⁷⁸, M. Gignac¹⁶⁷, M. Gilchriese¹⁶, T.P.S. Gillam³⁰, D. Gillberg³¹, G. Gilles¹⁷⁴, D.M. Gingrich^{3,d}, N. Giokaris⁹, M.P. Giordani^{163a,163c}, F.M. Giorgi^{22a}, F.M. Giorgi¹⁷, P.F. Giraud¹³⁶, P. Giromini⁵⁸, D. Giugni^{92a}, F. Giuli¹²⁰, C. Giuliani¹⁰¹, M. Giulini^{59b}, B.K. Gjelsten¹¹⁹, S. Gkaitatzis¹⁵⁴, I. Gkialas¹⁵⁴, E.L. Gkougkousis¹¹⁷, L.K. Gladilin⁹⁹, C. Glasman⁸³, J. Glatzer⁵⁰, P.C.F. Glaysheer⁴⁸, A. Glazov⁴⁴, M. Goblirsch-Kolb²⁵, J. Godlewski⁴¹, S. Goldfarb⁸⁹, T. Golling⁵¹, D. Golubkov¹³⁰, A. Gomes^{126a,126b,126d}, R. Gonçalo^{126a}, J. Goncalves Pinto Firmino Da Costa¹³⁶, G. Gonella⁵⁰, L. Gonella¹⁹, A. Gongadze⁶⁶, S. González de la Hoz¹⁶⁶, G. Gonzalez Parra¹³, S. Gonzalez-Sevilla⁵¹, L. Goossens³², P.A. Gorbounov⁹⁷, H.A. Gordon²⁷, I. Gorelov¹⁰⁵, B. Gorini³², E. Gorini^{74a,74b}, A. Gorišek⁷⁶, E. Gornicki⁴¹, A.T. Goshaw⁴⁷, C. Gössling⁴⁵, M.I. Gostkin⁶⁶, C.R. Goudet¹¹⁷, D. Goujdami^{135c}, A.G. Goussiou¹³⁸, N. Govender^{145b,p}, E. Gozani¹⁵², L. Graber⁵⁶, I. Grabowska-Bold^{40a}, P.O.J. Gradin⁵⁷, P. Grafström^{22a,22b}, J. Gramling⁵¹, E. Gramstad¹¹⁹, S. Grancagnolo¹⁷, V. Gratchev¹²³, P.M. Gravila^{28e}, H.M. Gray³², E. Graziani^{134a}, Z.D. Greenwood^{80,q}, C. Grefe²³, K. Gregersen⁷⁹, I.M. Gregor⁴⁴, P. Grenier¹⁴³, K. Grevtsov⁵, J. Griffiths⁸, A.A. Grillo¹³⁷, K. Grimm⁷³, S. Grinstein^{13,r}, Ph. Gris³⁶, J.-F. Grivaz¹¹⁷, S. Groh⁸⁴, J.P. Grohs⁴⁶, E. Gross¹⁷¹, J. Grosse-Knetter⁵⁶, G.C. Grossi⁸⁰, Z.J. Grout⁷⁹, L. Guan⁹⁰, W. Guan¹⁷², J. Guenther⁶³, F. Guescini⁵¹, D. Guest¹⁶², O. Gueta¹⁵³, E. Guido^{52a,52b}, T. Guillemin⁵, S. Guindon², U. Gul⁵⁵, C. Gumpert³², J. Guo^{35e}, Y. Guo^{35b,o}, R. Gupta⁴², S. Gupta¹²⁰, G. Gustavino^{132a,132b}, P. Gutierrez¹¹³, N.G. Gutierrez Ortiz⁷⁹, C. Gutsche⁴⁶, C. Guyot¹³⁶, C. Gwenlan¹²⁰, C.B. Gwilliam⁷⁵, A. Haas¹¹⁰, C. Haber¹⁶, H.K. Hadavand⁸, N. Haddad^{135e}, A. Hadeef⁸⁶, S. Hageböck²³, Z. Hajduk⁴¹, H. Hakobyan^{176,*}, M. Haleem⁴⁴, J. Haley¹¹⁴, G. Halladjian⁹¹, G.D. Hallewell⁸⁶, K. Hamacher¹⁷⁴, P. Hamal¹¹⁵, K. Hamano¹⁶⁸, A. Hamilton^{145a}, G.N. Hamity¹³⁹, P.G. Hamnett⁴⁴, L. Han^{35b}, K. Hanagaki^{67,s}, K. Hanawa¹⁵⁵, M. Hance¹³⁷, B. Haney¹²², P. Hanke^{59a}, R. Hanna¹³⁶, J.B. Hansen³⁸, J.D. Hansen³⁸, M.C. Hansen²³, P.H. Hansen³⁸, K. Hara¹⁶⁰, A.S. Hard¹⁷², T. Harenberg¹⁷⁴, F. Hariri¹¹⁷, S. Harkusha⁹³, R.D. Harrington⁴⁸, P.F. Harrison¹⁶⁹, F. Hartjes¹⁰⁷, N.M. Hartmann¹⁰⁰, M. Hasegawa⁶⁸, Y. Hasegawa¹⁴⁰, A. Hasib¹¹³, S. Hassani¹³⁶, S. Haug¹⁸, R. Hauser⁹¹, L. Hauswald⁴⁶, M. Havranek¹²⁷, C.M. Hawkes¹⁹, R.J. Hawkings³², D. Hayakawa¹⁵⁷, D. Hayden⁹¹, C.P. Hays¹²⁰, J.M. Hays⁷⁷, H.S. Hayward⁷⁵, S.J. Haywood¹³¹, S.J. Head¹⁹, T. Heck⁸⁴, V. Hedberg⁸², L. Heelan⁸, S. Heim¹²², T. Heim¹⁶, B. Heinemann¹⁶, J.J. Heinrich¹⁰⁰, L. Heinrich¹¹⁰, C. Heinz⁵⁴, J. Hejbal¹²⁷, L. Helary³², S. Hellman^{146a,146b}, C. Helsen³², J. Henderson¹²⁰, R.C.W. Henderson⁷³, Y. Heng¹⁷², S. Henkelmann¹⁶⁷, A.M. Henriques Correia³², S. Henrot-Versille¹¹⁷, G.H. Herbert¹⁷, V. Herget¹⁷³, Y. Hernández Jiménez¹⁶⁶, G. Herten⁵⁰, R. Hertenberger¹⁰⁰, L. Hervas³², G.G. Hesketh⁷⁹, N.P. Hessey¹⁰⁷, J.W. Hetherly⁴², R. Hickling⁷⁷, E. Higón-Rodríguez¹⁶⁶, E. Hill¹⁶⁸, J.C. Hill³⁰, K.H. Hiller⁴⁴, S.J. Hillier¹⁹, I. Hinchliffe¹⁶, E. Hines¹²², R.R. Hinman¹⁶, M. Hirose⁵⁰, D. Hirschbuehl¹⁷⁴, J. Hobbs¹⁴⁸, N. Hod^{159a}, M.C. Hodgkinson¹³⁹, P. Hodgson¹³⁹, A. Hoecker³², M.R. Hoferkamp¹⁰⁵, F. Hoenig¹⁰⁰, D. Hohn²³, T.R. Holmes¹⁶, M. Homann⁴⁵, T.M. Hong¹²⁵, B.H. Hooberman¹⁶⁵, W.H. Hopkins¹¹⁶, Y. Hori¹⁰³, A.J. Horton¹⁴², J.-Y. Hostachy⁵⁷, S. Hou¹⁵¹, A. Houmada^{135a}, J. Howarth⁴⁴, M. Hrabovsky¹¹⁵, I. Hristova¹⁷, J. Hrivnac¹¹⁷, T. Hryn'ova⁵, A. Hrynevich⁹⁴, C. Hsu^{145c}, P.J. Hsu^{151,t}, S.-C. Hsu¹³⁸, D. Hu³⁷, Q. Hu^{35b}, S. Hu^{35e}, Y. Huang⁴⁴, Z. Hubacek¹²⁸, F. Hubaut⁸⁶, F. Huegging²³, T.B. Huffman¹²⁰, E.W. Hughes³⁷, G. Hughes⁷³, M. Huhtinen³², P. Huo¹⁴⁸, N. Huseynov^{66,b}, J. Huston⁹¹,

J. Huth⁵⁸, G. Iacobucci⁵¹, G. Iakovidis²⁷, I. Ibragimov¹⁴¹, L. Iconomidou-Fayard¹¹⁷, E. Ideal¹⁷⁵, Z. Idrissi^{135e}, P. Ingo³², O. Igonkina^{107,u}, T. Iizawa¹⁷⁰, Y. Ikegami⁶⁷, M. Ikeno⁶⁷, Y. Ilchenko^{11,v}, D. Iliadis¹⁵⁴, N. Ilic¹⁴³, T. Ince¹⁰¹, G. Introzzi^{121a,121b}, P. Ioannou^{9,*}, M. Iodice^{134a}, K. Iordanidou³⁷, V. Ippolito⁵⁸, N. Ishijima¹¹⁸, M. Ishino¹⁵⁵, M. Ishitsuka¹⁵⁷, R. Ishmukhametov¹¹¹, C. Issever¹²⁰, S. Istin^{20a}, F. Ito¹⁶⁰, J.M. Iturbe Ponce⁸⁵, R. Iuppa³⁰⁸, W. Iwanski⁶³, H. Iwasaki⁶⁷, J.M. Izen⁴³, V. Izzo^{104a}, S. Jabbar³, B. Jackson¹²², P. Jackson¹, V. Jain², K.B. Jakobi⁸⁴, K. Jakobs⁵⁰, S. Jakobsen³², T. Jakoubek¹²⁷, D.O. Jamin¹¹⁴, D.K. Jana⁸⁰, E. Jansen⁷⁹, R. Jansky⁶³, J. Janssen²³, M. Janus⁵⁶, G. Jarlskog⁸², N. Javadov^{66,b}, T. Javůrek⁵⁰, F. Jeanneau¹³⁶, L. Jeanty¹⁶, G.-Y. Jeng¹⁵⁰, D. Jennens⁸⁹, P. Jenni^{50,w}, C. Jeske¹⁶⁹, S. Jézéquel⁵, H. Ji¹⁷², J. Jia¹⁴⁸, H. Jiang⁶⁵, Y. Jiang^{35b}, S. Jiggins⁷⁹, J. Jimenez Pena¹⁶⁶, S. Jin^{35a}, A. Jinaru^{28b}, O. Jinnouchi¹⁵⁷, H. Jivan^{145c}, P. Johansson¹³⁹, K.A. Johns⁷, W.J. Johnson¹³⁸, K. Jon-And^{146a,146b}, G. Jones¹⁶⁹, R.W.L. Jones⁷³, S. Jones⁷, T.J. Jones⁷⁵, J. Jongmanns^{59a}, P.M. Jorge^{126a,126b}, J. Jovicevic^{159a}, X. Ju¹⁷², A. Juste Rozas^{13,r}, M.K. Köhler¹⁷¹, A. Kaczmarska⁴¹, M. Kado¹¹⁷, H. Kagan¹¹¹, M. Kagan¹⁴³, S.J. Kahn⁸⁶, T. Kaji¹⁷⁰, E. Kajomovitz⁴⁷, C.W. Kalderon¹²⁰, A. Kaluza⁸⁴, S. Kama⁴², A. Kamenshchikov¹³⁰, N. Kanaya¹⁵⁵, S. Kaneti³⁰, L. Kanjir⁷⁶, V.A. Kantserov⁹⁸, J. Kanzaki⁶⁷, B. Kaplan¹¹⁰, L.S. Kaplan¹⁷², A. Kapliy³³, D. Kar^{145c}, K. Karakostas¹⁰, A. Karamaoun³, N. Karastathis¹⁰, M.J. Kareem⁵⁶, E. Karentzos¹⁰, M. Karnevskiy⁸⁴, S.N. Karpov⁶⁶, Z.M. Karpova⁶⁶, K. Karthik¹¹⁰, V. Kartvelishvili⁷³, A.N. Karyukhin¹³⁰, K. Kasahara¹⁶⁰, L. Kashif¹⁷², R.D. Kass¹¹¹, A. Kastanas¹⁵, Y. Kataoka¹⁵⁵, C. Kato¹⁵⁵, A. Katre⁵¹, J. Katzy⁴⁴, K. Kawagoe⁷¹, T. Kawamoto¹⁵⁵, G. Kawamura⁵⁶, V.F. Kazanin^{109,c}, R. Keeler¹⁶⁸, R. Kehoe⁴², J.S. Keller⁴⁴, J.J. Kempster⁷⁸, K. Kentaro¹⁰³, H. Keoshkerian¹⁵⁸, O. Kepka¹²⁷, B.P. Kerševan⁷⁶, S. Kersten¹⁷⁴, R.A. Keyes⁸⁸, M. Khader¹⁶⁵, F. Khalil-zada¹², A. Khanov¹¹⁴, A.G. Kharlamov^{109,c}, T.J. Khoo⁵¹, V. Khovanskiy⁹⁷, E. Khramov⁶⁶, J. Khubua^{53b,x}, S. Kido⁶⁸, C.R. Kilby⁷⁸, H.Y. Kim⁸, S.H. Kim¹⁶⁰, Y.K. Kim³³, N. Kimura¹⁵⁴, O.M. Kind¹⁷, B.T. King⁷⁵, M. King¹⁶⁶, S.B. King¹⁶⁷, J. Kirk¹³¹, A.E. Kiryunin¹⁰¹, T. Kishimoto¹⁵⁵, D. Kisielewska^{40a}, F. Kiss⁵⁰, K. Kiuchi¹⁶⁰, O. Kivernyk¹³⁶, E. Kladiva^{144b}, M.H. Klein³⁷, M. Klein⁷⁵, U. Klein⁷⁵, K. Kleinknecht⁸⁴, P. Klimek¹⁰⁸, A. Klimentov²⁷, R. Klingenberg⁴⁵, J.A. Klinger¹³⁹, T. Klioutchnikova³², E.-E. Kluge^{59a}, P. Kluit¹⁰⁷, S. Kluth¹⁰¹, J. Knapik⁴¹, E. Kneringer⁶³, E.B.F.G. Knoop⁸⁶, A. Knue⁵⁵, A. Kobayashi¹⁵⁵, D. Kobayashi¹⁵⁷, T. Kobayashi¹⁵⁵, M. Kobel⁴⁶, M. Kocian¹⁴³, P. Kodys¹²⁹, N.M. Koehler¹⁰¹, T. Koffas³¹, E. Koffeman¹⁰⁷, T. Koi¹⁴³, H. Kolanoski¹⁷, M. Kolb^{59b}, I. Koletsou⁵, A.A. Komar^{96,*}, Y. Komori¹⁵⁵, T. Kondo⁶⁷, N. Kondrashova⁴⁴, K. Köneke⁵⁰, A.C. König¹⁰⁶, T. Kono^{67,y}, R. Konoplich^{110,z}, N. Konstantinidis⁷⁹, R. Kopeliansky⁶², S. Koperny^{40a}, L. Köpke⁸⁴, A.K. Kopp⁵⁰, K. Korcyl⁴¹, K. Kordas¹⁵⁴, A. Korn⁷⁹, A.A. Korol^{109,c}, I. Korolkov¹³, E.V. Korolkova¹³⁹, O. Kortner¹⁰¹, S. Kortner¹⁰¹, T. Kosek¹²⁹, V.V. Kostyukhin²³, A. Kotwal⁴⁷, A. Kourkouveli-Charalampidi^{121a,121b}, C. Kourkouvelis⁹, V. Kouskoura²⁷, A.B. Kowalewska⁴¹, R. Kowalewski¹⁶⁸, T.Z. Kowalski^{40a}, C. Kozakai¹⁵⁵, W. Kozanecki¹³⁶, A.S. Kozhin¹³⁰, V.A. Kramarenko⁹⁹, G. Kramberger⁷⁶, D. Krasnopevtsev⁹⁸, M.W. Krasny⁸¹, A. Krasznahorkay³², A. Kravchenko²⁷, M. Kretz^{59c}, J. Kretzschmar⁷⁵, K. Kreutzfeldt⁵⁴, P. Krieger¹⁵⁸, K. Krizka³³, K. Kroeninger⁴⁵, H. Kroha¹⁰¹, J. Kroll¹²², J. Kroseberg²³, J. Krstic¹⁴, U. Kruchonak⁶⁶, H. Krüger²³, N. Krumnack⁶⁵, A. Kruse¹⁷², M.C. Kruse⁴⁷, M. Kruskal²⁴, T. Kubota⁸⁹, H. Kucuk⁷⁹, S. Kudah^{4b}, J.T. Kuechler¹⁷⁴, S. Kuehn⁵⁰, A. Kugel^{59c}, F. Kuger¹⁷³, A. Kuhl¹³⁷, T. Kuhl⁴⁴, V. Kukhtin⁶⁶, R. Kukla¹³⁶, Y. Kulchitsky⁹³, S. Kuleshov^{34b}, M. Kuna^{132a,132b}, T. Kunigo⁶⁹, A. Kupco¹²⁷, H. Kurashige⁶⁸, Y.A. Kurochkin⁹³, V. Kus¹²⁷, E.S. Kuwertz¹⁶⁸, M. Kuze¹⁵⁷, J. Kvita¹¹⁵, T. Kwan¹⁶⁸, D. Kyriazopoulos¹³⁹, A. La Rosa¹⁰¹, J.L. La Rosa Navarro^{26d}, L. La Rotonda^{39a,39b}, C. Lacasta¹⁶⁶, F. Lacava^{132a,132b}, J. Lacey³¹, H. Lacker¹⁷, D. Lacour⁸¹, V.R. Lacuesta¹⁶⁶, E. Ladygin⁶⁶, R. Lafaye⁵, B. Laforge⁸¹, T. Lagouri¹⁷⁵, S. Lai⁵⁶, S. Lammers⁶², W. Lampl⁷, E. Lançon¹³⁶, U. Landgraf⁵⁰, M.P.J. Landon⁷⁷, M.C. Lanfermann⁵¹, V.S. Lang^{59a}, J.C. Lange¹³, A.J. Lankford¹⁶², F. Lanni²⁷, K. Lantzsck²³, A. Lanza^{121a}, S. Laplace⁸¹, C. Lapoire³², J.F. Laporte¹³⁶, T. Lari^{92a}, F. Lasagni Manghi^{22a,22b}, M. Lassnig³², P. Laurelli⁴⁹, W. Lavrijsen¹⁶, A.T. Law¹³⁷, P. Laycock⁷⁵,

T. Lazovich⁵⁸, M. Lazzaroni^{92a,92b}, B. Le⁸⁹, O. Le Dortz⁸¹, E. Le Guirriec⁸⁶, E.P. Le Quilleuc¹³⁶,
 M. LeBlanc¹⁶⁸, T. LeCompte⁶, F. Ledroit-Guillon⁵⁷, C.A. Lee²⁷, S.C. Lee¹⁵¹, L. Lee¹, B. Lefebvre⁸⁸,
 G. Lefebvre⁸¹, M. Lefebvre¹⁶⁸, F. Legger¹⁰⁰, C. Leggett¹⁶, A. Lehan⁷⁵, G. Lehmann Miotto³², X. Lei⁷,
 W.A. Leight³¹, A. Leisos^{154,aa}, A.G. Leister¹⁷⁵, M.A.L. Leite^{26d}, R. Leitner¹²⁹, D. Lellouch¹⁷¹,
 B. Lemmer⁵⁶, K.J.C. Leney⁷⁹, T. Lenz²³, B. Lenzi³², R. Leone⁷, S. Leone^{124a,124b}, C. Leonidopoulos⁴⁸,
 S. Leontsinis¹⁰, G. Lerner¹⁴⁹, C. Leroy⁹⁵, A.A.J. Lesage¹³⁶, C.G. Lester³⁰, M. Levchenko¹²³,
 J. Levêque⁵, D. Levin⁹⁰, L.J. Levinson¹⁷¹, M. Levy¹⁹, D. Lewis⁷⁷, A.M. Leyko²³, M. Leyton⁴³,
 B. Li^{35b,o}, C. Li^{35b}, H. Li¹⁴⁸, H.L. Li³³, L. Li⁴⁷, L. Li^{35e}, Q. Li^{35a}, S. Li⁴⁷, X. Li⁸⁵, Y. Li¹⁴¹, Z. Liang^{35a},
 B. Liberti^{133a}, A. Liblong¹⁵⁸, P. Lichard³², K. Lie¹⁶⁵, J. Liebal²³, W. Liebig¹⁵, A. Limosani¹⁵⁰,
 S.C. Lin^{151,ab}, T.H. Lin⁸⁴, B.E. Lindquist¹⁴⁸, A.E. Lioni⁵¹, E. Lipeles¹²², A. Lipniacka¹⁵, M. Lisovyi^{59b},
 T.M. Liss¹⁶⁵, A. Lister¹⁶⁷, A.M. Litke¹³⁷, B. Liu^{151,ac}, D. Liu¹⁵¹, H. Liu⁹⁰, H. Liu²⁷, J. Liu⁸⁶,
 J.B. Liu^{35b}, K. Liu⁸⁶, L. Liu¹⁶⁵, M. Liu⁴⁷, M. Liu^{35b}, Y.L. Liu^{35b}, Y. Liu^{35b}, M. Livan^{121a,121b},
 A. Lleres⁵⁷, J. Llorente Merino^{35a}, S.L. Lloyd⁷⁷, F. Lo Sterzo¹⁵¹, E.M. Lobodzinska⁴⁴, P. Loch⁷,
 W.S. Lockman¹³⁷, F.K. Loebinger⁸⁵, A.E. Loevschall-Jensen³⁸, K.M. Loew²⁵, A. Loginov^{175,*},
 T. Lohse¹⁷, K. Lohwasser⁴⁴, M. Lokajicek¹²⁷, B.A. Long²⁴, J.D. Long¹⁶⁵, R.E. Long⁷³, L. Longo^{74a,74b},
 K.A. Looper¹¹¹, L. Lopes^{126a}, D. Lopez Mateos⁵⁸, B. Lopez Paredes¹³⁹, I. Lopez Paz¹³,
 A. Lopez Solis⁸¹, J. Lorenz¹⁰⁰, N. Lorenzo Martinez⁶², M. Losada²¹, P.J. Lösel¹⁰⁰, X. Lou^{35a},
 A. Lounis¹¹⁷, J. Love⁶, P.A. Love⁷³, H. Lu^{61a}, N. Lu⁹⁰, H.J. Lubatti¹³⁸, C. Luci^{132a,132b}, A. Lucotte⁵⁷,
 C. Luedtke⁵⁰, F. Luehring⁶², W. Lukas⁶³, L. Luminari^{132a}, O. Lundberg^{146a,146b}, B. Lund-Jensen¹⁴⁷,
 P.M. Luzi⁸¹, D. Lynn²⁷, R. Lysak¹²⁷, E. Lytken⁸², V. Lyubushkin⁶⁶, H. Ma²⁷, L.L. Ma^{35d}, Y. Ma^{35d},
 G. Maccarrone⁴⁹, A. Macchiolo¹⁰¹, C.M. Macdonald¹³⁹, B. Maček⁷⁶, J. Machado Miguens^{122,126b},
 D. Madaffari⁸⁶, R. Madar³⁶, H.J. Maddocks¹⁶⁴, W.F. Mader⁴⁶, A. Madsen⁴⁴, J. Maeda⁶⁸, S. Maeland¹⁵,
 T. Maeno²⁷, A. Maevskiy⁹⁹, E. Magradze⁵⁶, J. Mahlstedt¹⁰⁷, C. Maiani¹¹⁷, C. Maidantchik^{26a},
 A.A. Maier¹⁰¹, T. Maier¹⁰⁰, A. Maio^{126a,126b,126d}, S. Majewski¹¹⁶, Y. Makida⁶⁷, N. Makovec¹¹⁷,
 B. Malaescu⁸¹, Pa. Malecki⁴¹, V.P. Maleev¹²³, F. Malek⁵⁷, U. Mallik⁶⁴, D. Malon⁶, C. Malone¹⁴³,
 S. Maltezos¹⁰, S. Malyukov³², J. Mamuzic¹⁶⁶, G. Mancini⁴⁹, B. Mandelli³², L. Mandelli^{92a}, I. Mandić⁷⁶,
 J. Maneira^{126a,126b}, L. Manhaes de Andrade Filho^{26b}, J. Manjarres Ramos^{159b}, A. Mann¹⁰⁰,
 A. Manousos³², B. Mansoulie¹³⁶, J.D. Mansour^{35a}, R. Mantifel⁸⁸, M. Mantoani⁵⁶, S. Manzoni^{92a,92b},
 L. Mapelli³², G. Marceca²⁹, L. March⁵¹, G. Marchiori⁸¹, M. Marcisovsky¹²⁷, M. Marjanovic¹⁴,
 D.E. Marley⁹⁰, F. Marroquim^{26a}, S.P. Marsden⁸⁵, Z. Marshall¹⁶, S. Marti-Garcia¹⁶⁶, B. Martin⁹¹,
 T.A. Martin¹⁶⁹, V.J. Martin⁴⁸, B. Martin dit Latour¹⁵, M. Martinez^{13,r}, V.I. Martinez Outschoorn¹⁶⁵,
 S. Martin-Haugh¹³¹, V.S. Martoiu^{28b}, A.C. Martyniuk⁷⁹, M. Marx¹³⁸, A. Marzin³², L. Masetti⁸⁴,
 T. Mashimo¹⁵⁵, R. Mashinistov⁹⁶, J. Masik⁸⁵, A.L. Maslennikov^{109,c}, I. Massa^{22a,22b}, L. Massa^{22a,22b},
 P. Mastrandrea⁵, A. Mastroberardino^{39a,39b}, T. Masubuchi¹⁵⁵, P. Mättig¹⁷⁴, J. Mattmann⁸⁴, J. Maurer^{28b},
 S.J. Maxfield⁷⁵, D.A. Maximov^{109,c}, R. Mazini¹⁵¹, S.M. Mazza^{92a,92b}, N.C. Mc Fadden¹⁰⁵,
 G. Mc Goldrick¹⁵⁸, S.P. Mc Kee⁹⁰, A. McCarn⁹⁰, R.L. McCarthy¹⁴⁸, T.G. McCarthy¹⁰¹,
 L.I. McClymont⁷⁹, E.F. McDonald⁸⁹, J.A. Mcfayden⁷⁹, G. Mchedlize⁵⁶, S.J. McMahan¹³¹,
 R.A. McPherson^{168,l}, M. Medinnis⁴⁴, S. Meehan¹³⁸, S. Mehlhase¹⁰⁰, A. Mehta⁷⁵, K. Meier^{59a},
 C. Meineck¹⁰⁰, B. Meirose⁴³, D. Melini¹⁶⁶, B.R. Mellado Garcia^{145c}, M. Melo^{144a}, F. Meloni¹⁸,
 A. Mengarelli^{22a,22b}, S. Menke¹⁰¹, E. Meoni¹⁶¹, S. Mergelmeyer¹⁷, P. Mermod⁵¹, L. Merola^{104a,104b},
 C. Meroni^{92a}, F.S. Merritt³³, A. Messina^{132a,132b}, J. Metcalfe⁶, A.S. Mete¹⁶², C. Meyer⁸⁴, C. Meyer¹²²,
 J-P. Meyer¹³⁶, J. Meyer¹⁰⁷, H. Meyer Zu Theenhausen^{59a}, F. Miano¹⁴⁹, R.P. Middleton¹³¹,
 S. Miglioranzi^{52a,52b}, L. Mijovic⁴⁸, G. Mikenberg¹⁷¹, M. Mikestikova¹²⁷, M. Mikuž⁷⁶, M. Milesi⁸⁹,
 A. Milic⁶³, D.W. Miller³³, C. Mills⁴⁸, A. Milov¹⁷¹, D.A. Milstead^{146a,146b}, A.A. Minaenko¹³⁰,
 Y. Minami¹⁵⁵, I.A. Minashvili⁶⁶, A.I. Mincer¹¹⁰, B. Mindur^{40a}, M. Mineev⁶⁶, Y. Ming¹⁷², L.M. Mir¹³,
 K.P. Mistry¹²², T. Mitani¹⁷⁰, J. Mitrevski¹⁰⁰, V.A. Mitsou¹⁶⁶, A. Miucci¹⁸, P.S. Miyagawa¹³⁹,
 J.U. Mjörnmark⁸², T. Moa^{146a,146b}, K. Mochizuki⁹⁵, S. Mohapatra³⁷, S. Molander^{146a,146b},

R. Moles-Valls²³, R. Monden⁶⁹, M.C. Mondragon⁹¹, K. Mönig⁴⁴, J. Monk³⁸, E. Monnier⁸⁶, A. Montalbano¹⁴⁸, J. Montejo Berlingen³², F. Monticelli⁷², S. Monzani^{92a,92b}, R.W. Moore³, N. Morange¹¹⁷, D. Moreno²¹, M. Moreno Llácer⁵⁶, P. Morettini^{52a}, S. Morgenstern³², D. Mori¹⁴², T. Mori¹⁵⁵, M. Morii⁵⁸, M. Morinaga¹⁵⁵, V. Morisbak¹¹⁹, S. Moritz⁸⁴, A.K. Morley¹⁵⁰, G. Mornacchi³², J.D. Morris⁷⁷, S.S. Mortensen³⁸, L. Morvaj¹⁴⁸, M. Mosidze^{53b}, J. Moss^{143,ad}, K. Motohashi¹⁵⁷, R. Mount¹⁴³, E. Mountricha²⁷, S.V. Mouraviev^{96,*}, E.J.W. Moyse⁸⁷, S. Muanza⁸⁶, R.D. Mudd¹⁹, F. Mueller¹⁰¹, J. Mueller¹²⁵, R.S.P. Mueller¹⁰⁰, T. Mueller³⁰, D. Muenstermann⁷³, P. Mullen⁵⁵, G.A. Mullier¹⁸, F.J. Munoz Sanchez⁸⁵, J.A. Murillo Quijada¹⁹, W.J. Murray^{169,131}, H. Musheghyan⁵⁶, M. Muškinja⁷⁶, A.G. Myagkov^{130,ae}, M. Myska¹²⁸, B.P. Nachman¹⁴³, O. Nackenhorst⁵¹, K. Nagai¹²⁰, R. Nagai^{67,y}, K. Nagano⁶⁷, Y. Nagasaka⁶⁰, K. Nagata¹⁶⁰, M. Nagel⁵⁰, E. Nagy⁸⁶, A.M. Nairz³², Y. Nakahama¹⁰³, K. Nakamura⁶⁷, T. Nakamura¹⁵⁵, I. Nakano¹¹², H. Namasivayam⁴³, R.F. Naranjo Garcia⁴⁴, R. Narayan¹¹, D.I. Narrias Villar^{59a}, I. Naryshkin¹²³, T. Naumann⁴⁴, G. Navarro²¹, R. Nayyar⁷, H.A. Neal⁹⁰, P.Yu. Nechaeva⁹⁶, T.J. Neep⁸⁵, A. Negri^{121a,121b}, M. Negrini^{22a}, S. Nektarijevic¹⁰⁶, C. Nellist¹¹⁷, A. Nelson¹⁶², S. Nemecek¹²⁷, P. Nemethy¹¹⁰, A.A. Nepomuceno^{26a}, M. Nessi^{32,af}, M.S. Neubauer¹⁶⁵, M. Neumann¹⁷⁴, R.M. Neves¹¹⁰, P. Nevski²⁷, P.R. Newman¹⁹, D.H. Nguyen⁶, T. Nguyen Manh⁹⁵, R.B. Nickerson¹²⁰, R. Nicolaidou¹³⁶, J. Nielsen¹³⁷, A. Nikiforov¹⁷, V. Nikolaenko^{130,ae}, I. Nikolic-Audit⁸¹, K. Nikolopoulos¹⁹, J.K. Nilsen¹¹⁹, P. Nilsson²⁷, Y. Ninomiya¹⁵⁵, A. Nisati^{132a}, R. Nisius¹⁰¹, T. Nobe¹⁵⁵, M. Nomachi¹¹⁸, I. Nomidis³¹, T. Nooney⁷⁷, S. Norberg¹¹³, M. Nordberg³², N. Norjoharuddeen¹²⁰, O. Novgorodova⁴⁶, S. Nowak¹⁰¹, M. Nozaki⁶⁷, L. Nozka¹¹⁵, K. Ntekas¹⁰, E. Nurse⁷⁹, F. Nuti⁸⁹, F. O'grady⁷, D.C. O'Neil¹⁴², A.A. O'Rourke⁴⁴, V. O'Shea⁵⁵, F.G. Oakham^{31,d}, H. Oberlack¹⁰¹, T. Obermann²³, J. Ocariz⁸¹, A. Ochi⁶⁸, I. Ochoa³⁷, J.P. Ochoa-Ricoux^{34a}, S. Oda⁷¹, S. Odaka⁶⁷, H. Ogren⁶², A. Oh⁸⁵, S.H. Oh⁴⁷, C.C. Ohm¹⁶, H. Ohman¹⁶⁴, H. Oide³², H. Okawa¹⁶⁰, Y. Okumura¹⁵⁵, T. Okuyama⁶⁷, A. Olariu^{28b}, L.F. Oleiro Seabra^{126a}, S.A. Olivares Pino⁴⁸, D. Oliveira Damazio²⁷, A. Olszewski⁴¹, J. Olszowska⁴¹, A. Onofre^{126a,126c}, K. Onogi¹⁰³, P.U.E. Onyisi^{11,v}, M.J. Oreglia³³, Y. Oren¹⁵³, D. Orestano^{134a,134b}, N. Orlando^{61b}, R.S. Orr¹⁵⁸, B. Osculati^{52a,52b,*}, R. Ospanov⁸⁵, G. Otero y Garzon²⁹, H. Otono⁷¹, M. Ouchrif^{135d}, F. Ould-Saada¹¹⁹, A. Ouraou¹³⁶, K.P. Oussoren¹⁰⁷, Q. Ouyang^{35a}, M. Owen⁵⁵, R.E. Owen¹⁹, V.E. Ozcan^{20a}, N. Ozturk⁸, K. Pachal¹⁴², A. Pacheco Pages¹³, L. Pacheco Rodriguez¹³⁶, C. Padilla Aranda¹³, M. Pagáčová⁵⁰, S. Pagan Griso¹⁶, F. Paige²⁷, P. Pais⁸⁷, K. Pajchel¹¹⁹, G. Palacino^{159b}, S. Palazzo^{39a,39b}, S. Palestini³², M. Palka^{40b}, D. Pallin³⁶, E.St. Panagiotopoulou¹⁰, C.E. Pandini⁸¹, J.G. Panduro Vazquez⁷⁸, P. Pani^{146a,146b}, S. Panitkin²⁷, D. Pantea^{28b}, L. Paolozzi⁵¹, Th.D. Papadopoulou¹⁰, K. Papageorgiou¹⁵⁴, A. Paramonov⁶, D. Paredes Hernandez¹⁷⁵, A.J. Parker⁷³, M.A. Parker³⁰, K.A. Parker¹³⁹, F. Parodi^{52a,52b}, J.A. Parsons³⁷, U. Parzefall⁵⁰, V.R. Pascuzzi¹⁵⁸, E. Pasqualucci^{132a}, S. Passaggio^{52a}, Fr. Pastore⁷⁸, G. Pásztor^{31,ag}, S. Pataria¹⁷⁴, J.R. Pater⁸⁵, T. Pauly³², J. Pearce¹⁶⁸, B. Pearson¹¹³, L.E. Pedersen³⁸, M. Pedersen¹¹⁹, S. Pedraza Lopez¹⁶⁶, R. Pedro^{126a,126b}, S.V. Peleganchuk^{109,c}, O. Penc¹²⁷, C. Peng^{35a}, H. Peng^{35b}, J. Penwell⁶², B.S. Peralva^{26b}, M.M. Perego¹³⁶, D.V. Perepelitsa²⁷, E. Perez Codina^{159a}, L. Perini^{92a,92b}, H. Pernegger³², S. Perrella^{104a,104b}, R. Peschke⁴⁴, V.D. Peshekhonov⁶⁶, K. Peters⁴⁴, R.F.Y. Peters⁸⁵, B.A. Petersen³², T.C. Petersen³⁸, E. Petit⁵⁷, A. Petridis¹, C. Petridou¹⁵⁴, P. Petroff¹¹⁷, E. Petrolo^{132a}, M. Petrov¹²⁰, F. Petrucci^{134a,134b}, N.E. Pettersson⁸⁷, A. Peyaud¹³⁶, R. Pezoa^{34b}, P.W. Phillips¹³¹, G. Piacquadio^{143,ah}, E. Pianori¹⁶⁹, A. Picazio⁸⁷, E. Piccaro⁷⁷, M. Piccinini^{22a,22b}, M.A. Pickering¹²⁰, R. Piegai²⁹, J.E. Pilcher³³, A.D. Pilkington⁸⁵, A.W.J. Pin⁸⁵, M. Pinamonti^{163a,163c,ai}, J.L. Pinfeld³, A. Pingel³⁸, S. Pires⁸¹, H. Pirumov⁴⁴, M. Pitt¹⁷¹, L. Plazak^{144a}, M.-A. Pleier²⁷, V. Pleskot⁸⁴, E. Plotnikova⁶⁶, P. Plucinski⁹¹, D. Pluth⁶⁵, R. Poettgen^{146a,146b}, L. Poggioli¹¹⁷, D. Pohl²³, G. Polesello^{121a}, A. Poley⁴⁴, A. Policicchio^{39a,39b}, R. Polifka¹⁵⁸, A. Polini^{22a}, C.S. Pollard⁵⁵, V. Polychronakos²⁷, K. Pommès³², L. Pontecorvo^{132a}, B.G. Pope⁹¹, G.A. Popeneciu^{28c}, A. Poppleton³², S. Pospisil¹²⁸, K. Potamianos¹⁶, I.N. Potrap⁶⁶, C.J. Potter³⁰, C.T. Potter¹¹⁶, G. Poulard³², J. Poveda³², V. Pozdnyakov⁶⁶,

M.E. Pozo Astigarraga³², P. Pralavorio⁸⁶, A. Pranko¹⁶, S. Prell⁶⁵, D. Price⁸⁵, L.E. Price⁶,
M. Primavera^{74a}, S. Prince⁸⁸, K. Prokofiev^{61c}, F. Prokoshin^{34b}, S. Protopopescu²⁷, J. Proudfoot⁶,
M. Przybycien^{40a}, D. Puddu^{134a,134b}, M. Purohit^{27,aj}, P. Puzo¹¹⁷, J. Qian⁹⁰, G. Qin⁵⁵, Y. Qin⁸⁵,
A. Quadt⁵⁶, W.B. Quayle^{163a,163b}, M. Queitsch-Maitland⁸⁵, D. Quilty⁵⁵, S. Raddum¹¹⁹, V. Radeka²⁷,
V. Radescu¹²⁰, S.K. Radhakrishnan¹⁴⁸, P. Radloff¹¹⁶, P. Rados⁸⁹, F. Ragusa^{92a,92b}, G. Rahal¹⁷⁷,
J.A. Raine⁸⁵, S. Rajagopalan²⁷, M. Rammensee³², C. Rangel-Smith¹⁶⁴, M.G. Ratti^{92a,92b},
F. Rauscher¹⁰⁰, S. Rave⁸⁴, T. Ravenscroft⁵⁵, I. Ravinovich¹⁷¹, M. Raymond³², A.L. Read¹¹⁹,
N.P. Readioff⁷⁵, M. Reale^{74a,74b}, D.M. Rebuffi^{121a,121b}, A. Redelbach¹⁷³, G. Redlinger²⁷, R. Reece¹³⁷,
K. Reeves⁴³, L. Rehnisch¹⁷, J. Reichert¹²², H. Reisin²⁹, C. Rembser³², H. Ren^{35a}, M. Rescigno^{132a},
S. Resconi^{92a}, O.L. Rezanova^{109,c}, P. Reznicek¹²⁹, R. Rezvani⁹⁵, R. Richter¹⁰¹, S. Richter⁷⁹,
E. Richter-Was^{40b}, O. Ricken²³, M. Ridel⁸¹, P. Rieck¹⁷, C.J. Riegel¹⁷⁴, J. Rieger⁵⁶, O. Rifki¹¹³,
M. Rijssenbeek¹⁴⁸, A. Rimoldi^{121a,121b}, M. Rimoldi¹⁸, L. Rinaldi^{22a}, B. Ristić⁵¹, E. Ritsch³², I. Riu¹³,
F. Rizatdinova¹¹⁴, E. Rizvi⁷⁷, C. Rizzi¹³, S.H. Robertson^{88,l}, A. Robichaud-Veronneau⁸⁸, D. Robinson³⁰,
J.E.M. Robinson⁴⁴, A. Robson⁵⁵, C. Roda^{124a,124b}, Y. Rodina⁸⁶, A. Rodriguez Perez¹³,
D. Rodriguez Rodriguez¹⁶⁶, S. Roe³², C.S. Rogan⁵⁸, O. Røhne¹¹⁹, A. Romaniouk⁹⁸, M. Romano^{22a,22b},
S.M. Romano Saez³⁶, E. Romero Adam¹⁶⁶, N. Rompotis¹³⁸, M. Ronzani⁵⁰, L. Roos⁸¹, E. Ros¹⁶⁶,
S. Rosati^{132a}, K. Rosbach⁵⁰, P. Rose¹³⁷, O. Rosenthal¹⁴¹, N.-A. Rosien⁵⁶, V. Rossetti^{146a,146b},
E. Rossi^{104a,104b}, L.P. Rossi^{52a}, J.H.N. Rosten³⁰, R. Rosten¹³⁸, M. Rotaru^{28b}, I. Roth¹⁷¹, J. Rothberg¹³⁸,
D. Rousseau¹¹⁷, C.R. Royon¹³⁶, A. Rozanov⁸⁶, Y. Rozen¹⁵², X. Ruan^{145c}, F. Rubbo¹⁴³,
M.S. Rudolph¹⁵⁸, F. Rühr⁵⁰, A. Ruiz-Martinez³¹, Z. Rurikova⁵⁰, N.A. Rusakovich⁶⁶, A. Ruschke¹⁰⁰,
H.L. Russell¹³⁸, J.P. Rutherford⁷, N. Ruthmann³², Y.F. Ryabov¹²³, M. Rybar¹⁶⁵, G. Rybkin¹¹⁷, S. Ryu⁶,
A. Ryzhov¹³⁰, G.F. Rzehorz⁵⁶, A.F. Saavedra¹⁵⁰, G. Sabato¹⁰⁷, S. Sacerdoti²⁹, H.F.-W. Sadrozinski¹³⁷,
R. Sadykov⁶⁶, F. Safai Tehrani^{132a}, P. Saha¹⁰⁸, M. Sahinsoy^{59a}, M. Saimpert¹³⁶, T. Saito¹⁵⁵,
H. Sakamoto¹⁵⁵, Y. Sakurai¹⁷⁰, G. Salamanna^{134a,134b}, A. Salamon^{133a,133b}, J.E. Salazar Loyola^{34b},
D. Salek¹⁰⁷, P.H. Sales De Bruin¹³⁸, D. Salihagic¹⁰¹, A. Salnikov¹⁴³, J. Salt¹⁶⁶, D. Salvatore^{39a,39b},
F. Salvatore¹⁴⁹, A. Salvucci^{61a}, A. Salzburger³², D. Sammel⁵⁰, D. Sampsonidis¹⁵⁴, A. Sanchez^{104a,104b},
J. Sánchez¹⁶⁶, V. Sanchez Martinez¹⁶⁶, H. Sandaker¹¹⁹, R.L. Sandbach⁷⁷, H.G. Sander⁸⁴,
M. Sandhoff¹⁷⁴, C. Sandoval²¹, R. Sandstroem¹⁰¹, D.P.C. Sankey¹³¹, M. Sannino^{52a,52b}, A. Sansoni⁴⁹,
C. Santoni³⁶, R. Santonico^{133a,133b}, H. Santos^{126a}, I. Santoyo Castillo¹⁴⁹, K. Sapp¹²⁵, A. Saponov⁶⁶,
J.G. Saraiva^{126a,126d}, B. Sarrazin²³, O. Sasaki⁶⁷, Y. Sasaki¹⁵⁵, K. Sato¹⁶⁰, G. Sauvage^{5,*}, E. Sauvan⁵,
G. Savage⁷⁸, P. Savard^{158,d}, N. Savic¹⁰¹, C. Sawyer¹³¹, L. Sawyer^{80,q}, J. Saxon³³, C. Sbarra^{22a},
A. Sbrizzi^{22a,22b}, T. Scanlon⁷⁹, D.A. Scannicchio¹⁶², M. Scarcella¹⁵⁰, V. Scarfone^{39a,39b},
J. Schaarschmidt¹⁷¹, P. Schacht¹⁰¹, B.M. Schachtner¹⁰⁰, D. Schaefer³², L. Schaefer¹²², R. Schaefer⁴⁴,
J. Schaeffer⁸⁴, S. Schaepe²³, S. Schaezel^{59b}, U. Schäfer⁸⁴, A.C. Schaffer¹¹⁷, D. Schaile¹⁰⁰,
R.D. Schamberger¹⁴⁸, V. Scharf^{59a}, V.A. Schegelsky¹²³, D. Scheirich¹²⁹, M. Schernau¹⁶²,
C. Schiavi^{52a,52b}, S. Schier¹³⁷, C. Schillo⁵⁰, M. Schioppa^{39a,39b}, S. Schlenker³²,
K.R. Schmidt-Sommerfeld¹⁰¹, K. Schmieden³², C. Schmitt⁸⁴, S. Schmitt⁴⁴, S. Schmitz⁸⁴,
B. Schneider^{159a}, U. Schnoor⁵⁰, L. Schoeffel¹³⁶, A. Schoening^{59b}, B.D. Schoenrock⁹¹, E. Schopf²³,
M. Schott⁸⁴, J. Schovancova⁸, S. Schramm⁵¹, M. Schreyer¹⁷³, N. Schuh⁸⁴, A. Schulte⁸⁴,
M.J. Schultens²³, H.-C. Schultz-Coulon^{59a}, H. Schulz¹⁷, M. Schumacher⁵⁰, B.A. Schumm¹³⁷,
Ph. Schune¹³⁶, A. Schwartzman¹⁴³, T.A. Schwarz⁹⁰, H. Schweiger⁸⁵, Ph. Schwemling¹³⁶,
R. Schwienhorst⁹¹, J. Schwindling¹³⁶, T. Schwindt²³, G. Sciolla²⁵, F. Scuri^{124a,124b}, F. Scutti⁸⁹,
J. Searcy⁹⁰, P. Seema²³, S.C. Seidel¹⁰⁵, A. Seiden¹³⁷, F. Seifert¹²⁸, J.M. Seixas^{26a}, G. Sekhniaidze^{104a},
K. Sekhon⁹⁰, S.J. Sekula⁴², D.M. Seliverstov^{123,*}, N. Semprini-Cesari^{22a,22b}, C. Serfon¹¹⁹, L. Serin¹¹⁷,
L. Serkin^{163a,163b}, M. Sessa^{134a,134b}, R. Seuster¹⁶⁸, H. Severini¹¹³, T. Sfiligoi⁷⁶, F. Sforza³², A. Sfyrla⁵¹,
E. Shabalina⁵⁶, N.W. Shaikh^{146a,146b}, L.Y. Shan^{35a}, R. Shang¹⁶⁵, J.T. Shank²⁴, M. Shapiro¹⁶,
P.B. Shatalov⁹⁷, K. Shaw^{163a,163b}, S.M. Shaw⁸⁵, A. Shcherbakova^{146a,146b}, C.Y. Shehu¹⁴⁹, P. Sherwood⁷⁹,

L. Shi^{151.ak}, S. Shimizu⁶⁸, C.O. Shimmin¹⁶², M. Shimojima¹⁰², M. Shiyakova^{66.al}, A. Shmeleva⁹⁶, D. Shoaleh Saadi⁹⁵, M.J. Shochet³³, S. Shojaii^{92a,92b}, S. Shrestha¹¹¹, E. Shulga⁹⁸, M.A. Shupe⁷, P. Sicho¹²⁷, A.M. Sickles¹⁶⁵, P.E. Sidebo¹⁴⁷, O. Sidiropoulou¹⁷³, D. Sidorov¹¹⁴, A. Sidoti^{22a,22b}, F. Siegert⁴⁶, Dj. Sijacki¹⁴, J. Silva^{126a,126d}, S.B. Silverstein^{146a}, V. Simak¹²⁸, Lj. Simic¹⁴, S. Simion¹¹⁷, E. Simioni⁸⁴, B. Simmons⁷⁹, D. Simon³⁶, M. Simon⁸⁴, P. Sinervo¹⁵⁸, N.B. Sinev¹¹⁶, M. Sioli^{22a,22b}, G. Siragusa¹⁷³, S.Yu. Sivoklokov⁹⁹, J. Sjölin^{146a,146b}, M.B. Skinner⁷³, H.P. Skottowe⁵⁸, P. Skubic¹¹³, M. Slater¹⁹, T. Slavicek¹²⁸, M. Slawinska¹⁰⁷, K. Sliwa¹⁶¹, R. Slovak¹²⁹, V. Smakhtin¹⁷¹, B.H. Smart⁵, L. Smestad¹⁵, J. Smiesko^{144a}, S.Yu. Smirnov⁹⁸, Y. Smirnov⁹⁸, L.N. Smirnova^{99.am}, O. Smirnova⁸², M.N.K. Smith³⁷, R.W. Smith³⁷, M. Smizanska⁷³, K. Smolek¹²⁸, A.A. Snesev⁹⁶, S. Snyder²⁷, R. Sobie^{168.l}, F. Socher⁴⁶, A. Soffer¹⁵³, D.A. Soh¹⁵¹, G. Sokhrannyi⁷⁶, C.A. Solans Sanchez³², M. Solar¹²⁸, E.Yu. Soldatov⁹⁸, U. Soldevila¹⁶⁶, A.A. Solodkov¹³⁰, A. Soloshenko⁶⁶, O.V. Solovyanov¹³⁰, V. Solovyev¹²³, P. Sommer⁵⁰, H. Son¹⁶¹, H.Y. Song^{35b.an}, A. Sood¹⁶, A. Sopczak¹²⁸, V. Sopko¹²⁸, V. Sorin¹³, D. Sosa^{59b}, C.L. Sotiropoulou^{124a,124b}, R. Soualah^{163a,163c}, A.M. Soukharev^{109.c}, D. South⁴⁴, B.C. Sowden⁷⁸, S. Spagnolo^{74a,74b}, M. Spalla^{124a,124b}, M. Spangenberg¹⁶⁹, F. Spanò⁷⁸, D. Sperlich¹⁷, F. Spettel¹⁰¹, R. Spighi^{22a}, G. Spigo³², L.A. Spiller⁸⁹, M. Spousta¹²⁹, R.D. St. Denis^{55,*}, A. Stabile^{92a}, R. Stamen^{59a}, S. Stamm¹⁷, E. Stanecka⁴¹, R.W. Stanek⁶, C. Stanescu^{134a}, M. Stanescu-Bellu⁴⁴, M.M. Stanitzki⁴⁴, S. Stapnes¹¹⁹, E.A. Starchenko¹³⁰, G.H. Stark³³, J. Stark⁵⁷, P. Staroba¹²⁷, P. Starovoitov^{59a}, S. Stärz³², R. Staszewski⁴¹, P. Steinberg²⁷, B. Stelzer¹⁴², H.J. Stelzer³², O. Stelzer-Chilton^{159a}, H. Stenzel⁵⁴, G.A. Stewart⁵⁵, J.A. Stillings²³, M.C. Stockton⁸⁸, M. Stoebe⁸⁸, G. Stoicea^{28b}, P. Stolte⁵⁶, S. Stonjek¹⁰¹, A.R. Stradling⁸, A. Straessner⁴⁶, M.E. Stramaglia¹⁸, J. Strandberg¹⁴⁷, S. Strandberg^{146a,146b}, A. Strandlie¹¹⁹, M. Strauss¹¹³, P. Strizenc^{144b}, R. Ströhmer¹⁷³, D.M. Strom¹¹⁶, R. Stroynowski⁴², A. Strubig¹⁰⁶, S.A. Stucci²⁷, B. Stugu¹⁵, N.A. Styles⁴⁴, D. Su¹⁴³, J. Su¹²⁵, S. Suchek^{59a}, Y. Sugaya¹¹⁸, M. Suk¹²⁸, V.V. Sulin⁹⁶, S. Sultansoy^{4c}, T. Sumida⁶⁹, S. Sun⁵⁸, X. Sun^{35a}, J.E. Sundermann⁵⁰, K. Suruliz¹⁴⁹, G. Susinno^{39a,39b}, M.R. Sutton¹⁴⁹, S. Suzuki⁶⁷, M. Svatos¹²⁷, M. Swiatlowski³³, I. Sykora^{144a}, T. Sykora¹²⁹, D. Ta⁵⁰, C. Taccini^{134a,134b}, K. Tackmann⁴⁴, J. Taenzer¹⁵⁸, A. Taffard¹⁶², R. Tafirout^{159a}, N. Taiblum¹⁵³, H. Takai²⁷, R. Takashima⁷⁰, T. Takeshita¹⁴⁰, Y. Takubo⁶⁷, M. Talby⁸⁶, A.A. Talyshv^{109.c}, K.G. Tan⁸⁹, J. Tanaka¹⁵⁵, M. Tanaka¹⁵⁷, R. Tanaka¹¹⁷, S. Tanaka⁶⁷, B.B. Tannenwald¹¹¹, S. Tapia Araya^{34b}, S. Tapprogge⁸⁴, S. Tarem¹⁵², G.F. Tartarelli^{92a}, P. Tas¹²⁹, M. Tasevsky¹²⁷, T. Tashiro⁶⁹, E. Tassi^{39a,39b}, A. Tavares Delgado^{126a,126b}, Y. Tayalati^{135e}, A.C. Taylor¹⁰⁵, G.N. Taylor⁸⁹, P.T.E. Taylor⁸⁹, W. Taylor^{159b}, F.A. Teischinger³², P. Teixeira-Dias⁷⁸, K.K. Temming⁵⁰, D. Temple¹⁴², H. Ten Kate³², P.K. Teng¹⁵¹, J.J. Teoh¹¹⁸, F. Tepel¹⁷⁴, S. Terada⁶⁷, K. Terashi¹⁵⁵, J. Terron⁸³, S. Terzo¹³, M. Testa⁴⁹, R.J. Teuscher^{158.l}, T. Thevenaux-Pelzer⁸⁶, J.P. Thomas¹⁹, J. Thomas-Wilsker⁷⁸, E.N. Thompson³⁷, P.D. Thompson¹⁹, A.S. Thompson⁵⁵, L.A. Thomsen¹⁷⁵, E. Thomson¹²², M. Thomson³⁰, M.J. Tibbetts¹⁶, R.E. Ticse Torres⁸⁶, V.O. Tikhomirov^{96,ao}, Yu.A. Tikhonov^{109.c}, S. Timoshenko⁹⁸, P. Tipton¹⁷⁵, S. Tisserant⁸⁶, K. Todome¹⁵⁷, T. Todorov^{5,*}, S. Todorova-Nova¹²⁹, J. Tojo⁷¹, S. Tokár^{144a}, K. Tokushuku⁶⁷, E. Tolley⁵⁸, L. Tomlinson⁸⁵, M. Tomoto¹⁰³, L. Tompkins^{143.ap}, K. Toms¹⁰⁵, B. Tong⁵⁸, E. Torrence¹¹⁶, H. Torres¹⁴², E. Torró Pastor¹³⁸, J. Toth^{86.aq}, F. Touchard⁸⁶, D.R. Tovey¹³⁹, T. Trefzger¹⁷³, A. Tricoli²⁷, I.M. Trigger^{159a}, S. Trincaz-Duvoid⁸¹, M.F. Tripiana¹³, W. Trischuk¹⁵⁸, B. Trocme⁵⁷, A. Trofymov⁴⁴, C. Troncon^{92a}, M. Trotter-McDonald¹⁶, M. Trovatelli¹⁶⁸, L. Truong^{163a,163c}, M. Trzebinski⁴¹, A. Trzupek⁴¹, J.C-L. Tseng¹²⁰, P.V. Tsiarehka⁹³, G. Tsipolitis¹⁰, N. Tsirintanis⁹, S. Tsiskaridze¹³, V. Tsiskaridze⁵⁰, E.G. Tskhadadze^{53a}, K.M. Tsui^{61a}, I.I. Tsukerman⁹⁷, V. Tsulaia¹⁶, S. Tsuno⁶⁷, D. Tsybychev¹⁴⁸, Y. Tu^{61b}, A. Tudorache^{28b}, V. Tudorache^{28b}, A.N. Tuna⁵⁸, S.A. Tuppiti^{22a,22b}, S. Turchikhin⁶⁶, D. Turecek¹²⁸, D. Turgeman¹⁷¹, R. Turra^{92a,92b}, A.J. Turvey⁴², P.M. Tuts³⁷, M. Tyndel¹³¹, G. Ucchielli^{22a,22b}, I. Ueda¹⁵⁵, M. Ughetto^{146a,146b}, F. Ukegawa¹⁶⁰, G. Unal³², A. Undrus²⁷, G. Unel¹⁶², F.C. Ungaro⁸⁹, Y. Unno⁶⁷, C. Unverdorben¹⁰⁰, J. Urban^{144b}, P. Urquijo⁸⁹, P. Urrejola⁸⁴, G. Usai⁸, A. Usanova⁶³, L. Vacavant⁸⁶, V. Vacek¹²⁸, B. Vachon⁸⁸, C. Valderanis¹⁰⁰,

E. Valdes Santurio^{146a,146b}, N. Valencic¹⁰⁷, S. Valentinetti^{22a,22b}, A. Valero¹⁶⁶, L. Valery¹³, S. Valkar¹²⁹, J.A. Valls Ferrer¹⁶⁶, W. Van Den Wollenberg¹⁰⁷, P.C. Van Der Deijl¹⁰⁷, H. van der Graaf¹⁰⁷, N. van Eldik¹⁵², P. van Gemmeren⁶, J. Van Nieuwkoop¹⁴², I. van Vulpen¹⁰⁷, M.C. van Woerden³², M. Vanadia^{132a,132b}, W. Vandelli³², R. Vanguri¹²², A. Vaniachine¹³⁰, P. Vankov¹⁰⁷, G. Vardanyan¹⁷⁶, R. Vari^{132a}, E.W. Varnes⁷, T. Varol⁴², D. Varouchas⁸¹, A. Vartapetian⁸, K.E. Varvell¹⁵⁰, J.G. Vasquez¹⁷⁵, F. Vazeille³⁶, T. Vazquez Schroeder⁸⁸, J. Veatch⁵⁶, V. Veeraraghavan⁷, L.M. Veloce¹⁵⁸, F. Veloso^{126a,126c}, S. Veneziano^{132a}, A. Ventura^{74a,74b}, M. Venturi¹⁶⁸, N. Venturi¹⁵⁸, A. Venturini²⁵, V. Vercesi^{121a}, M. Verducci^{132a,132b}, W. Verkerke¹⁰⁷, J.C. Vermeulen¹⁰⁷, A. Vest^{46,ar}, M.C. Vetterli^{142,d}, O. Viazlo⁸², I. Vichou^{165,*}, T. Vickey¹³⁹, O.E. Vickey Boeriu¹³⁹, G.H.A. Viehhauser¹²⁰, S. Viel¹⁶, L. Vigani¹²⁰, M. Villa^{22a,22b}, M. Villaplana Perez^{92a,92b}, E. Vilucchi⁴⁹, M.G. Vincter³¹, V.B. Vinogradov⁶⁶, C. Vittori^{22a,22b}, I. Vivarelli¹⁴⁹, S. Vlachos¹⁰, M. Vlasak¹²⁸, M. Vogel¹⁷⁴, P. Vokac¹²⁸, G. Volpi^{124a,124b}, M. Volpi⁸⁹, H. von der Schmitt¹⁰¹, E. von Toerne²³, V. Vorobel¹²⁹, K. Vorobev⁹⁸, M. Vos¹⁶⁶, R. Voss³², J.H. Vossebeld⁷⁵, N. Vranjes¹⁴, M. Vranjes Milosavljevic¹⁴, V. Vrba¹²⁷, M. Vreeswijk¹⁰⁷, R. Vuillermet³², I. Vukotic³³, Z. Vykydal¹²⁸, P. Wagner²³, W. Wagner¹⁷⁴, H. Wahlberg⁷², S. Wahrmond⁴⁶, J. Wakabayashi¹⁰³, J. Walder⁷³, R. Walker¹⁰⁰, W. Walkowiak¹⁴¹, V. Wallangen^{146a,146b}, C. Wang^{35c}, C. Wang^{35d,86}, F. Wang¹⁷², H. Wang¹⁶, H. Wang⁴², J. Wang⁴⁴, J. Wang¹⁵⁰, K. Wang⁸⁸, R. Wang⁶, S.M. Wang¹⁵¹, T. Wang²³, T. Wang³⁷, W. Wang^{35b}, X. Wang¹⁷⁵, C. Wanotayaroj¹¹⁶, A. Warburton⁸⁸, C.P. Ward³⁰, D.R. Wardrope⁷⁹, A. Washbrook⁴⁸, P.M. Watkins¹⁹, A.T. Watson¹⁹, M.F. Watson¹⁹, G. Watts¹³⁸, S. Watts⁸⁵, B.M. Waugh⁷⁹, S. Webb⁸⁴, M.S. Weber¹⁸, S.W. Weber¹⁷³, J.S. Webster⁶, A.R. Weidberg¹²⁰, B. Weinert⁶², J. Weingarten⁵⁶, C. Weiser⁵⁰, H. Weits¹⁰⁷, P.S. Wells³², T. Wenaus²⁷, T. Wengler³², S. Wenig³², N. Wermes²³, M. Werner⁵⁰, M.D. Werner⁶⁵, P. Werner³², M. Wessels^{59a}, J. Wetter¹⁶¹, K. Whalen¹¹⁶, N.L. Whallon¹³⁸, A.M. Wharton⁷³, A. White⁸, M.J. White¹, R. White^{34b}, D. Whiteson¹⁶², F.J. Wickens¹³¹, W. Wiedenmann¹⁷², M. Wielers¹³¹, P. Wienemann²³, C. Wiglesworth³⁸, L.A.M. Wiik-Fuchs²³, A. Wildauer¹⁰¹, F. Wilk⁸⁵, H.G. Wilkens³², H.H. Williams¹²², S. Williams¹⁰⁷, C. Willis⁹¹, S. Willocq⁸⁷, J.A. Wilson¹⁹, I. Wingerter-Seez⁵, F. Winklmeier¹¹⁶, O.J. Winston¹⁴⁹, B.T. Winter²³, M. Wittgen¹⁴³, J. Wittkowski¹⁰⁰, T.M.H. Wolf¹⁰⁷, M.W. Wolter⁴¹, H. Wolters^{126a,126c}, S.D. Worm¹³¹, B.K. Wosiek⁴¹, J. Wotschack³², M.J. Woudstra⁸⁵, K.W. Wozniak⁴¹, M. Wu⁵⁷, M. Wu³³, S.L. Wu¹⁷², X. Wu⁵¹, Y. Wu⁹⁰, T.R. Wyatt⁸⁵, B.M. Wynne⁴⁸, S. Xella³⁸, D. Xu^{35a}, L. Xu²⁷, B. Yabsley¹⁵⁰, S. Yacoob^{145a}, D. Yamaguchi¹⁵⁷, Y. Yamaguchi¹¹⁸, A. Yamamoto⁶⁷, S. Yamamoto¹⁵⁵, T. Yamanaka¹⁵⁵, K. Yamauchi¹⁰³, Y. Yamazaki⁶⁸, Z. Yan²⁴, H. Yang^{35e}, H. Yang¹⁷², Y. Yang¹⁵¹, Z. Yang¹⁵, W-M. Yao¹⁶, Y.C. Yap⁸¹, Y. Yasu⁶⁷, E. Yatsenko⁵, K.H. Yau Wong²³, J. Ye⁴², S. Ye²⁷, I. Yeletskikh⁶⁶, A.L. Yen⁵⁸, E. Yildirim⁸⁴, K. Yorita¹⁷⁰, R. Yoshida⁶, K. Yoshihara¹²², C. Young¹⁴³, C.J.S. Young³², S. Youssef²⁴, D.R. Yu¹⁶, J. Yu⁸, J.M. Yu⁹⁰, J. Yu⁶⁵, L. Yuan⁶⁸, S.P.Y. Yuen²³, I. Yusuff^{30,as}, B. Zabinski⁴¹, R. Zaidan^{35d}, A.M. Zaitsev^{130,ae}, N. Zakharchuk⁴⁴, J. Zalieckas¹⁵, A. Zaman¹⁴⁸, S. Zambito⁵⁸, L. Zanello^{132a,132b}, D. Zanzi⁸⁹, C. Zeitnitz¹⁷⁴, M. Zeman¹²⁸, A. Zemla^{40a}, J.C. Zeng¹⁶⁵, Q. Zeng¹⁴³, K. Zengel²⁵, O. Zenin¹³⁰, T. Ženiš^{144a}, D. Zerwas¹¹⁷, D. Zhang⁹⁰, F. Zhang¹⁷², G. Zhang^{35b,an}, H. Zhang^{35c}, J. Zhang⁶, L. Zhang⁵⁰, R. Zhang²³, R. Zhang^{35b,at}, X. Zhang^{35d}, Z. Zhang¹¹⁷, X. Zhao⁴², Y. Zhao^{35d}, Z. Zhao^{35b}, A. Zhemchugov⁶⁶, J. Zhong¹²⁰, B. Zhou⁹⁰, C. Zhou⁴⁷, L. Zhou³⁷, L. Zhou⁴², M. Zhou¹⁴⁸, N. Zhou^{35f}, C.G. Zhu^{35d}, H. Zhu^{35a}, J. Zhu⁹⁰, Y. Zhu^{35b}, X. Zhuang^{35a}, K. Zhukov⁹⁶, A. Zibell¹⁷³, D. Zieminska⁶², N.I. Zimine⁶⁶, C. Zimmermann⁸⁴, S. Zimmermann⁵⁰, Z. Zinonos⁵⁶, M. Zinser⁸⁴, M. Ziolkowski¹⁴¹, L. Živković¹⁴, G. Zobernig¹⁷², A. Zoccoli^{22a,22b}, M. zur Nedden¹⁷, L. Zwalinski³².

¹ Department of Physics, University of Adelaide, Adelaide, Australia

² Physics Department, SUNY Albany, Albany NY, United States of America

³ Department of Physics, University of Alberta, Edmonton AB, Canada

⁴ (a) Department of Physics, Ankara University, Ankara; (b) Istanbul Aydin University, Istanbul; (c)

Division of Physics, TOBB University of Economics and Technology, Ankara, Turkey

⁵ LAPP, CNRS/IN2P3 and Université Savoie Mont Blanc, Annecy-le-Vieux, France

⁶ High Energy Physics Division, Argonne National Laboratory, Argonne IL, United States of America

⁷ Department of Physics, University of Arizona, Tucson AZ, United States of America

⁸ Department of Physics, The University of Texas at Arlington, Arlington TX, United States of America

⁹ Physics Department, University of Athens, Athens, Greece

¹⁰ Physics Department, National Technical University of Athens, Zografou, Greece

¹¹ Department of Physics, The University of Texas at Austin, Austin TX, United States of America

¹² Institute of Physics, Azerbaijan Academy of Sciences, Baku, Azerbaijan

¹³ Institut de Física d'Altes Energies (IFAE), The Barcelona Institute of Science and Technology, Barcelona, Spain, Spain

¹⁴ Institute of Physics, University of Belgrade, Belgrade, Serbia

¹⁵ Department for Physics and Technology, University of Bergen, Bergen, Norway

¹⁶ Physics Division, Lawrence Berkeley National Laboratory and University of California, Berkeley CA, United States of America

¹⁷ Department of Physics, Humboldt University, Berlin, Germany

¹⁸ Albert Einstein Center for Fundamental Physics and Laboratory for High Energy Physics, University of Bern, Bern, Switzerland

¹⁹ School of Physics and Astronomy, University of Birmingham, Birmingham, United Kingdom

²⁰ ^(a) Department of Physics, Bogazici University, Istanbul; ^(b) Department of Physics Engineering, Gaziantep University, Gaziantep; ^(d) Istanbul Bilgi University, Faculty of Engineering and Natural Sciences, Istanbul, Turkey; ^(e) Bahcesehir University, Faculty of Engineering and Natural Sciences, Istanbul, Turkey, Turkey

²¹ Centro de Investigaciones, Universidad Antonio Narino, Bogota, Colombia

²² ^(a) INFN Sezione di Bologna; ^(b) Dipartimento di Fisica e Astronomia, Università di Bologna, Bologna, Italy

²³ Physikalisches Institut, University of Bonn, Bonn, Germany

²⁴ Department of Physics, Boston University, Boston MA, United States of America

²⁵ Department of Physics, Brandeis University, Waltham MA, United States of America

²⁶ ^(a) Universidade Federal do Rio De Janeiro COPPE/EE/IF, Rio de Janeiro; ^(b) Electrical Circuits Department, Federal University of Juiz de Fora (UFJF), Juiz de Fora; ^(c) Federal University of Sao Joao del Rei (UFSJ), Sao Joao del Rei; ^(d) Instituto de Fisica, Universidade de Sao Paulo, Sao Paulo, Brazil

²⁷ Physics Department, Brookhaven National Laboratory, Upton NY, United States of America

²⁸ ^(a) Transilvania University of Brasov, Brasov, Romania; ^(b) National Institute of Physics and Nuclear Engineering, Bucharest; ^(c) National Institute for Research and Development of Isotopic and Molecular Technologies, Physics Department, Cluj Napoca; ^(d) University Politehnica Bucharest, Bucharest; ^(e) West University in Timisoara, Timisoara, Romania

²⁹ Departamento de Física, Universidad de Buenos Aires, Buenos Aires, Argentina

³⁰ Cavendish Laboratory, University of Cambridge, Cambridge, United Kingdom

³¹ Department of Physics, Carleton University, Ottawa ON, Canada

³² CERN, Geneva, Switzerland

³³ Enrico Fermi Institute, University of Chicago, Chicago IL, United States of America

³⁴ ^(a) Departamento de Física, Pontificia Universidad Católica de Chile, Santiago; ^(b) Departamento de Física, Universidad Técnica Federico Santa María, Valparaíso, Chile

³⁵ ^(a) Institute of High Energy Physics, Chinese Academy of Sciences, Beijing; ^(b) Department of Modern Physics, University of Science and Technology of China, Anhui; ^(c) Department of Physics, Nanjing University, Jiangsu; ^(d) School of Physics, Shandong University, Shandong; ^(e) Department of

Physics and Astronomy, Shanghai Key Laboratory for Particle Physics and Cosmology, Shanghai Jiao Tong University, Shanghai; (also affiliated with PKU-CHEP); ^(f) Physics Department, Tsinghua University, Beijing 100084, China

³⁶ Laboratoire de Physique Corpusculaire, Clermont Université and Université Blaise Pascal and CNRS/IN2P3, Clermont-Ferrand, France

³⁷ Nevis Laboratory, Columbia University, Irvington NY, United States of America

³⁸ Niels Bohr Institute, University of Copenhagen, Kobenhavn, Denmark

³⁹ ^(a) INFN Gruppo Collegato di Cosenza, Laboratori Nazionali di Frascati; ^(b) Dipartimento di Fisica, Università della Calabria, Rende, Italy

⁴⁰ ^(a) AGH University of Science and Technology, Faculty of Physics and Applied Computer Science, Krakow; ^(b) Marian Smoluchowski Institute of Physics, Jagiellonian University, Krakow, Poland

⁴¹ Institute of Nuclear Physics Polish Academy of Sciences, Krakow, Poland

⁴² Physics Department, Southern Methodist University, Dallas TX, United States of America

⁴³ Physics Department, University of Texas at Dallas, Richardson TX, United States of America

⁴⁴ DESY, Hamburg and Zeuthen, Germany

⁴⁵ Lehrstuhl für Experimentelle Physik IV, Technische Universität Dortmund, Dortmund, Germany

⁴⁶ Institut für Kern- und Teilchenphysik, Technische Universität Dresden, Dresden, Germany

⁴⁷ Department of Physics, Duke University, Durham NC, United States of America

⁴⁸ SUPA - School of Physics and Astronomy, University of Edinburgh, Edinburgh, United Kingdom

⁴⁹ INFN Laboratori Nazionali di Frascati, Frascati, Italy

⁵⁰ Fakultät für Mathematik und Physik, Albert-Ludwigs-Universität, Freiburg, Germany

⁵¹ Section de Physique, Université de Genève, Geneva, Switzerland

⁵² ^(a) INFN Sezione di Genova; ^(b) Dipartimento di Fisica, Università di Genova, Genova, Italy

⁵³ ^(a) E. Andronikashvili Institute of Physics, Iv. Javakishvili Tbilisi State University, Tbilisi; ^(b) High Energy Physics Institute, Tbilisi State University, Tbilisi, Georgia

⁵⁴ II Physikalisches Institut, Justus-Liebig-Universität Giessen, Giessen, Germany

⁵⁵ SUPA - School of Physics and Astronomy, University of Glasgow, Glasgow, United Kingdom

⁵⁶ II Physikalisches Institut, Georg-August-Universität, Göttingen, Germany

⁵⁷ Laboratoire de Physique Subatomique et de Cosmologie, Université Grenoble-Alpes, CNRS/IN2P3, Grenoble, France

⁵⁸ Laboratory for Particle Physics and Cosmology, Harvard University, Cambridge MA, United States of America

⁵⁹ ^(a) Kirchhoff-Institut für Physik, Ruprecht-Karls-Universität Heidelberg, Heidelberg; ^(b) Physikalisches Institut, Ruprecht-Karls-Universität Heidelberg, Heidelberg; ^(c) ZITI Institut für technische Informatik, Ruprecht-Karls-Universität Heidelberg, Mannheim, Germany

⁶⁰ Faculty of Applied Information Science, Hiroshima Institute of Technology, Hiroshima, Japan

⁶¹ ^(a) Department of Physics, The Chinese University of Hong Kong, Shatin, N.T., Hong Kong; ^(b) Department of Physics, The University of Hong Kong, Hong Kong; ^(c) Department of Physics, The Hong Kong University of Science and Technology, Clear Water Bay, Kowloon, Hong Kong, China

⁶² Department of Physics, Indiana University, Bloomington IN, United States of America

⁶³ Institut für Astro- und Teilchenphysik, Leopold-Franzens-Universität, Innsbruck, Austria

⁶⁴ University of Iowa, Iowa City IA, United States of America

⁶⁵ Department of Physics and Astronomy, Iowa State University, Ames IA, United States of America

⁶⁶ Joint Institute for Nuclear Research, JINR Dubna, Dubna, Russia

⁶⁷ KEK, High Energy Accelerator Research Organization, Tsukuba, Japan

⁶⁸ Graduate School of Science, Kobe University, Kobe, Japan

⁶⁹ Faculty of Science, Kyoto University, Kyoto, Japan

- 70 Kyoto University of Education, Kyoto, Japan
- 71 Department of Physics, Kyushu University, Fukuoka, Japan
- 72 Instituto de Física La Plata, Universidad Nacional de La Plata and CONICET, La Plata, Argentina
- 73 Physics Department, Lancaster University, Lancaster, United Kingdom
- 74 ^(a) INFN Sezione di Lecce; ^(b) Dipartimento di Matematica e Fisica, Università del Salento, Lecce, Italy
- 75 Oliver Lodge Laboratory, University of Liverpool, Liverpool, United Kingdom
- 76 Department of Physics, Jožef Stefan Institute and University of Ljubljana, Ljubljana, Slovenia
- 77 School of Physics and Astronomy, Queen Mary University of London, London, United Kingdom
- 78 Department of Physics, Royal Holloway University of London, Surrey, United Kingdom
- 79 Department of Physics and Astronomy, University College London, London, United Kingdom
- 80 Louisiana Tech University, Ruston LA, United States of America
- 81 Laboratoire de Physique Nucléaire et de Hautes Energies, UPMC and Université Paris-Diderot and CNRS/IN2P3, Paris, France
- 82 Fysiska institutionen, Lunds universitet, Lund, Sweden
- 83 Departamento de Física Teórica C-15, Universidad Autónoma de Madrid, Madrid, Spain
- 84 Institut für Physik, Universität Mainz, Mainz, Germany
- 85 School of Physics and Astronomy, University of Manchester, Manchester, United Kingdom
- 86 CPPM, Aix-Marseille Université and CNRS/IN2P3, Marseille, France
- 87 Department of Physics, University of Massachusetts, Amherst MA, United States of America
- 88 Department of Physics, McGill University, Montreal QC, Canada
- 89 School of Physics, University of Melbourne, Victoria, Australia
- 90 Department of Physics, The University of Michigan, Ann Arbor MI, United States of America
- 91 Department of Physics and Astronomy, Michigan State University, East Lansing MI, United States of America
- 92 ^(a) INFN Sezione di Milano; ^(b) Dipartimento di Fisica, Università di Milano, Milano, Italy
- 93 B.I. Stepanov Institute of Physics, National Academy of Sciences of Belarus, Minsk, Republic of Belarus
- 94 National Scientific and Educational Centre for Particle and High Energy Physics, Minsk, Republic of Belarus
- 95 Group of Particle Physics, University of Montreal, Montreal QC, Canada
- 96 P.N. Lebedev Physical Institute of the Russian Academy of Sciences, Moscow, Russia
- 97 Institute for Theoretical and Experimental Physics (ITEP), Moscow, Russia
- 98 National Research Nuclear University MEPhI, Moscow, Russia
- 99 D.V. Skobeltsyn Institute of Nuclear Physics, M.V. Lomonosov Moscow State University, Moscow, Russia
- 100 Fakultät für Physik, Ludwig-Maximilians-Universität München, München, Germany
- 101 Max-Planck-Institut für Physik (Werner-Heisenberg-Institut), München, Germany
- 102 Nagasaki Institute of Applied Science, Nagasaki, Japan
- 103 Graduate School of Science and Kobayashi-Maskawa Institute, Nagoya University, Nagoya, Japan
- 104 ^(a) INFN Sezione di Napoli; ^(b) Dipartimento di Fisica, Università di Napoli, Napoli, Italy
- 105 Department of Physics and Astronomy, University of New Mexico, Albuquerque NM, United States of America
- 106 Institute for Mathematics, Astrophysics and Particle Physics, Radboud University Nijmegen/Nikhef, Nijmegen, Netherlands
- 107 Nikhef National Institute for Subatomic Physics and University of Amsterdam, Amsterdam, Netherlands

- ¹⁰⁸ Department of Physics, Northern Illinois University, DeKalb IL, United States of America
- ¹⁰⁹ Budker Institute of Nuclear Physics, SB RAS, Novosibirsk, Russia
- ¹¹⁰ Department of Physics, New York University, New York NY, United States of America
- ¹¹¹ Ohio State University, Columbus OH, United States of America
- ¹¹² Faculty of Science, Okayama University, Okayama, Japan
- ¹¹³ Homer L. Dodge Department of Physics and Astronomy, University of Oklahoma, Norman OK, United States of America
- ¹¹⁴ Department of Physics, Oklahoma State University, Stillwater OK, United States of America
- ¹¹⁵ Palacký University, RCPTM, Olomouc, Czech Republic
- ¹¹⁶ Center for High Energy Physics, University of Oregon, Eugene OR, United States of America
- ¹¹⁷ LAL, Univ. Paris-Sud, CNRS/IN2P3, Université Paris-Saclay, Orsay, France
- ¹¹⁸ Graduate School of Science, Osaka University, Osaka, Japan
- ¹¹⁹ Department of Physics, University of Oslo, Oslo, Norway
- ¹²⁰ Department of Physics, Oxford University, Oxford, United Kingdom
- ¹²¹ ^(a) INFN Sezione di Pavia; ^(b) Dipartimento di Fisica, Università di Pavia, Pavia, Italy
- ¹²² Department of Physics, University of Pennsylvania, Philadelphia PA, United States of America
- ¹²³ National Research Centre "Kurchatov Institute" B.P.Konstantinov Petersburg Nuclear Physics Institute, St. Petersburg, Russia
- ¹²⁴ ^(a) INFN Sezione di Pisa; ^(b) Dipartimento di Fisica E. Fermi, Università di Pisa, Pisa, Italy
- ¹²⁵ Department of Physics and Astronomy, University of Pittsburgh, Pittsburgh PA, United States of America
- ¹²⁶ ^(a) Laboratório de Instrumentação e Física Experimental de Partículas - LIP, Lisboa; ^(b) Faculdade de Ciências, Universidade de Lisboa, Lisboa; ^(c) Department of Physics, University of Coimbra, Coimbra; ^(d) Centro de Física Nuclear da Universidade de Lisboa, Lisboa; ^(e) Departamento de Física, Universidade do Minho, Braga; ^(f) Departamento de Física Teórica y del Cosmos and CAFPE, Universidad de Granada, Granada (Spain); ^(g) Dep Física and CEFITEC of Faculdade de Ciências e Tecnologia, Universidade Nova de Lisboa, Caparica, Portugal
- ¹²⁷ Institute of Physics, Academy of Sciences of the Czech Republic, Praha, Czech Republic
- ¹²⁸ Czech Technical University in Prague, Praha, Czech Republic
- ¹²⁹ Faculty of Mathematics and Physics, Charles University in Prague, Praha, Czech Republic
- ¹³⁰ State Research Center Institute for High Energy Physics (Protvino), NRC KI, Russia
- ¹³¹ Particle Physics Department, Rutherford Appleton Laboratory, Didcot, United Kingdom
- ¹³² ^(a) INFN Sezione di Roma; ^(b) Dipartimento di Fisica, Sapienza Università di Roma, Roma, Italy
- ¹³³ ^(a) INFN Sezione di Roma Tor Vergata; ^(b) Dipartimento di Fisica, Università di Roma Tor Vergata, Roma, Italy
- ¹³⁴ ^(a) INFN Sezione di Roma Tre; ^(b) Dipartimento di Matematica e Fisica, Università Roma Tre, Roma, Italy
- ¹³⁵ ^(a) Faculté des Sciences Ain Chock, Réseau Universitaire de Physique des Hautes Energies - Université Hassan II, Casablanca; ^(b) Centre National de l'Énergie des Sciences Techniques Nucleaires, Rabat; ^(c) Faculté des Sciences Semlalia, Université Cadi Ayyad, LPHEA-Marrakech; ^(d) Faculté des Sciences, Université Mohamed Premier and LTPM, Oujda; ^(e) Faculté des sciences, Université Mohammed V, Rabat, Morocco
- ¹³⁶ DSM/IRFU (Institut de Recherches sur les Lois Fondamentales de l'Univers), CEA Saclay (Commissariat à l'Énergie Atomique et aux Énergies Alternatives), Gif-sur-Yvette, France
- ¹³⁷ Santa Cruz Institute for Particle Physics, University of California Santa Cruz, Santa Cruz CA, United States of America
- ¹³⁸ Department of Physics, University of Washington, Seattle WA, United States of America

- ¹³⁹ Department of Physics and Astronomy, University of Sheffield, Sheffield, United Kingdom
- ¹⁴⁰ Department of Physics, Shinshu University, Nagano, Japan
- ¹⁴¹ Fachbereich Physik, Universität Siegen, Siegen, Germany
- ¹⁴² Department of Physics, Simon Fraser University, Burnaby BC, Canada
- ¹⁴³ SLAC National Accelerator Laboratory, Stanford CA, United States of America
- ¹⁴⁴ ^(a) Faculty of Mathematics, Physics & Informatics, Comenius University, Bratislava; ^(b) Department of Subnuclear Physics, Institute of Experimental Physics of the Slovak Academy of Sciences, Kosice, Slovak Republic
- ¹⁴⁵ ^(a) Department of Physics, University of Cape Town, Cape Town; ^(b) Department of Physics, University of Johannesburg, Johannesburg; ^(c) School of Physics, University of the Witwatersrand, Johannesburg, South Africa
- ¹⁴⁶ ^(a) Department of Physics, Stockholm University; ^(b) The Oskar Klein Centre, Stockholm, Sweden
- ¹⁴⁷ Physics Department, Royal Institute of Technology, Stockholm, Sweden
- ¹⁴⁸ Departments of Physics & Astronomy and Chemistry, Stony Brook University, Stony Brook NY, United States of America
- ¹⁴⁹ Department of Physics and Astronomy, University of Sussex, Brighton, United Kingdom
- ¹⁵⁰ School of Physics, University of Sydney, Sydney, Australia
- ¹⁵¹ Institute of Physics, Academia Sinica, Taipei, Taiwan
- ¹⁵² Department of Physics, Technion: Israel Institute of Technology, Haifa, Israel
- ¹⁵³ Raymond and Beverly Sackler School of Physics and Astronomy, Tel Aviv University, Tel Aviv, Israel
- ¹⁵⁴ Department of Physics, Aristotle University of Thessaloniki, Thessaloniki, Greece
- ¹⁵⁵ International Center for Elementary Particle Physics and Department of Physics, The University of Tokyo, Tokyo, Japan
- ¹⁵⁶ Graduate School of Science and Technology, Tokyo Metropolitan University, Tokyo, Japan
- ¹⁵⁷ Department of Physics, Tokyo Institute of Technology, Tokyo, Japan
- ¹⁵⁸ Department of Physics, University of Toronto, Toronto ON, Canada
- ¹⁵⁹ ^(a) TRIUMF, Vancouver BC; ^(b) Department of Physics and Astronomy, York University, Toronto ON, Canada
- ¹⁶⁰ Faculty of Pure and Applied Sciences, and Center for Integrated Research in Fundamental Science and Engineering, University of Tsukuba, Tsukuba, Japan
- ¹⁶¹ Department of Physics and Astronomy, Tufts University, Medford MA, United States of America
- ¹⁶² Department of Physics and Astronomy, University of California Irvine, Irvine CA, United States of America
- ¹⁶³ ^(a) INFN Gruppo Collegato di Udine, Sezione di Trieste, Udine; ^(b) ICTP, Trieste; ^(c) Dipartimento di Chimica, Fisica e Ambiente, Università di Udine, Udine, Italy
- ¹⁶⁴ Department of Physics and Astronomy, University of Uppsala, Uppsala, Sweden
- ¹⁶⁵ Department of Physics, University of Illinois, Urbana IL, United States of America
- ¹⁶⁶ Instituto de Física Corpuscular (IFIC) and Departamento de Física Atomica, Molecular y Nuclear and Departamento de Ingeniería Electrónica and Instituto de Microelectrónica de Barcelona (IMB-CNM), University of Valencia and CSIC, Valencia, Spain
- ¹⁶⁷ Department of Physics, University of British Columbia, Vancouver BC, Canada
- ¹⁶⁸ Department of Physics and Astronomy, University of Victoria, Victoria BC, Canada
- ¹⁶⁹ Department of Physics, University of Warwick, Coventry, United Kingdom
- ¹⁷⁰ Waseda University, Tokyo, Japan
- ¹⁷¹ Department of Particle Physics, The Weizmann Institute of Science, Rehovot, Israel
- ¹⁷² Department of Physics, University of Wisconsin, Madison WI, United States of America

- ¹⁷³ Fakultät für Physik und Astronomie, Julius-Maximilians-Universität, Würzburg, Germany
- ¹⁷⁴ Fakultät für Mathematik und Naturwissenschaften, Fachgruppe Physik, Bergische Universität Wuppertal, Wuppertal, Germany
- ¹⁷⁵ Department of Physics, Yale University, New Haven CT, United States of America
- ¹⁷⁶ Yerevan Physics Institute, Yerevan, Armenia
- ¹⁷⁷ Centre de Calcul de l'Institut National de Physique Nucléaire et de Physique des Particules (IN2P3), Villeurbanne, France
- ^a Also at Department of Physics, King's College London, London, United Kingdom
- ^b Also at Institute of Physics, Azerbaijan Academy of Sciences, Baku, Azerbaijan
- ^c Also at Novosibirsk State University, Novosibirsk, Russia
- ^d Also at TRIUMF, Vancouver BC, Canada
- ^e Also at Department of Physics & Astronomy, University of Louisville, Louisville, KY, United States of America
- ^f Also at Department of Physics, California State University, Fresno CA, United States of America
- ^g Also at Department of Physics, University of Fribourg, Fribourg, Switzerland
- ^h Also at Departament de Física de la Universitat Autònoma de Barcelona, Barcelona, Spain
- ⁱ Also at Departamento de Física e Astronomia, Faculdade de Ciências, Universidade do Porto, Portugal
- ^j Also at Tomsk State University, Tomsk, Russia
- ^k Also at Università di Napoli Parthenope, Napoli, Italy
- ^l Also at Institute of Particle Physics (IPP), Canada
- ^m Also at National Institute of Physics and Nuclear Engineering, Bucharest, Romania
- ⁿ Also at Department of Physics, St. Petersburg State Polytechnical University, St. Petersburg, Russia
- ^o Also at Department of Physics, The University of Michigan, Ann Arbor MI, United States of America
- ^p Also at Centre for High Performance Computing, CSIR Campus, Rosebank, Cape Town, South Africa
- ^q Also at Louisiana Tech University, Ruston LA, United States of America
- ^r Also at Institutio Catalana de Recerca i Estudis Avancats, ICREA, Barcelona, Spain
- ^s Also at Graduate School of Science, Osaka University, Osaka, Japan
- ^t Also at Department of Physics, National Tsing Hua University, Taiwan
- ^u Also at Institute for Mathematics, Astrophysics and Particle Physics, Radboud University Nijmegen/Nikhef, Nijmegen, Netherlands
- ^v Also at Department of Physics, The University of Texas at Austin, Austin TX, United States of America
- ^w Also at CERN, Geneva, Switzerland
- ^x Also at Georgian Technical University (GTU), Tbilisi, Georgia
- ^y Also at O Chadai Academic Production, Ochanomizu University, Tokyo, Japan
- ^z Also at Manhattan College, New York NY, United States of America
- ^{aa} Also at Hellenic Open University, Patras, Greece
- ^{ab} Also at Academia Sinica Grid Computing, Institute of Physics, Academia Sinica, Taipei, Taiwan
- ^{ac} Also at School of Physics, Shandong University, Shandong, China
- ^{ad} Also at Department of Physics, California State University, Sacramento CA, United States of America
- ^{ae} Also at Moscow Institute of Physics and Technology State University, Dolgoprudny, Russia
- ^{af} Also at Section de Physique, Université de Genève, Geneva, Switzerland
- ^{ag} Also at Eotvos Lorand University, Budapest, Hungary
- ^{ah} Also at Departments of Physics & Astronomy and Chemistry, Stony Brook University, Stony Brook NY, United States of America
- ^{ai} Also at International School for Advanced Studies (SISSA), Trieste, Italy
- ^{aj} Also at Department of Physics and Astronomy, University of South Carolina, Columbia SC, United States of America

- ak* Also at School of Physics and Engineering, Sun Yat-sen University, Guangzhou, China
- al* Also at Institute for Nuclear Research and Nuclear Energy (INRNE) of the Bulgarian Academy of Sciences, Sofia, Bulgaria
- am* Also at Faculty of Physics, M.V.Lomonosov Moscow State University, Moscow, Russia
- an* Also at Institute of Physics, Academia Sinica, Taipei, Taiwan
- ao* Also at National Research Nuclear University MEPhI, Moscow, Russia
- ap* Also at Department of Physics, Stanford University, Stanford CA, United States of America
- aq* Also at Institute for Particle and Nuclear Physics, Wigner Research Centre for Physics, Budapest, Hungary
- ar* Also at Flensburg University of Applied Sciences, Flensburg, Germany
- as* Also at University of Malaya, Department of Physics, Kuala Lumpur, Malaysia
- at* Also at CPPM, Aix-Marseille Université and CNRS/IN2P3, Marseille, France
- * Deceased